Full-duplex for cellular networks : a stochastic geometry approach

Hernan Arrano Scharager

INSTITUT POLYTECHNIQUE DE PARIS

NNT : 2020IPPAT001

Thèse de doctorat

Full-Duplex for Cellular Networks: A Stochastic Geometry Approach

Thèse de doctorat de l'Institut Polytechnique de Paris
préparée à Télécom Paris

École doctorale n°626 Institut Polytechnique de Paris (ED IP Paris)
Spécialité de doctorat : Informatique, Données, Intelligence Artificielle

Thèse présentée et soutenue à Paris, le 30 janvier 2020, par

HERNÁN FELIPE ARRAÑO SCHARAGER

Composition du Jury :

Véronique Vèque Professeur, Université Paris-Saclay	Président
Mohamed-Slim Alouini Professeur, King Abdula University of Science and Technology	Rapporteur
Marco Di Renzo Directeur de Recherche CNRS, CentraleSupélec	Rapporteur
Anastasios Giovanidis Chargé de Recherche CNRS, Sorbonne Université	Examinateur
Juan Antonio Cordero Fuertes Maître de Conférences, École Polytechnique	Examinateur
Marceau Coupechoux Professeur, Telecom Paris	Directeur de thèse
Jean-Marc Kelif Ingénieur de Recherche, Orange Labs	Co-directeur de thèse

Titre : Full-duplex pour les réseaux cellulaires : une approche basée sur la géométrie stochastique

Mots clés : full-duplex, géométrie stochastique, réseaux cellulaires

Résumé : Le full-duplex (FD) est un principe selon lequel un appareil peut recevoir et émettre sur la même ressource radio temporaux-fréquentiel. Le principe a été longtemps considéré comme irréaliste en raison de la forte auto-interférence qui se produit lors de la transmission et la réception dans le même bloc de ressources. En supposant une annulation parfaite de l'auto-interférence (self-IC), il peut potentiellement doubler l'efficacité spectrale (SE) d'une communication point à point donnée. Dans la pratique, il n'est toutefois pas possible d'obtenir la caractéristique susmentionnée. En outre, dans le contexte d'un réseau cellulaire, la performance du FD n'est pas limité seulement par l'efficacité du self-IC, puisque des interférences supplémentaires sont créées par les stations de base (BS) et les équipements des utilisateurs (UEs). Toutefois, même avec des niveaux des interférences plus élevés, les liens en voie-descendantes (DLs) obtient ainsi de meilleures performances en termes de SE, tandis que les liaisons montantes (UL) sont généralement gravement dégradées par rapport au half-duplex (HD).
Nous focalisons notre travail sur l'étude d'alternatives qui peuvent aider à améliorer les UL dégradés dans les réseaux basés sur FD, tout en essayant de profiter des gains obtenus par les DLs. À cet égard, nous utilisons la géométrie stochastique pour caractériser les indicateurs clés de performance des réseaux cellulaires, tels que : probabilité de couverture, SE moyenne et débit de données. La thèse est divisé en trois grandes études. Premièrement, nous proposons une politique qui permet aux BSs de opérer en FD ou HD en fonction des conditions UL et DL. Deuxièmement, nous étudions la performance des réseaux hybrides HD/FD dans un contexte d'ondes millimétriques. Finalement, nous proposons un algorithme basé sur l'accès multiple non orthogonal (NOMA) et l'annulation d'interférences successives (SIC), qui permet aux stations de base de coordonner leurs schémas de transmission respectifs pour réduire les interférences BS vers BS.
Nous démontrons que les modèles présentés permettent d'équilibrer les gains d'une liaison par rapport à l'autre ; réduisant la dégradation de l'UL, tout en maintenant les gains DL. En outre, nous montrons que les scénarios dans lesquels les équipement sont capables de former des faisceaux sont idéaux pour les déploiements FD, puisqu'ils réduisent directement l'intérference co-canal.

Title : Full-duplex for cellular networks: a stochastic geometry approach

Keywords : full-duplex, stochastic geometry, cellular networks

Abstract : Full-duplex (FD) is a principle in which a transceiver can receive and transmit on the same time-frequency radio resource. The principle was long held as impractical due to the high self-interference that arises when simultaneously transmitting and receiving in the same resource block. When assuming perfect self-interference cancellation, FD can potentially double the spectral efficiency (SE) of a given point-to-point communication. In practice though, it is not possible to achieve the aforementioned characteristic. Moreover, under a cellular network context, not only the self-interference limits the performance, since additional co-channel interference is created by base stations (BSs) and users equipment (UEs). However, even with the higher interference dowlinks (DLs) still obtain higher SE performances, whereas uplinks (ULs) are generally critically degraded, when compared to half-duplex (HD).
We focus our work in the study of alternatives that can help improve the impaired ULs in FD networks, while still trying to profit from the gains experienced by DLs. In this regard, we use stochastic geometry along the thesis as a means to characterize key performance indicators of cellular networks, such as: coverage probability, average SE and data rates. The thesis is divided into three major studies. Firstly, we propose a duplex-switching policy which enables BSs to operate in FD- or HD- depending on the UL and DL conditions. Secondly, we investigate the performance of hybrid HD/FD networks under a millimeter wave context. Finally, we propose a novel algorithm based on non-orthogonal multiple-access (NOMA) and successive interference cancellation (SIC), which allows BSs to coordinate on their respective transmission schemes to reduce the BS-to-BS interference.
We demonstrate that the models presented in the thesis allow to balance the gains of one link over the other; reducing the UL degradation, while maintaining DL gains. In addition, we show that scenarios in which equipment is able to perform beamforming are ideal for FD deployments, since they directly reduce the co-channel interference.

Institut Polytechnique de Paris
91120 Palaiseau, France

Table of contents

List of figures

List of tables

Nomenclature and Acronyms

Roman Symbols

$\mathbf{B}$	Borel set
B	System bandwidth
$d(i,j)$	Distance between points i and j
f_R	Contact distribution and nearest neighbor distribution of homogeneous PPPs
f_{R_0}	Distance between UE and its serving BS
I	Interference
$L(i,j)$	Deterministic distance dependent loss between points i and j
P	Power
P	Distribution of point process
R	Rotation function
v_D	Lebesgue measure in dimension D
x	Position of a base station
y	Position of a user equipment

Greek Symbols

β	Residual self-interference parameter
Γ_m	Mean rate gains with respect to a FD network of a link $m \in \{u,d\}$
η	Path-loss exponent

γ	Signal-to-interference-plus-noise ratio
κ	Link reference path-loss at 1 meter
Λ	Intensity measure of a point process
λ_u	Intensity function of user equipment point process
$\lambda_u^{(\mathrm{BS})}$	Intensity function of UE point process as seen from a typical BS
μ	Ratio between user equipment power and base station power
Ω	Set of RBs over the system bandwidth
ω	RB bandwidth
Φ	Point process (when in a cellular network context, it represents the position of BSs)
$\hat{\Phi}$	Marked point process
Ψ	Point process representing the position of UEs
σ^2	Noise power
τ	Resource block
ϑ_m	FD-to-HD average spectral efficiency ratio of a link $m \in \{u, d\}$

Superscripts

D	Dimension size
d	Effect generated towards an element in downlink
mode	Duplex mode (full-duplex or half-duplex)
u	Effect generated towards an element in uplink

Subscripts

BS	Effect generated by base stations
d	Characteristic in downlink
m	Characteristic in dowlink or uplink
u	Characteristic in uplink

UE Effect generated by user equipment

Other Symbols

$\mathbb{1}$ Indicator function

$\mathscr{C}$ Instantaneous link capacity

$\overline{\mathscr{C}}$ Ergodic capacity

$\mathbb{E}$ Expectation

$\mathscr{L}$ Laplace transform

$\mathbb{M}$ Space of marks of point processes

$\mathscr{M}$ Borel σ-algebra in $\mathbb{M}$

M Distribution of marks of point processes

$\mathscr{N}$ σ-algebra on $\mathbb{N}$

$\mathbb{N}$ Family of all sequences of points locally finite and simple

$\mathscr{O}$ Origin

$\mathscr{P}$ Coverage probability

$\mathbb{P}$ Probability

$\mathbb{R}$ Real line

$\mathscr{R}$ Rate

$\mathscr{T}$ Throughput

Acronyms / Abbreviations

1D One-dimensional

2D Two-dimensional

2G Second-generation

3D Three-dimensional

3G Third-generation

4G Fourth-generation

5G Fifth-generation

ADC Analog-to-digital converter

ASE Average spectral efficiency

BS Base station

CCDF Complementary cumulative distribution function

CDF Cumulative distribution function

CoMP Coordinated multi point

CRAN Centralized radio access network

DAC Digital-to-analog converter

DL Downlink

DS Duplex-switching

FDD Frequency division duplexing

FD Full-duplex

GPS Global positioning system

HD Half-duplex

HPA High power amplifier

i.i.d Independent and identically distributed

ISD Inter-site distance

LNA Low noise amplifier

LOS Line-of-sight

MAC Media access control

MC Macro-cell

MIMO Multiple-input multiple-output

mmWave Millimeter wave

NGWN Next-generation wireless network

NLOS Non-line-of-sight

NOMA Non-orthogonal multiple access

OUT Outage

PA Power amplifier

PCF Pair correlation function

PDF Probability density function

PGFL Probability generating functional

PP Point process

PPP Poisson point process

RB Resource block

RSI Residual self-interference

RV Random variable

SC Small-cell

Self-IC Self-Interference Cancellation

SE Spectral efficiency

SIC Successive interference cancellation

SINR Signal-to-interference-plus-noise ratio

SNR Signal-to-noise-ratio

TDD Time division duplexing

UE User equipment

UL Uplink

UMi Urban micro-cell deployment

Chapter 1

Introduction

1.1 Context and motivation

Designing, deploying and managing next-generation wireless networks (NGWNs) is a highly constrained problem due to the existence of a limited and scarce available frequency-domain spectrum. This is a great issue, firstly, because there is a continuously increasing number of devices entering mobile networks and, secondly, due to a growing demand for greater data rates. In this regard, we may think of three different approaches to increase the throughput and capacity of NGWNs:

1. Improve the spectral efficiency (SE) ,
2. Densify networks, and
3. Increase the bandwidth of systems.

Item 2 mostly depends on the deployment strategies of network operators, while item 3 on the ability of, firstly, releasing spectrum in currently used bands (a fact that depends not only on operators, but also on spectrum owners, e.g. governments and regulators) and, secondly, on the use of new frequency-domain bands, such as the millimeter wave (mmWave) spectrum. For item 1, we find different physical layer techniques that might help improve the SE, such as: massive multiple-input multiple-output (MIMO) , three-dimensional (3D) beamforming, non-orthogonal multiple access (NOMA), new channel codes, etc [1]. But, it remains to be seen if these techniques will be sufficient to address NGWNs scenarios and performance demands, e.g. as the ones expected in fifth-generation (5G) cellular networks where multiple technologies operating in nearby frequency bands are supposed to provide different services and coexist in highly dense radio environments.

In this thesis we are interested in full-duplex which is a technique based on interference cancellation. However, we will not look at the signal processing aspects, but at the impact that full-duplex implementation would have on the network performance, when focusing on the cellular context. On this matter, we will see that the gains achieved by full-duplex in point-to-point communications are not necessarily up to the theoretical expectations and, hence, new approaches to manage the interference are needed.

1.1.1 What is full-duplex? Definition and promises

In literature, a *duplex* represents a set of connected parties that can communicate between each other. In this regard, a *half-duplex* (HD) system commonly represents the case in which these parties cannot communicate between each other simultaneously. The "walkie-talkie" example is arguably the most used to represent this scenario. Further, *full-duplex* (FD) is frequently used to represent the case in which the point-to-point communication between the different parties can be achieved simultaneously in both directions by using two separate channels (or seemingly simultaneously by adjacent time slots on a single radio channel). Therefore, and according to this definition, it is not difficult to find references to telephony (fixed or mobile) as an example of a FD system, since in a telephone call the communication process between the two parties can be carried out simultaneously without needing one of them to finish communicating a message, to let the other proceed. These definitions are for example given in the rather old reference [2].

However, in this thesis we consider:

- Half-duplex, for the case in which radio channels cannot be used simultaneously for transmission and reception, and
- Full-duplex, for the case in which radio channels can be used simultaneously for transmission and reception.

With this new definitions of HD and FD, if we observe how the different equipment work at the physical and media access control (MAC) levels, we notice that neither walkie-talkies, nor mobile network equipment use the same radio channel for transmission and reception simultaneously. Hence, they all form HD-based systems. Nonetheless, if we analyze the problem from an application level point of view, the aforementioned telephone call example can eventually be interpreted as FD, in the sense that the involved parties can communicate simultaneously (or seemingly simultaneously).

On this matter, frequency division duplexing (FDD) and time division duplexing (TDD) are two techniques widely used in mobile networks to enable two-way communications. In

FDD, equipment can transmit simultaneously but on different frequency channels. Hence, in FDD, the uplink (UL) and downlink (DL) channels are separated in two frequencies. On the other hand, in TDD the mobile phone and the base station (BS) transmit alternatively on different channels. On this matter, the UL and DL channels are time-separated. FDD and TDD approaches are traditionally adopted to avoid interference between links. However, the notion of FD challenges the concepts of TDD and FDD historically present in cellular networks, as in a FD system the UL and DL channels are no longer separated in terms of time, nor frequency.

In this thesis we will study FD systems, in which equipment are capable of simultaneously receiving and transmitting data in a given frequency channel. With FD, one could potentially double the total communication throughput or use half as many resources for a given throughput compared to HD systems (depending on the desired system performance and approach used).

1.1.2 Main practical limitations

Even though the theoretical FD principle is promising, successfully conceiving FD-based systems is a complex subject. This explains why FD is not exploited by nowadays wireless networks. In this sense, we separate the main practical drawbacks of FD in two main categories:

- Self-interference, and
- Inter- and intra-cell interference.

Self-interference related challenges

Full-duplex was long held as impractical, due to the high self-interference that arises from the fact of having a transceiver receiving and transmitting in the same frequency band. We can arguably say that this impairment is the most important and limiting factor of "real-life" FD transceivers. Roughly, this process is like the action of talking to someone, while this other person is simultaneously talking to you and being able to process/understand the received message, which should be almost impossible for any normal human being. To grasp the latter impairment, let us consider the following example.

Example 1.1.1. *Let us take into account a single cell scenario according to typical values found in cellular networks. Hence, we consider a small-cell FD-enabled BS (located in B)*

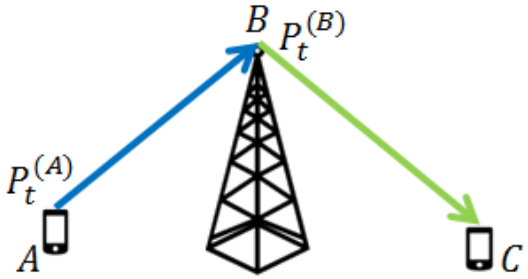

Fig. 1.1 Two user terminals served by a base station in FD.

which transmits at its maximum power capabilities, i.e., $P_t^{(B)} = 30$ *dBm, with two scheduled users, one in UL (located in A) and the other in DL (located in C), as seen in Fig. 1.1. The UL user transmits at its maximum power capability, i.e.,* $P_t^{(A)} = 23$ *dBm. According to Friss free-space transmission equation, the received power (*P_r*) of a given point-to-point link is given by:*

$$P_r = G_t G_r \left(\frac{w_l}{4\pi d}\right)^2 P_t, \tag{1.1}$$

where G_t *and* G_r *are the transmitter and receiver antenna gains, respectively,* w_l *is the wavelength, d the distance between the transmitter and receiver and* P_t *the transmit power. In this example, all elements have isotropic antennas (hence,* $G_r = G_t = 1$ *in all cases), they operate in the 2600 MHz band and A and C are respectively at* 100 *m from the BS. By using* (1.1)*, the power of the signal received in B coming from the UL user in A is approximately -87 dBm. Now, let us assume that the BS in B has no particular system integrated to cancel the self-interference. Thus, the total transmitted power from B towards C, will interfere the useful signal received from A, with difference of* $-87\,dBm - 30\,dBm = -117\,dB$*. This is a huge difference, if we know that receivers usually operates at signal-to-interference-plus-noise ratio (SINR) levels above* -10 *dB in a classical network. Thus, the useful UL signal at B is approximately* 1×10^{-12} *times smaller than the self-interference power.*

On this matter, we could arguably say that as a transceiver already knows its transmitted signal, cancelling it afterwards from the received (total) signal should be an “easy task”. Yet as we will further see in Section 1.2, in practice, different effects heavily distort the received version of the transmitted message, which critically complexes the self-interference cancellation process.

Because there exists a trade-off between the power that should be radiated towards a receiver and the self-interference generated from this operation, power allocation and optimal transmission schemes are also more complex under the FD context. Hence, different

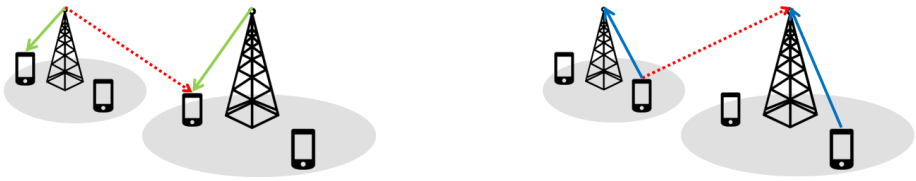

(a) Downlink in HD (b) Uplink in HD

Fig. 1.2 Interference created in HD-based networks, where the red-dotted lines represent an interfering link. For the downlink in (a), the interference is generated by other DLs (transmitting BSs). For the uplink in (b), the interference is generated by other ULs (transmitting UEs).

approaches could be adopted depending on the quality of service requirements. In this sense, the system might aim to privilege the performance of one of the link directions (signals towards or from a given FD transceiver), or on the other hand, find an optimal solution to balance the power of the signal received by the intended user and the level of self-interference, e.g. [3, 4].

Moreover, the complexity and cost of a FD-capable element is considerable higher when comparing it with respect to its HD counterpart. Full-duplex is complex and costly mainly because it is necessary to cancel the self-interference. As we will further discuss in Section 1.2, this processes requires the addition of physical barriers to prevent that the transmitted signals of a FD-transceiver are received by its own receiver-end and, subsequently, extra circuits must be added to cancel all of those signals that still remain after the physical isolation. In this regard, FD considerably consumes more energy than HD [5, 6].

Some other factors that may impair the performance or increase the complexity of FD-based systems, and that remain as subjects of interest for further researches are, e.g., channel estimation [7, 8], coding (for self-interference or regular transmission scenario), MAC layer protocol design [6, 9–11], modulation techniques [12], among others.

1.1.3 Inter- and intra-cell interference

Implementing FD in a network context, i.e., where more than one FD-enabled transceiver is transmitting a signal, increases the co-channel interference. This is due to the simultaneous use of a given channel for UL and DL traffics. In fact, self-interference is actually a sub-case of co-channel interference, but here we refer to the interference that arises between different network equipment.

To grasp the previous idea, let us observe Fig. 1.2, which depicts the interference suffered by DLs and ULs on HD-based networks. For the DL case in Fig. 1.2 (a), we observe that a user equipment (UE) receiving information from his serving BS is only interfered by other

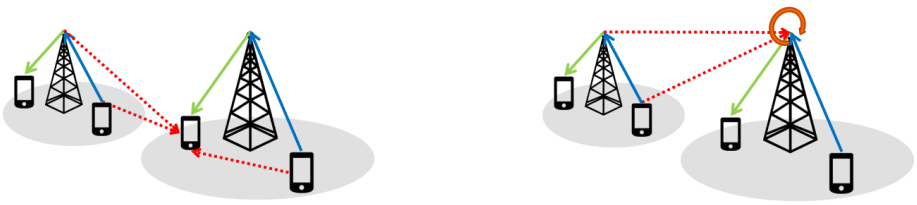

(a) Downlink in FD (b) Uplink in FD

Fig. 1.3 Interference created in a three-node FD network, where the red-dotted lines represent an interfering link and the orange loop in (b) the self-interference. For downlinks in (a), the interference is generated by other DLs and by all ULs. For uplinks in (b), the interference is generated by other DLs and ULs, additionally, the BS suffers from self-interference.

BSs that are also transmitting (by using the same channel) towards their respective UEs. On the other hand, when focusing on the UL in Fig. 1.2 (b), we see that a BS receiving data from one of his scheduled UE, is only interfered by other UL transmissions that are using the same frequency-band. In this regard, it is important to mention that when TDD is used, networks are usually synchronised, hence in a given instant the network only has DLs or ULs, but not both. Hence, the nature of the interference for the DL case comes only from other DLs, and vice versa for the UL case.

Yet, when considering the case in which BSs are FD capable, the picture is different. Indeed, let us consider Fig. 1.3 and proceed with a similar analysis as the one previously done for a HD network. In the present case, we can firstly note that by using the same channel for UL and DL, a BS is capable of serving an UL and DL user simultaneously, which is a positive effect in terms of SE. But, if we observe more in detail the DL panorama in Fig. 1.3 (a), we see that a UE is not only interfered by other BSs, but also by users in UL. Moreover, for the UL case in Fig. 1.3 (b), a BS receiving a signal from one of its scheduled UE is interfered by other UL users, by other BSs and, also, by itself, i.e., a BS is self-interfered. This increase in co-channel interference for both DL and UL limits the SE gain of FD-capable networks.

Nevertheless, current results show that when compared to traditional HD cellular systems, FD implementation may enhance the overall per-cell SE [13–17]. The whole gain is however captured by the DL, while the UL suffers from a severe degradation [18]. On the DL, the additional interference seen by a UE is compensated by the additional radio resource that are available with FD. On the contrary, and even when considering that it is possible to perfectly cancel the self-interence, neighboring BSs which are transmitting with high power compared to UEs (in UL) create a huge interference that degrades the UL performance. As a consequence, FD is only envisioned for small-cells (SCs) because they transmit at lower power and they benefit, under rooftops, from obstructed propagation between BSs [19, 20].

In this regard, optimal power allocation or innovative transmission schemes, can serve as a means to cope with co-channel interference between equipment. Different approaches can enable FD transceivers that are susceptible to strongly interfere others, to reduce their transmitted powers or their data rates towards their intended receivers, not only for the sake of reducing the self-interference, but also to minimize the net inference floor in the network. Moreover, those elements that do not necessary impair other, can profit from this radio conditions and can operate with greater freedom. On this matter, Chapter 5 presents and analyzes a novel system in which base station coordination allows to enhance the system performance by reducing the co-channel interference between FD-enabled elements.

1.1.4 Thesis objectives

As we will see in the next section, recent advances in self-interference cancellation make the development of FD-transceivers more and more realistic. So arguably, the next challenges that should be addressed to eventually achieve the implementation of FD in NGWNs are to: reduce/manage the interference and reduce the network level complexity.

The objective of the thesis is to evaluate the performance of a FD cellular network and propose solutions to mitigate the co-channel interference, in particular on the UL.

1.2 Self-interference cancellation

In this section, we provide a short literature study on self-interference cancellation. Even though this is not the subject of the thesis, it is important to have in mind the state-of-the-art in this domain to see which performance is today achievable.

Great efforts have been made by researchers and some private institutions (notably Kumu Networks) to create *self-interference cancellation* (self-IC) systems which enable FD implementation and practical results already show that levels of self-IC are getting close to be sufficiently enough to enable FD communication. In this regard, and even though the focus of this thesis is not on analyzing the signal processing aspects of FD (i.e. self-IC), without self-IC, FD would remain a utopia. Hence, it seems fundamental to us to be able to understand how this process is carried out in a general way and what is the state-of-the-art on the achieved performance, which is the main goal of the current section.

As noted in [6, 9, 20–22], the three main techniques to perform self-IC are:

- Propagation domain cancellation,
- Analog cancellation, and

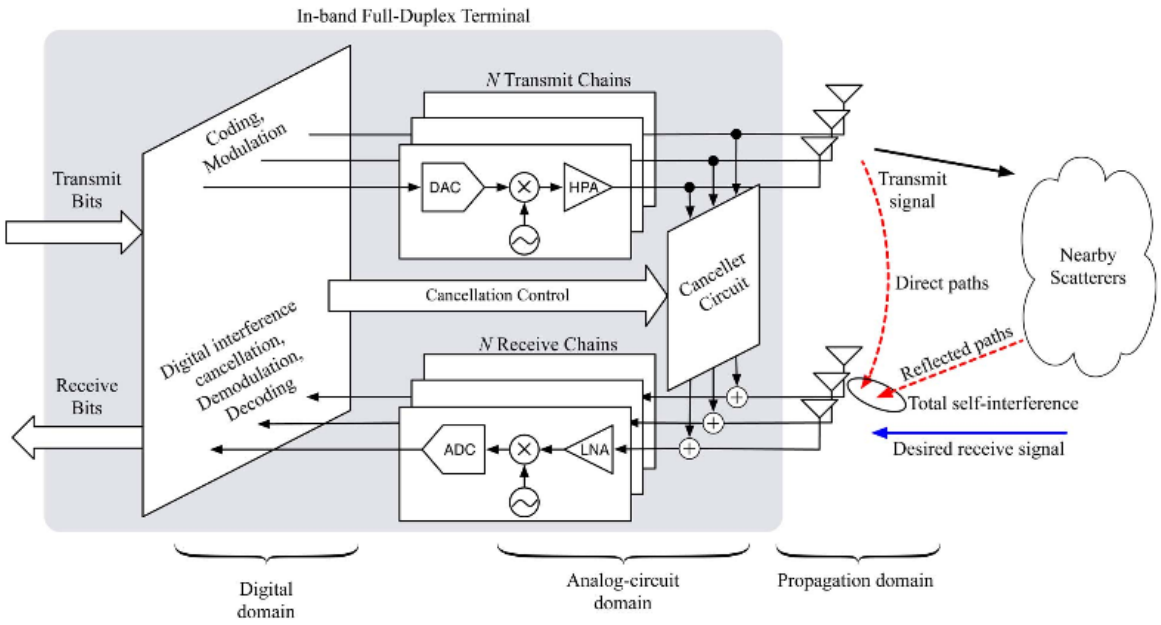

Fig. 1.4 Anatomy of a separate-antenna full-duplex terminal, where DAC stands for digital-to-analog converter, HPA for high power amplifier and LNA for low noise amplifier. (Figure taken from [20])

- Digital cancellation.

These can be implemented separately or simultaneously, depending on the needs and constraints of the system. The typical "anatomy" of a FD transceiver is depicted in Fig. 1.4, where, indeed, the three techniques are implemented in cascade to achieve lower residual self-interference (RSI) levels. We see on this figure that the steps that should be performed for self-IC are:

1. Sample the output of the transmitter,
2. Pass this signal through a canceller circuit which models the changes that the transmitted signal might suffer before arriving to the receiving antennas, creating a 'cancellation signal',
3. Mix the total received signal (equivalent to the desired signal and the self-interference) with the cancellation signal to ideally end up with a signal consisting only of the desired signal.

Let us notice from the figure, that the propagation domain cancellation technique is directly related with item 1 and impacts the total received signal. Moreover, the analog and digital cancellation techniques are performed in the canceller circuit described in item 2. Finally,

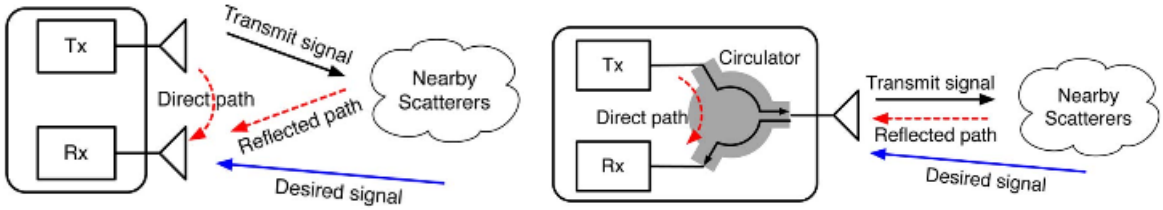

(a) Separated antennas (b) Shared antennas

Fig. 1.5 Representation of the architecture of separated and shared antennas in a FD transceiver. (Figure taken from [20])

the performance of the self-IC system is represented after the process described in item 3. Each of these techniques are now described in more detail.

1.2.1 Propagation domain cancellation

Depending on the system characteristics and demands, the FD transceiver can be conceived by a single antenna that shares the transmission and reception chains, or by separated antennas[1], as seen in Fig. 1.5. In case of separated antennas, the propagation domain cancellation can be achieved by effectively separating the antennas, through beamforming (directivity), cross polarization and/or by placing absorptive shielding between antennas [23]. In the shared antenna case, the latter can be achieved by using a circulator [6, 20, 22]. In either case, these different techniques aim at reducing as much as possible the direct path interference, which, given the small size of these systems (in relation to the separation between a transmitter and the user for which the message is intended) are usually extremely strong signals. On this matter, whatever technique is used, propagation domain cancellation can reduce the self-interference by around 15 to 30 dB [22]. Yet, as seen in Example 1.1.1 and in [20, 22], the transmitted signal cancellation should be around 100 dB to achieve a signal-to-noise-ratio (SNR) performance similar to the one of HD systems (of course, depending on the power of the transmit signal).

1.2.2 Analog cancellation

In an ideal scenario, where direct path signals are negligible or when the self-interference power is considerably low, one might think that, given its (arguably) simpler implementation, digital cancellation circuit might be enough to reduce the RSI. Under this consideration, instead of sampling the signal of the transmitter in its output, this could be done before,

[1] In this context, we could think of having separated antennas as: one transmitter and receiver antenna, or multiple ones (in case of MIMO) for each chain.

i.e., in the digital domain (baseband). Hence, simplifying the self-interference canceller by avoiding a analog cancellation circuit. This could reduce costs, complexity and space, while obviously decreasing to some extent the effectiveness of the cancellation of non-linearity distortions created by the high power amplifiers (HPAs) or oscillators phase-noise, which in some cases can be considerable [24, 25]. But, as rightly stated in [21], digital cancellation without analog cancellation does not yield an interesting system. Otherwise, FD would not be a challenge and would be arguably mass-deployed in wireless networks.

Analog circuits are usually more expensive and space consuming when compared to their digital counterpart. But they are necessary, that is the reality. Since, as just mentioned, in practice propagation domain cancellation can generally only cancel up to 30 dB of the self-interference and analog-to-digital converters (ADCs) do not have sufficient dynamic range to achieve 100 dB (or more) of cancellation. Besides, as authors show in [21], when analog cancellation achieves large suppression, applying digital cancellation afterwards can increase the noise in the system. Moreover, it is also demonstrated here that when applying digital cancellation after the analog one, the digital canceller performance decreases as the analog canceller performance increases. But, analog-domain circuits are expected to achieve up to 60 dB of cancellation [22]. Hence, a single analog cancellation circuit is not enough to deal with cases as the one presented in Example 1.1.1. This explains why a canceller circuit is achieved by mixing a digital and analog part. Here, both consist of a number of taps composed of attenuators, phase shifters and delay elements, as seen in Fig. 1.6.

As it is not easy in practice to create delays for the taps in an analog circuit, the analog cancellation part is mostly used to cancel the interference generated by direct paths (see Figs.1.4 and 1.5), since these are received practically in an instantaneous fashion by the

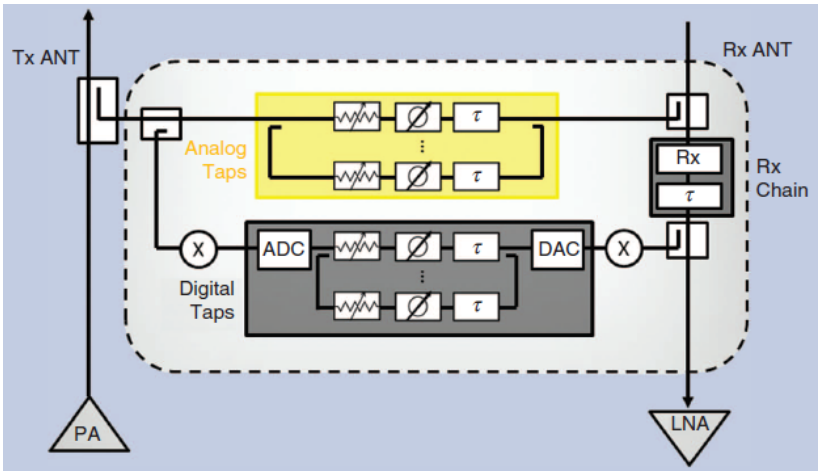

Fig. 1.6 Basic architecture of the canceller circuit, in which an analog and digital circuit are mixed. In the figure, PA stands for power amplifier. (Figure taken from [22])

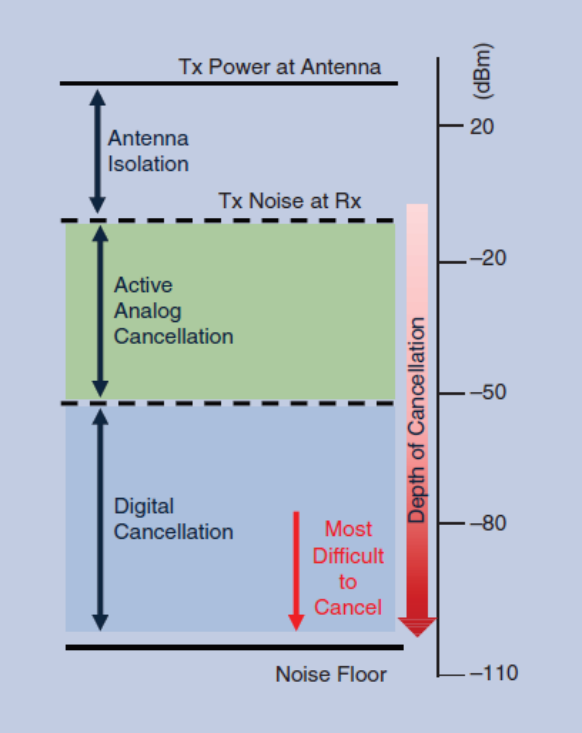

Fig. 1.7 A mixed solution between antenna isolation, analog and digital cancellation can achieve favourable self-IC levels. (Figure taken from [22])

receiving antennas. Moreover, modelling the parameters of direct paths is arguably easier than the ones of time-evolving multi-path environments, as they are generally constant. Hence, this simplifies the choice of parameters for the circuit taps.

The hardware design of analog self-interference canceller drastically increases when considering FD MIMO systems, preventing an accurate analog cancellation. On this matter, some alternative approaches have been proposed. For instance, in [26], a reduced number of taps and simple multiplexers are used to efficiently route the signals among the transmit and receive radio frequency chains. Contrary to other analog cancellation architectures, the values for each tap and the configuration of the multiplexers are jointly designed with the digital beamforming filters. Here, the number of taps does not increase with the number of transmit or receive antenna elements and results show the superiority of the proposed low complexity FD MIMO in terms of RSI and average rate.

1.2.3 Digital cancellation

The digital canceller circuits aims to suppress the distortions created by self-interference signals that travelled trough a (sometimes) complex environment and the interference remaining

after the analog cancellation[2]. Implementing digital signal processing is, arguably, simpler than what can be achieved in the analog domain. However, as previously stated, digital cancellation is limited by the range of ADCs. On this matter, and as noted in [22], there exists tuning algorithms that allow the digital canceller to adapt to changes in the environment at the rate of a few hundred of microseconds, that have similar processing power and code-space requirements compared to the typical algorithms used in MIMO systems. However, in this respect, different approaches regarding digital cancellation for FD-enabled transceivers have been presented by several scholars. For instance, and as example we can consider [27, 28]. In the first work, an adaptive filter with gradient descent based algorithms to estimate the filter coefficients is proposed, leading to 77% less computations. On the other hand, in [28] authors propose digital canceller that utilizes a Volterra series with sparse memory to model the RSI signal. This methods enables to reconstruct the self-interference even under a heavily nonlinear transmitter power amplifier.

Fig. 1.7 summarizes the operation of a self-IC solution by mixing antenna isolation and analog and digital cancellation. In this regard, experimental results already show that it is possible to obtain self-IC levels close to 110 dB, e.g. [28–31]. This is the order of magnitude we will consider in this thesis. We may assume even higher values while anticipating the progress of self-interference cancellation.

1.3 Cellular network context: full-duplex vs half-duplex

If we consider perfect self-IC in the single-cell scenario in Example 1.1.1, we observe that FD can potentially double the SE of the UL point-to-point communication. The same applies for the DL, if we assume that the UL user does not interfere the DL user. This makes FD an appealing candidate to be implemented in NGWNs. Nonetheless, it is not feasible in practical applications to achieve a perfect self-IC and some kind of scheme (or particular radio condition) has to exist to prevent the co-channel interference between the two users using the same radio resource simultaneously.

However, what interests us is the study of cellular networks. Under this context, and as seen in Fig. 1.3, the co-channel interference increases, limiting even more the performance of FD. We could think of two ways of conceiving FD-based networks: the two- and three-node models, which are shown in Fig. 1.8. In the two-node FD model, BSs and UEs are FD-capable. Hence, a given radio resource is simultaneously shared between a single user and its serving BS. For the three-node FD case, only BSs are FD capable, while users are HD-capable equipment, i.e., they can only send or receive signals. On this subject, by

[2]We could also imagine that the analog canceller circuit can, as well, distort the signal travelling through it.

(a) Two-node FD

(b) Three-node FD

Fig. 1.8 Different FD network models.

considering Section 1.2, it is arguably easier to implement the FD capability in BSs, given the constraints imposed by a user terminal (limited battery life, reduced space to implement self-IC circuits and isolation between antennas). Hence, otherwise stated, we consider along the thesis the three-node FD model, which is arguably more realistic according to current technological advances [19, 32].

Before continuing, it is important to mention that along the thesis, we say that a UE is *attached* to a BS, when the user is connected to the BS under mutual accordance, and therefore, it is only with this station with which it can eventually exchange data packets (in UL or DL) while the connection is established. We refer to a UE being *served* or *scheduled* by a BS, when not only there exists an established connection with the BS, but when there is also user data being transferred by using a given radio resource. We say in this case, that the radio resource has been allocated to this specific user to satisfy its UL or DL demands. Hence, a UE might be attached to a BS, while not being served, but not vice versa. Finally, we say that a BS is *active*, when it is serving one of its attached UE. In this event, we say that the user being served is also an *active* UE. Notice, that a BS might be active, but not transmitting, if in a given instant it is only serving UL users. To resume:

- A user has to be attached to a BS to transmit or receive data,
- A user is served by its attached BS when there are data packets flowing in UL or DL directions, and
- An active equipment is the one that is sending or receiving data packets.

1.3.1 Spectrum utilization

Let us define the *resource utilization ratio* of a link m as:

$$\alpha_m^{(\text{mode})} = \frac{B_m}{B_T^{(\text{mode})}}, \tag{1.2}$$

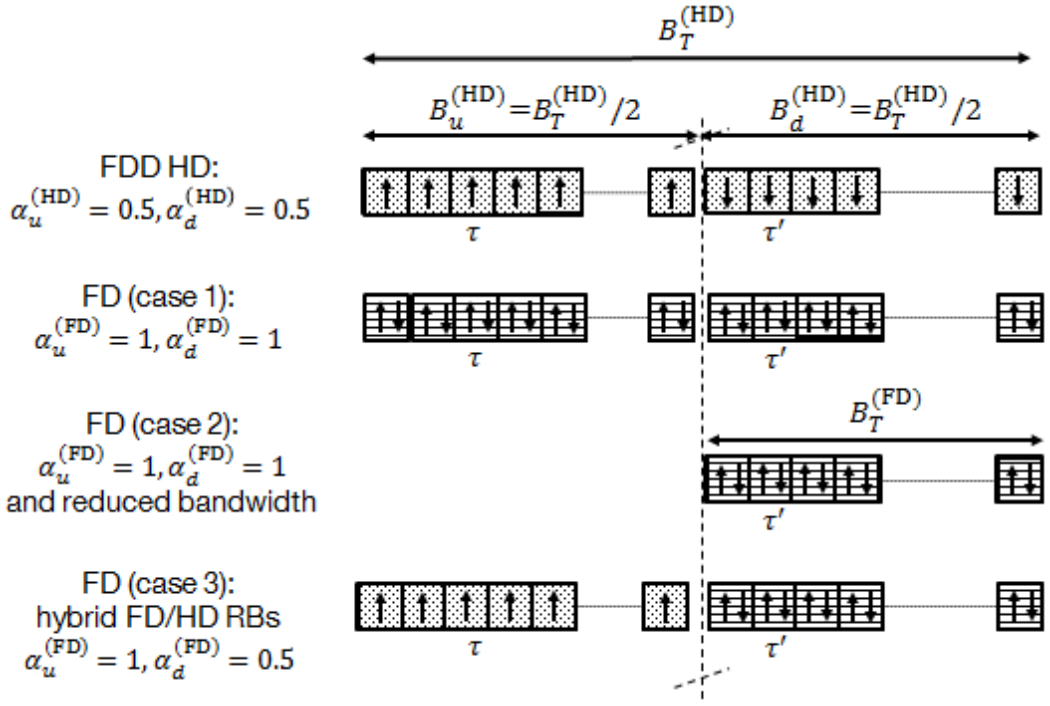

Fig. 1.9 Use of the spectrum in HD, FD and when RBs can be used for HD or FD. Each squared box represents a RB and arrows are for the direction of the links that the RBs are serving (↑ is for UL and ↓ for DL).

where $m \in \{u,d\}$ represents the link direction (u for UL and d for DL), 'mode' is the duplex-mode of the BS, B_m is the bandwidth allocated for m and $B_T^{(\text{mode})}$ is the total system bandwidth.

Generally, FDD-based cellular HD systems divide the total bandwidth, B, into equal parts for DL and UL. In each of these parts, the frequency-domain resource blocks (RBs) can only be used to satisfy the corresponding communication purpose (link direction demand). Hence, for this case,

$$B_T^{(\text{HD})} = B_u + B_d \tag{1.3}$$

and $\alpha_m^{(\text{HD})} = 1/2, \forall m$ (see 'FDD HD' in Fig. 1.9). However, if the system needs to allocate more bandwidth to a particular link, the only way of proceeding is by replacing and using RBs that were previously used for the other link. Thus, for HD systems the following holds:

$$\alpha_u^{(\text{HD})} + \alpha_d^{(\text{HD})} = 1. \tag{1.4}$$

On the contrary, in FD a RB can be used for UL and DL simultaneously. So, indeed, if each RB in $B_T^{(\text{FD})}$ is actually used for both purposes (see 'FD (case 1)' in Fig. 1.9), then

$\alpha_m^{(\mathrm{FD})} = 1, \forall m$. Hence, in this particular case we have that:

$$\alpha_u^{(\mathrm{FD})} + \alpha_d^{(\mathrm{FD})} = 2 \tag{1.5}$$

and $B_T^{(\mathrm{FD})} = B_u = B_d$.

However, as FD can potentially increase the SE, it is possible to think of two alternative options:

1. A fraction of the spectrum might be released, while still achieving similar throughput performances as in the HD scenario (see 'FD (case 2)' in Fig. 1.9), or

2. If individual RBs can adopt HD- or FD-mode, then if the system needs to enhance the performance of one of the links, e.g. the UL, we can increase α_u, while maintaining the value of α_d constant with respect to the HD case. This is achieved by allowing RBs of the link which is not intended to be improved, to be in FD (see 'FD (case 3)' in Fig. 1.9).

Let us notice that by implementing option 1, we free spectrum bandwidth that can be used for other purposes. This is extremely useful for NGWNs due to the limited and scarce available frequency-domain spectrum. Yet, in this case, the resource utilization ratio for UL and DL, remains unchanged. Consequently, we still have that $\alpha_m^{(\mathrm{FD})} = 1, \forall m$. Furthermore, with option 2, RBs can be used in HD- and FD-fashion, according to specific system performance requirements. Without loss of generality, we refer to option 2 as well as a FD-mode case. For instance, in the 'FD (case 3)' example presented in Fig. 1.9, the system aims to enhance the UL performance by using half of the spectrum exclusively for ULs and the rest in FD mode, which gives us: $\alpha_m^{(\mathrm{FD})} = 1$ and $\alpha_d^{(\mathrm{FD})} = 1/2$. Therefore, we see that we can define $B_T^{(\mathrm{mode})}$ as:

$$B_T^{(\mathrm{mode})} = B_u + B_d - (B_u \cap B_d), \tag{1.6}$$

where $(B_u \cap B_d)$ represents the bandwidth overlap between UL and DL parts or, equivalently, the bandwidth of RBs operating in FD-mode. And finally, that for all cases, we have that:

$$1 \leq \alpha_u^{(\mathrm{mode})} + \alpha_d^{(\mathrm{mode})} \leq 2. \tag{1.7}$$

1.3.2 Signal-to-interference-plus-noise ratio: a general overview

Let us consider a network with an available bandwidth $B_T^{(\mathrm{mode})}$, where Ω is the set of all RBs. Each RB is of bandwidth ω.

Locations of BSs and UEs are describe by sets X and Y, respectively. Each BS in this model has at least two UEs to serve inside its coverage region[3] and that the network is fully-loaded[4]. Base stations perform random scheduling[5]. Thus, if we observe the network in a given time t and at an specific RB τ, the positions of served users in UL and DL, which we respectively write as $Y_u(t,\tau)$ and $Y_d(t,\tau)$, can be seen as a subset of Y, which we write as $Y(t,\tau)$.

In a HD network, $B = B_u + B_d$ (as seen in Fig.1.9) and a RB is used for the transmission on a single link at a time, meaning that:

$$Y(t,\tau) = \begin{cases} Y_u(t,\tau), & \text{if } \tau \in B_u, \\ Y_d(t,\tau), & \text{if } \tau \in B_d. \end{cases} \tag{1.8}$$

For the SINR expressions, we consider a generic time-slot, t. Hence, as a result, we eliminate the time dependence for simplicity.

Half-duplex SINR expressions

The downlink SINR at a RB $\tau \in B_d$, between a BS located in x and its served UE in y is given by:

$$\gamma_d^{(\mathrm{HD})}(x,y,\tau) = \frac{P_{x,y}(\tau)}{I_{\mathrm{BS}}^{(d)}(y,\tau) + \sigma^2}, \tag{1.9}$$

where $P_{x,y}(\tau)$ is the received power at x of the useful signal transmitted by y on RB τ, σ^2 is the noise power and

$$I_{\mathrm{BS}}^{(d)}(y,\tau) = \sum_{x' \in X \setminus \{x\}} P_{x',y}(\tau), \tag{1.10}$$

is the interference generated by other DLs towards location y. On the other hand, the UL SINR between a served UE in y and its BS located in x is:

$$\gamma_u^{(\mathrm{HD})}(x,y,\tau) = \frac{P_{y,x}(\tau)}{I_{\mathrm{UE}}^{(u)}(x,\tau) + \sigma^2}, \tag{1.11}$$

where

$$I_{\mathrm{UE}}^{(u)}(x,\tau) = \sum_{y' \in Y_u(\tau) \setminus \{y\}} P_{y',x}(\tau), \tag{1.12}$$

[3]By saying this, we assume that in each cell there is always UL and DL traffic.
[4]There is 'infinite' data to be sent in all directions and the system always uses all of the available RBs.
[5]Each BS randomly chooses a pair of its attached UEs to perform UL and DL.

is the interference generated by other ULs towards location x. A graphical representation of useful and interference signals involved in an HD-based network can be found in Fig. 1.2.

Full-duplex SINR expressions

In the three-node FD scenario, a RB τ can be used for UL and DL simultaneously, hence $Y(\tau) = Y_u(\tau) \cup Y_d(\tau)$. Thus, we have that the DL SINR experienced at RB τ is:

$$\gamma_d^{(\mathrm{FD})}(x,y,\tau) = \frac{P_{x,y}(\tau)}{I_{\mathrm{BS}}^{(d)}(y,\tau) + I_{\mathrm{UE}}^{(d)}(y,\tau) + \sigma^2}, \tag{1.13}$$

where

$$I_{\mathrm{UE}}^{(d)}(y,\tau) = \sum_{y' \in Y_u(\tau) \setminus \{y\}} P_{y',y}(\tau) \tag{1.14}$$

is the interference created in y by all UL users sending information to their serving BSs (even the one in the same cell of y). This term represents the UE-to-UE interference that arises when implementing FD.

Furthermore, the UL the SINR is given by:

$$\gamma_u^{(\mathrm{FD})}(x,y,\tau) = \frac{P_{y,x}(\tau)}{I_{\mathrm{BS}}^{(u)}(y,\tau) + I_{\mathrm{UE}}^{(u)}(y,\tau) + I_{\mathrm{RSI}} + \sigma^2}, \tag{1.15}$$

where I_{RSI} is the residual self-interference after applying the different self-IC techniques in the transceiver of the BS in x and

$$I_{\mathrm{BS}}^{(u)}(x,\tau) = \sum_{x' \in X \setminus \{x\}} P_{x',x}(\tau) \tag{1.16}$$

is the interference created by all other BSs having DL towards the BS in x. This last term is the BS-to-BS interference that arises when implementing FD. A diagram representing the useful and interference signals in a three-node FD network can be found in Fig. 1.3.

By analyzing the previous SINR expressions for both HD and FD cases, we can notice that the interference is greater in FD scenarios, i.e.:

$$\begin{aligned} \gamma_d^{(\mathrm{HD})}(x,y,\tau) &\geq \gamma_d^{(\mathrm{FD})}(x,y,\tau), \\ \gamma_u^{(\mathrm{HD})}(x,y,\tau) &\geq \gamma_u^{(\mathrm{FD})}(x,y,\tau), \end{aligned} \tag{1.17}$$

which shows that implementing FD impairs the SINR performance.

1.3.3 Systems having similarities with full-duplex

Co-channel interference impairments are arguably going to be more frequent in NGWNs due to the existence of a scarce electromagnetic spectrum and the expected highly dense radio environments in which different technologies and services will mutually interact. As an example, we can consider the probable interference that could arise between current 3.4-3.8 GHz fourth-generation (4G) bands and future 5G networks, due to their near operating frequencies [33]. Additionally, co-channel interference also arises in other communication systems that are proposed for NGWNs, such as: dynamic TDD [34, 35] and NOMA-based systems [36–40]. Or even, in systems that suffer from channel-adjacent interference in transmitters that use the same technology. Thus, the study of solutions to address inter- and intra-cell interference in FD networks can be useful to solve similar technical impairments in other communication systems. In this regard, the solutions further presented in Chapters 3 and 5 can serve as a flexible solution to be implemented in other contexts.

1.4 Contributions and outline of the thesis

In order to reduce the UL performance degradation observed in FD cellular networks due to additional co-channel interference, we propose in this thesis three different approaches:

- A policy that allows BSs to switch between HD and FD,
- The use of FD BSs in conjunction with beamforming in millimeter waves bands,
- A NOMA-based FD system.

1.4.1 The duplex-switching policy

The first approach is based in a duplex-switching (DS) policy in which BSs can adopt FD- or HD-mode according to the position of their scheduled users, when using sub-6 GHz frequencies for transmissions. This DS policy offers a flexible tool for operators to favor more or less one link (UL/DL) against the other.

The contributions regarding this part of the work are the following:

- A new DS policy for cellular networks is proposed, where BSs can adopt either FD- or HD-mode. Particularly, we have that if the distance between the UL user and its serving BS is less than some threshold and the distance between the UL and the DL user is greater than some other threshold, FD is activated at the BS. Otherwise HD is

adopted. The goal is to allow FD only in good radio propagation conditions and low intra-cell interference.

- The system is modeled using the theory of stochastic geometry and analytical expressions are derived for the SINR distribution and the SE.
- The impact of the two introduced thresholds on the system performance is studied. We show that it is possible to trade-off the DL performance for an UL improvement. But also, that the parameters can be set in order to meet a maximum UL degradation constraint. In some special cases, we show that both UL and DL can be improved over a HD system. Moreover, we demonstrate that if a high UL degradation is acceptable, the DL performance can be further enhanced, with respect to the the standard FD case. Finally, we show that when the parameters are optimized, our policy even outperforms both HD and FD networks, in terms of cell performance (i.e. UL+DL).

1.4.2 Hybrid HD/FD in millimeter wave scenarios

In the second work, we investigate the possibility for BSs to switch between HD and FD in the mmWave spectrum to reduce interference, while users equipment and BSs employ beamforming techniques.

Our contributions in this part are the following:

- We model the mmWave hybrid-duplex cellular network using the theory of stochastic geometry, deriving analytical expressions for the coverage probability and SE.
- The RSI in FD-enabled elements is modeled by considering the geometry of the transmitted and received beams in the BSs.
- We show that contrary to sub-6 GHz, hybrid-duplex schemes are not required in mmWave cellular networks.
- We investigate the advantage of performing power control at FD BSs and show that reducing their power avoids UL degradation, while still enabling to enhance the DL performance with respect to a HD deployment.

1.4.3 NOMA-based FD system

In the last approach, we propose a method based on NOMA and SIC to reduce the BS-to-BS interference present in FD cellular networks. The approach consists in coordinating BSs to enable the decoding and the suppression of undesired signals that impair UL transmissions.

Our contributions in this part are the following:

- We analyze the proposed network using stochastic geometry tools and propose closed-form equations for the coverage probability and mean data rates.
- We show that our approach is promising in scenarios in which FD ULs are critically degraded due to strong BS-to-BS co-channel interference. In fact, results show that for particular settings, it is even possible to outperform the performance of HD ULs. However, this arbitrarily degrades the DLs. So we propose an alternative configuration in which the UL is enhanced by a 25% (with respect to the traditional FD case) while retaining the gains in the DL due to FD implementation.
- We show that our algorithm is flexible enough to be implemented in other systems or scenarios suffering from co-channel interference.

1.4.4 Structure of thesis

The Thesis is organized as follows. In Chapter 2, we introduce stochastic geometry tools in order to analyze some key performance indicators of HD and FD cellular networks. Chapter 3 proposes and evaluates the DS policy. In Chapter 4 the analysis of hybrid FD/HD models in mmWave-based system is carried. Chapter 5 proposes and analyses the performance of a FD cellular network, in which NOMA is used to reduce the co-channel interference. Finally, Chapter 6 is for conclusions and future works.

1.4.5 List of publications

Patents

- Hernán-Felipe Arraño-Scharager, Marceau Coupechoux, Jean-Marc Kelif, “Procédé de communication et dispositifs d’un réseau de communication sans fil” (Communication method and devices of a wireless communication network), *filed to the French National Institute of Industrial Property (INPI)*, reference number FR1901833, Feb. 2019, France.
- Jean-Marc Kelif, Marceau Coupechoux, Hernán-Felipe Arraño-Scharager, “Procédé de Communication en Full-Duplex Dans un Réseau Cellulaire” (Full-Duplex Communication Process in a Cellular Network), *filed to the INPI*, reference number FR1763277, Dec. 2017, France.

Journal articles

- Hernán-Felipe Arraño-Scharager, Marceau Coupechoux, Jean-Marc Kelif, "A NOMA Based BS Coordination Scheme for Full Duplex Cellular Networks", *submitted to* IEEE Transactions on Wireless Communications, Jan. 2020.

Conference articles

- Hernán-Felipe Arraño-Scharager, Jean-Marc Kelif, Marceau Coupechoux, "Performance Evaluation of Millimeter Wave Full-Duplex Cellular Networks", *IEEE Global Communications Conference (GLOBECOM) Workshops: Full-Duplex Communications for Future Wireless Networks*, Dec. 2018, Abu Dhabi, United Arab Emirates.
- Hernán-Felipe Arraño-Scharager, Marceau Coupechoux, Jean-Marc Kelif, "Full and Half Duplex-Switching Policy for Cellular Networks under Uplink Degradation Constraint", *IEEE International Communications Conference (ICC)*, May 2018, Kansas City, United States of America.

Chapter 2

Short introduction to stochastic geometry

We have seen how FD systems experience higher interference levels when compared to HD ones, which may prevent performance enhancements. Yet, in order to mathematically quantify the impact towards the performance of different key indicators concerning cellular networks (as the coverage probability, capacity, spectral efficiency, among other), it is necessary to introduce some tools that can help us do so.

Traditionally, cellular networks have been analyzed by using the hexagonal grid model in which the area covered by a BS is an hexagon. Yet, this model arguably does not represents the topology of real cellular networks, as in most cases it is not possible to have this kind of uniform and rigid grid. This is due to the diverse distribution of users (demand) along the network and, in addition, to the difficulties imposed by the topology of cities, in which buildings, streets or cost constraints do not allow to freely install cellular equipment. This is depicted in Fig. 2.1.

Moreover, the hexagonal grid model does not offer simple mathematical tractability to model various performance indicators of interest for operators to deploy their networks. In this regard, stochastic geometry arises as a solution to the previously mentioned issues. Firstly, because certain point processes allow to accurately model the topology of true networks and, on the other hand, because with them we can gain many engineering insights from the equations.

In this part, we introduce some of the main properties regarding point processes and give some useful results that allow us to characterize and analyze the different models presented in the following Chapters of this thesis. To do so, we mainly use as references [42–44]. We highly encourage the reader to check these references, as they further develop most of the introduced notions and hold more detailed information, that can serve as a support to

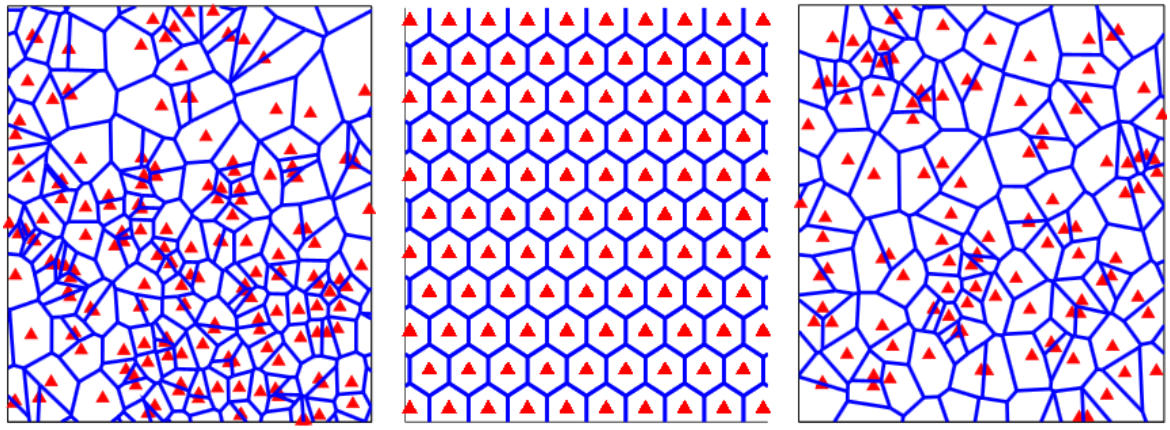

(a) Random deployment (b) Hexagonal deployment (c) Actual 4G network

Fig. 2.1 Comparison an stochastic geometry based deployment, an hexagonal one and a real 4G network. (Figure taken from [41])

the following Sections. For a more concise introduction to stochastic geometry and point processes, we also recommend [45].

2.1 Basic definitions, properties and tools

The current Section presents general point processes and their mathematical characterization. Several basic definitions, propositions and theorems are here introduced. These results and their respective proofs can be found in the suggested literature.

We can think of a point process as a set of points scattered along a certain space, where each point is drawn distributed according to a certain distribution or law, which translates formally to:

Definition 2.1.1 (Point process)**.** *A point process (PP) is a countable random collection of points that reside in some measure space, usually the Euclidean space* $\mathbb{R}^D$ *[42].*

In this thesis we consider $D = 2$ for simplicity, i.e., points are distributed in the two-dimensional (2D) plane.

Along this work, we use Φ to represent a given PP. According to Definition 2.1.1, we can interpret a PP as a random point pattern (a collection or sequence of points $\Phi = \{x_1, x_2, \ldots\}$) or, also, as a random counting measure, i.e., for a Borel set $\mathbf{B}$, the symbol $\Phi(\mathbf{B})$ denotes the random number of points of Φ which lie in $\mathbf{B}$ [43]. The first description of a point process

concern the random set formalism and the other to random measure formalism. In this regard, and as introduced in [43, Section 4.1], we can mathematically define a PP on $\mathbb{R}^D$ as a random variable taking values in a measurable space $[\mathbb{N}, \mathscr{N}]$, where $\mathbb{N}$ is the family of all sequences φ of points in $\mathbb{R}^D$ satisfying two regularity conditions:

- the sequence φ is *locally finite*, i.e., each bounded subset of $\mathbb{R}^D$ must contain only a finite number of points of φ,
- the sequence is *simple*, i.e., $x_i \neq x_j$, if $i \neq j$,

and $\mathscr{N}$ is the σ-algebra, defined as the smallest σ-algebra on $\mathbb{N}$ to make all mapping $\varphi \mapsto \varphi(B)$ measurable, for $\mathbf{B}$ running through the bounded Borel sets. Here, again, $\varphi(\mathbf{B})$ represents the number of points in $\mathbf{B}$ and, in order to avoid confusions, we consider that a PP Φ is, simply, a random choice of one of the processes $\varphi \in \mathbb{N}$.

We now introduce some other useful definitions, properties and results concerning point processes:

Definition 2.1.2 (Distribution)**.** *The distribution of a point process Φ, which we will represent as P, is determined by the probabilities:*

$$\begin{aligned} \mathsf{P}(Y) &= \mathbb{P}(\Phi \in Y) \\ &= \mathbb{P}(\{w \in \Omega : \Phi(w) \in Y\}), \end{aligned} \tag{2.1}$$

where $Y \in \mathscr{N}$. The term $\Phi \in Y$ means that Φ has some property, then, $\mathbb{P}(\Phi \in Y)$ denotes the probability that Φ has this property [43].

Definition 2.1.3 (Stationarity)**.** *A point process $\Phi = \{x_n\} \in \mathbb{R}^D$ is stationary if $\forall b \in \mathbb{R}^D$, $\Phi' = \{x_n + b\} \in \mathbb{R}^D$ has the same distribution of Φ.*

Definition 2.1.4 (Isotropy)**.** *A point process $\Phi = \{x_n\} \in \mathbb{R}^D$ is isotropic if for all rotated processes $\mathsf{R}(\Phi) = \{\mathsf{R}(x_n)\}$, $\mathsf{R}(\Phi)$ has the same distribution of Φ.*

Definition 2.1.5 (Motion-invariant)**.** *A point process $\Phi \in \mathbb{R}^D$ is motion-invariant if it is stationary and isotropic.*

Definition 2.1.6 (Intensity measure)**.** *The intensity measure, Λ, of a point process $\Phi \in \mathbb{R}^D$ is defined as:*

$$\begin{aligned} \Lambda(B) &= \mathbb{E}\left[\Phi(\mathbf{B})\right], \\ &= \int \varphi(\mathbf{B}) \mathsf{P}(\mathrm{d}\varphi), \end{aligned} \tag{2.2}$$

for all Borel set $\mathbf{B} \in \mathbb{R}^D$. Hence, the intensity measure is the mean number of points in B.

Proposition 2.1.1. *If a point process $\Phi \in \mathbb{R}^D$ is stationary, then the $\Lambda(\mathbf{B})$ is a translation-invariant measure such that:*

$$\Lambda(\mathbf{B}) = \lambda v_D(\mathbf{B}), \quad \forall \mathbf{B} \in \mathbb{R}^D, \tag{2.3}$$

where v_D is the Lebesgue measure (volume) in $\mathbb{R}^D$ and λ is called the density or intensity function of a point process [43, Section 1.9].

Remark 2.1.1. *In general and based on Proposition 2.1.1, Λ can be written as:*

$$\Lambda(\mathbf{B}) = \int_{\mathbf{B}} \lambda(x)\, \mathrm{d}x. \tag{2.4}$$

This is not true, for example, when the points are arranged on a lattice [43].

Definition 2.1.7 (Contact distribution function and void probability)**.** *For a convex compact $\mathbf{B} \in \mathbb{R}^D$, with the origin, $\mathscr{O} \in \mathbf{B}$, and $v_D(\mathbf{B}) > 0$. The* contact distribution function*, $H_{\mathbf{B}}(r)$, of*

a stationary point process, Φ, is defined as:

$$H_{\mathbf{B}}(r) = 1 - \mathbb{P}\left(\Phi(r\mathbf{B}) = 0\right) \tag{2.5}$$

for $r \leq 0$. Moreover, the term $\mathbb{P}\left(\Phi(r\mathbf{B}) = 0\right)$ is known as the void probability.

When, $r\mathbf{B} = \mathbf{B}(\mathscr{O}, r)$, i.e., the ball centered in $\mathscr{O}$ and radius r, then the contact distribution function is called the *first contact distribution function* and it can be interpreted as the distance from the origin to the closest point in Φ. In this regard, we can also define the *nearest-neighbor distance* for a point $x \in \Phi$ as:

$$\arg\min_{x' \in \Phi} \|x' - x\|. \tag{2.6}$$

As we will further see, these distance will allow us to characterize the interaction between points in PPs that model cellular networks.

2.1.1 Sums and products over point processes

All previous definitions allow us to understand how PPs can be mathematically characterized. Yet, as previously mentioned, our goal is to be able to use this mathematical tractability, in order to analyze different performance indicators of the different systems. Firstly, we have Campbell's Theorem, which states that:

Theorem 2.1.1 (Campbell)**.** *For any non-negative measurable function $f(x)$, it holds that:*

$$\begin{aligned} \mathbb{E}\left[\sum_{x \in \Phi} f(x)\right] &= \int_{\mathbb{N}} \sum_{x \in \varphi} f(x) \mathsf{P}(\mathrm{d}\varphi), \\ &= \int f(x) \Lambda(\mathrm{d}x). \end{aligned} \tag{2.7}$$

Thus, by considering (2.3) and Campbell's theorem, we can derive that for an stationary PP:

$$\mathbb{E}\left[\sum_{x \in \Phi} f(x)\right] = \lambda \int f(x) \mathrm{d}x. \tag{2.8}$$

Moreover, when the point process has an intensity function, then:

$$\mathbb{E}\left[\sum_{x\in\Phi} f(x)\right] = \int f(x)\lambda(x)\mathrm{d}x. \tag{2.9}$$

Let us notice that using the previous theorem allow us to perform sums over different points in a given PP. This is particularly useful, for example, in order to model the sum of interfering signals when transmitters are assumed to form a given PP.

Further, we have the *probability generating functional* (PGFL) of a PP, which is defined as:

Definition 2.1.8 (Probability generating functional of a point process)**.** *Let V be the family of all measurable functions $v : \mathbb{R}^D \mapsto [0,1]$, such that $1-v$ has bounded support. For $v \in V$, the PGFL of a point process Φ is given by:*

$$\begin{aligned} G(v) &= \mathbb{E}\left[\prod_{x\in\Phi} v(x)\right] \\ &= \int \prod_{x\in\varphi} v(x)\mathbb{P}(\mathrm{d}\varphi). \end{aligned} \tag{2.10}$$

Hence, the PGFL allow us to model the product of points in PPs. Arguably, (2.10) by itself does not allow us, at this point, to grasp the true potential and application of the PGFL towards our goal. Yet, we will see later (particularly when analyzing the Poisson point processes) how it can be directly used.

2.1.2 Transforming, mapping or displacing a point processes

As we will further see in Chapter 4, it is sometimes useful to transform a point process that lies in a given space, into another simpler space, e.g. transform a 2D point process into a one-dimensional one. We, thus, define the *random transformation of a point process* as:

Definition 2.1.9 (Random transformation of a PP)**.** *Let us consider a PP, $\Phi \in \mathbb{R}^D$, and $\mathbf{B}_p \in \mathbb{R}^{D_p}$ a bounded set. Let $p(x,\mathbf{B}_p)$ be a probability kernel from $\mathbb{R}^D$ to $\mathbb{R}^{D_p}$ for every point $x \in \Phi$. Hence $p(x,B_p)$ is a probability measure on $\mathbb{R}^{D_p}$, i.e., a real-valued function defined*

on a set of events in a probability space that satisfies measure properties. We then have that the transformed point process *of* Φ *is the point process* Φ_p*, that is defined by the probability kernell* $p(x,\mathbf{B}_p) = \mathbb{P}(x_p \in \mathbf{B}_p|\Phi)$*, where* $x_p \in \mathbb{R}^{D_p}$ *is a point of* Φ_p *[45].*

Hence, we see that Φ_p is obtained by randomly and independently displacing each point of $\Phi \in \mathbb{R}^D$ to another location on $\mathbb{R}^{D_p}$, according to the kernel $p(x,\mathbf{B}_p)$, i.e., the probability that the displaced version of x lies in $\mathbf{B}_p$.

2.1.3 Marking and thinning of point processes

Marking a point process refers to the fact of adding an specific characteristic, or mark, to every point in the process. In this regard, if $\Phi = \{x_n\}$, we can think of a marked PP as another sequence $\hat{\Phi} = \{x_n, m_n\}$, where m_n are the marks related to the different points x_n. The nature of the marks can vary depending on the model and we say that they belong to the space $\mathbb{M}$, where the Borel σ-algebra in $\mathbb{M}$ is denoted by $\mathscr{M}$.

We refer to *independent marks*, when the marks form mutually independent sequences on $\mathbb{R}^M$, that may only depend on the position of each point. In this regard, we characterize an independently marked PP as:

Corollary 2.1.1 (Characterization of an independent marked PP)**.** *A point process* $\hat{\Phi} = \{x_n, m_n\}$ *is said to be independently marked when a given mark* $m_i \in \{m_n\}$ *may only depend on its respective point* $x_i \in \{x_n\}$*, yet not on* x_j *nor* m_j*, for* $j \neq i$*. In this case, we write the distribution of marks as* M_x*.*

Furthermore, when the marks are independent and identically distributed (i.i.d) distributed random variables (RVs), then the marks distribution is independent of the location of the original PP and we simply write M. We refer to this case as the *i.i.d marked point process*.

On the other hand, *thinning* refers to the operation in which the points of a point process are deleted according to a given rule. Thus, if Φ is the original PP, then the thinned process Φ_t is such that:

$$\Phi_t \subset \Phi. \tag{2.11}$$

The simplest way of thinning a PP, is by applying the *p-thinning rule*, in which each point of Φ is independently retained with probability p (hence, deleted from the original PP with

probability $1-p$). Additionally, we could also consider the case in which the probability of retention is such that: $0 \leq p(x) \leq 1$ for a point $x \in \Phi$. Thus, a point is deleted (or not) according to its location. We denote the latter operation as $p(x)$-*thinning*. Once again, with this operation, the retention probability of a given point is independent of the action applied to other points.

More interestingly, is the case in which the thinning of a point depends as well on the thinning of others, we call this *dependent thinning*. This allows to generate repulsion of points or clusters of them and can be useful to model more precisely several scenarios. We might take as an example the actual deployment of the 4G network in Fig. 2.1 (c), where we see that unlike the random deployment shown in Fig. 2.1 (a), in reality BSs tend to be more distant from each other, since this reduces the possible co-channel interference. However, given their higher complexity, the mathematical tractability can also be reduced when applying this kind of thinning operation.

2.2 Palm theory

Palm theory refers to all operations in which we consider the fact that a PP has a point placed in a given location. Particularly, the *Palm distribution* is the conditional point process distribution given that a point exists at a specific location, note here as[1]:

$$\mathsf{P}_x(Y) \triangleq \mathbb{P}(\Phi \in Y | x \in \Phi), \quad \forall Y \in \mathscr{N}. \tag{2.12}$$

Palm theory formalized the notion of a *typical point* or typical element of a PP. In fact, this notion refers to the random selection of a point in the PP, where the choice of a given element is equiprobable for all the point in the process. Yet, in general when using Palm probabilities it is preferable not to consider the point to which the distribution is conditioned on. For example, when analyzing the signal-to-interference ratio at of a PP-based network, we consider a given point as a reference and the rest as interferers. Hence, we need to exclude this reference point from the interference sum to avoid considering a self-interference factor. This leads us to define the *reduced Palm distribution*, which is written as:

$$\mathsf{P}^{!}_x(Y) \triangleq \mathbb{P}(\Phi \backslash \{x\} \in Y | x \in \Phi). \tag{2.13}$$

[1]Given the randomness of the point processes, the above definition and its respective probability should not exist, since the conditional event has zero probability. For this reason, we encourage the reader to use the recommended references for a further and deeper discussion.

Notice that here, the point we condition on is not considered in the distribution. This notation is also used along this work for other mathematical operators, e.g. the expectation with respect to the Palm and reduced Palm measures are written as $\mathbb{E}_x[\cdot]$ and $\mathbb{E}_x^![\cdot]$, respectively.

In order to fully exploit the potential of the reduced Palm theory, in the next section we introduce the Slivnyak-Mecke Theorem which represents a powerful result that we use along this work.

2.3 Poisson point process

Arguably, the most important PP for this work is the Poisson point process (PPP). A point process Φ of intensity function $\lambda(x)$ is a (inhomogeneous) PPP if:

1. The number of points in any bounded set $\mathbf{B} \in \mathbb{R}^2$ has a Poisson distribution with mean:

$$\Lambda(\mathbf{B}) = \int_{\mathbf{B}} \lambda(x)\,\mathrm{d}x, \tag{2.14}$$

   i.e. that;

$$\mathbb{P}(\Phi(\mathbf{B}) = k) = \frac{(\Lambda(\mathbf{B}))^k}{k!} \exp(-\Lambda(\mathbf{B})). \tag{2.15}$$

2. The number of points in disjoints sets are independent, i.e., $\forall\{\mathbf{B}_1, \mathbf{B}_2\} \in \mathbb{R}^2$ with $\mathbf{B}_1 \cap \mathbf{B}_2 = \emptyset$, then $\Phi(\mathbf{B}_1)$ and $\Phi(\mathbf{B}_2)$ are independent.

Moreover, we say that a PPP is *homogeneous* when $\lambda(x) = \lambda$ in (2.14). Hence, we have that:

$$\Lambda(\mathbf{B}) = \lambda v_d(\mathbf{B}). \tag{2.16}$$

Implying that it is a motion-invariant point process.

Corollary 2.3.1 (Void probability, contact distribution and nearest neighbor distance in a PPP)**.** *For an homogeneous PPP, Φ, with intensity function λ, the void probability reads:*

$$\mathbb{P}(\Phi(r\mathbf{B}) = 0) = \exp(-\lambda v_d(r\mathbf{B})). \tag{2.17}$$

Hence, when $r\mathbf{B} = \mathbf{B}(\mathscr{O}, r)$, the contact distribution function is:

$$H_{\mathbf{B}}(r) = 1 - \exp\left(-\lambda \pi r^2\right). \tag{2.18}$$

Interestingly and as noted in [42], for the PPP, the contact distribution function and nearest-neighbor distribution function are identical.

Let us now define R as the RV that describes the distance between a typical point of PPP and its n-th neighbor. Then, for the homogeneous case and by using (2.15), we can derive that the probability density function (PDF) of R is [46, Section 3.2]:

$$f_R(r,n) = \frac{2(\pi\lambda)^n}{(n-1)!} r^{2n-1} \mathrm{e}^{-\lambda\pi r^2}. \tag{2.19}$$

Moreover, for the homogeneous PPP and as seen in [43, Section 3.1.7], the contact distribution function represents the cumulative distribution function (CDF) of the distance between the origin and the nearest neighbor. Hence, by taking the derivative of (2.18) to obtain the PDF of this distance we get:

$$f_R(r) \triangleq 2\pi\lambda r \mathrm{e}^{\left(-\pi\lambda r^2\right)} = f_R(r,1) \tag{2.20}$$

which is, in fact, equivalent to setting $n = 1$ in (2.19).

Corollary 2.3.2 (Probability generating functional of a PPP)**.** *If Φ is a PPP with intensity measure Λ, then its PGFL is:*

$$G(v) = \exp\left(-\int (1-v(x))\Lambda(\mathrm{d}x)\right) \quad \textit{for } v \in V. \tag{2.21}$$

Hence, if the PPP has a intensity function λ, we also have:

$$G(v) = \exp\left(-\int (1-v(x))\lambda(x)\,\mathrm{d}x\right). \tag{2.22}$$

Theorem 2.3.1 (Displacement theorem)**.** *Let us consider the random transformation of a PP introduced in Definition 2.1.9, where we consider that Φ is a PPP of intensity measure $\Lambda(\mathrm{d}x) = \lambda(x)\mathrm{d}x$ and $l_p(\cdot) : \mathbb{R}^D \to \mathbb{R}^{D_p}$ is the displacement function described by the probability kernel $p(x,\mathbf{B}_p)$. Then we have that the transformed PP, Φ_p, has an intensity*

measure:

$$\begin{aligned}\Lambda_p(B_p) &= \int_{\mathbb{R}^D} p(x,\mathbf{B}_p)\Lambda(\mathrm{d}x),\\ &= \int_{\mathbb{R}^D} \mathbb{P}\left(x_p \in \mathbf{B}_p|\Phi\right)\Lambda(\mathrm{d}x),\\ &= \int_{\mathbb{R}^D} \mathbb{P}\left(x_p = l_p(x) \in \mathbf{B}_p\right)\lambda(x)\mathrm{d}x,\\ &= \int_{\mathbb{R}^D} \mathbb{1}\{l_p(x) \in \mathbf{B}_p\}\lambda(x)\mathrm{d}x.\end{aligned} \tag{2.23}$$

Thus, we observe by comparing (2.23) *with* (2.14)*, that independent displacements preserve the Poisson characteristic of the PP.*

Theorem 2.3.2 (Marking of PPPs)**.** *Let Φ be a PPP with intensity measure $\Lambda(\mathrm{d}x) \in \mathbb{R}^D$ and marks with distribution $\mathsf{M}_x(\mathrm{d}m) \in \mathbb{R}^M$. The independently marked PP $\hat{\Phi}$ is a PPP on $\mathbb{R}^D \times \mathbb{R}^M$, such that its intensity measure is:*

$$\hat{\Lambda}(\mathrm{d}x,\mathrm{d}m) = \mathsf{M}_x(\mathrm{d}m)\Lambda(\mathrm{d}x). \tag{2.24}$$

Theorem 2.3.3 (Thinning of PPPs)**.** *When $p(x)$-thinning is applied to a PPP of intensity measure $\Lambda(\mathrm{d}x)$, we have that:*

$$\Lambda_t(\mathrm{d}x) = p(x)\Lambda(\mathrm{d}x). \tag{2.25}$$

Hence, we see that the $p(x)$-thinning of a PPP creates another PPP and also, that it is an application of the displacement theorem.

Theorem 2.3.4 (Slivnyak-Mecke)**.** *The reduced Palm distribution of a PPP is equal to its original distribution, i.e.:*

$$\mathsf{P}_x^!(Y) = \mathsf{P}(Y), \tag{2.26}$$

where $Y \in \mathscr{N}$.

Let us notice that Slivnyak-Mecke theorem, implies that for a PPP, we can add or remove a point while still maintaining the distribution of the other points. This derives from the fact,

that the contact distribution function of a PPP is actually the distribution of the distance from an arbitrary point to its nearest neighbor. Yet, more importantly, it allows us to directly use the reduced Palm measures to analyze PPPs, which as we have previously seen, have a high mathematical tractability.

2.4 Moment measures

In this section we introduce different *moment measures* of a point process. We will use these measures to derive the main characteristics of UEs point processes in Section 2.4.1. Indeed, in general, the position of active users depend on the distribution of their serving BSs. Hence, even when considering that the position of BSs in a cellular network is a PPP, the PP describing active users is not a PPP.

Firstly, we are looking for to characterize the interaction between BSs and active users, to accurately model the interference of users in FD uplinks and the distance from a served UE to its BS. And secondly, we are interested in modeling the interaction between active users, for the UE-to-UE interference that affects FD downlinks.

The *first-moment measure* (or 'mean') is simply the intensity measure of a PP, i.e., $\Lambda(\mathbf{B})$, for a Borel set $\mathbf{B}$. Further, the *second-order measure* is defined as:

$$\begin{aligned}\mu^{(2)}(\mathbf{B_1}\times\mathbf{B_2}) &\triangleq \mathbb{E}\left[\Phi(\mathbf{B_1})\Phi(\mathbf{B_2})\right]\\ &= \mathbb{E}\left[\sum_{x_1,x_2\in\Phi} \mathbb{1}\{x_1\in\mathbf{B_1}\}\mathbb{1}\{x_2\in\mathbf{B_2}\}\right],\end{aligned} \tag{2.27}$$

where $\mathbb{1}\{\cdot\}$ is the indicator function and, $\mathbf{B_1}$ and $\mathbf{B_2}$ are two Borel sets. The second-order measure enables to calculate the variance and covariance of a PP. The previous sum can be divided into two sums. First, the one over distinct points $\{x_1,x_2\}\in\Phi$, and secondly, over equal points $x_1=x_2\in\Phi$. Hence, for a homogeneous PPP of intensity function λ, we obtain that:

$$\mu^{(2)}(\mathbf{B_1}\times\mathbf{B_2}) = \lambda^2 v_d(\mathbf{B_1})v_d(\mathbf{B_2}) + \lambda v_d(\mathbf{B_1}\cap\mathbf{B_2}). \tag{2.28}$$

For the previous measure, we might only be interested in considering the sum over distinct points $\{x_1,x_2\}\in\Phi$, which can be written as:

$$\alpha^{(2)}(\mathbf{B_1}\times\mathbf{B_2}) = \mathbb{E}\left[\sum_{x_1,x_2\in\Phi}^{\neq} \mathbb{1}\{x_1\in\mathbf{B_1}\}\mathbb{1}\{x_2\in\mathbf{B_2}\}\right]. \tag{2.29}$$

Here, $\alpha^2(\mathbf{B_1}\times\mathbf{B_2})$ is defined as the *second-order factorial moment measure* of Φ. For the homogeneous PPP, this derives simply in subtracting the second term of (2.28), i.e.:

$$\alpha^{(2)}(\mathbf{B_1}\times\mathbf{B_2}) = \lambda^2 v_d(\mathbf{B_1})v_d(\mathbf{B_2}) = \Lambda(\mathbf{B_1})\Lambda(\mathbf{B_2}). \tag{2.30}$$

The density of $\alpha^{(2)}$ with respect to the Lebesgue measure, $\rho^{(2)}(x_1,x_2)$, is known as the *second-order product density*, and can be derived from:

$$\alpha^{(2)}(\mathbf{B_1}\times\mathbf{B_2}) = \int_{\mathbf{B_2}}\int_{\mathbf{B_1}} \rho^{(2)}(x_1,x_2)\mathrm{d}x_1\mathrm{d}x_2. \tag{2.31}$$

By considering (2.30) we obtain that for the homogeneous PPP we have that:

$$\rho^{(2)}(x_1,x_2) = \lambda^2. \tag{2.32}$$

Moreover, as a homogeneous PPP is a motion-invariant point process, then $\rho^{(2)}(x_1,x_2)$ only depends on the distance between x_1 and x_2, hence we write it as $\rho^{(2)}(r) = \rho^{(2)}(x_1,x_2)$, where $r = \|x_1 - x_2\|$.

For the stationary case, we can use the Palm distribution to express the second-order factorial moment measure:

$$\alpha^{(2)}(\mathbf{B_1}\times\mathbf{B_2}) = \lambda^2 \int_{\mathbf{B_1}} \mathscr{K}(\mathbf{B_2} - x)\mathrm{d}x, \tag{2.33}$$

where $\mathscr{K}(\cdot)$ is known as the *reduced second moment measure* and is defined as:

$$\lambda\mathscr{K}(\mathbf{B}) = \int \varphi(\mathbf{B})\mathsf{P}^{!}_{\mathscr{O}}(\mathrm{d}\varphi) \tag{2.34}$$

Hence, $\lambda\mathscr{K}(\mathbf{B})$ can be considered as the mean number of points in $\mathbf{B}\backslash\{\mathscr{O}\}$, conditioned on the fact that $\mathscr{O}\in\mathbf{B}$. By taking (2.31), the reduced second moment measure can be also written as:

$$\lambda^2\mathscr{K}(\mathbf{B}) = \int_{\mathbf{B}} \rho^{(2)}(x)\mathrm{d}x. \tag{2.35}$$

For a motion-invariant scenario, we can write:

$$\mathscr{K}(\mathbf{B}(\mathscr{O},r)) = K(r), \tag{2.36}$$

where $K(r)$ is the *reduced second moment function*, also known as *Ripley's K-function*. From this, we define:

$$g(r) \triangleq \frac{1}{2\pi r}\frac{\mathrm{d}K(r)}{\mathrm{d}r}, \tag{2.37}$$

as the *pair correlation function* (PCF). Thus, the PCF can be interpreted as a local average density at a given distance r from the origin. By taking (2.35), for the motion-invariant case we can derive the following result:

$$g(r) = \frac{\rho^{(2)}(r)}{\lambda^2}. \tag{2.38}$$

The previous measures allow us to characterize PPs but, at the same time, they enable us to approximate complex point processes with another simpler ones, as PPPs. This idea is developed in the following section and taken from [47].

2.4.1 Distribution of users attached to BSs

As we will further see in the following Chapters, when having a PPP, Φ, it is useful to consider the case in which there is another point process, Φ', whose nodes depend on the position of each original point in Φ. This is normally the case in modeling users point processes whose location depends on their serving BS. In general, the expressions describing the latter processes have higher complexity than the ones of PPPs and, consequently, lower tractability. Hence, in this part we present a way of calculating the PCF of these processes and, further, on how to approximate them with a PPP. The results introduced here are taken from the development found in [47] and we strongly encourage the reader to come back to this reference for further details and proofs.

Let us consider that Φ is a homogeneous PPP with intensity function λ. Further, Φ' is formed by uniformly and randomly placing a point x' inside the Voronoi cell of each original node $x \in \Phi$. The PCF of Φ' is given by:

$$g'(r) = 1 - \exp\left(-(9/4)\sqrt{\lambda}r\right) + 0.5\lambda r^2 \exp\left(-(5/4)\lambda r^2\right). \tag{2.39}$$

For this scenario, the distribution of the RV describing the distance between nearest points in Φ', D, is:

$$f_D(r) = 50r^3 \mathrm{e}^{-5r^2}. \tag{2.40}$$

Furthermore, the distribution of the RV describing the distance between a point in Φ' and its nearest neighbor in Φ, R_0, is:

$$f_{R_0}(r) = 2(1.3)\pi\lambda r \mathrm{e}^{-(1.3)\pi\lambda r^2}. \tag{2.41}$$

This can be interpreted as the distribution of the random variable that describes the distance between a user and the station that serves him.

Additionally, we use Palm theory to analyze the effect of interfering points in Φ' towards a typical point in Φ. For this case we consider $\Phi^{!}_{\mathscr{O}}$ instead of the original Φ, i.e., we condition on the fact that the origin is a point in Φ and we do not consider it for the corresponding mathematical development. For this scenario, the pair correlation function is given by:

$$g'^{(\Phi)}(r) = 1 - \exp\left(-(13/2)\lambda r^2\right) + (2/7)\lambda r^2 \exp\left(-(13/9)\lambda r^2\right). \tag{2.42}$$

For tractability reasons, the goal now is to approximate Φ' with a PPP. To do so, we consider that Φ' has a general intensity function λ and we would like to find a PPP, Φ_{PPP} such that for all $f : \mathbb{R}^2 \mapsto \mathbb{R}^+$:

$$\mathbb{E}^{!}_{\mathscr{O}}\left[\sum_{x\in\Phi'} f(x)\right] = \mathbb{E}\left[\sum_{x\in\Phi_{\text{PPP}}} f(x)\right]. \tag{2.43}$$

By using Campbell's theorem, we find that:

$$\lambda \int_{\mathbb{R}^2} f(x)g(\|x\|)\mathrm{d}x = \int_{\mathbb{R}^2} f(x)\lambda_{\text{PPP}}(\|x\|)\mathrm{d}x. \tag{2.44}$$

Which results in the fact that:

$$\lambda_{\text{PPP}}(r) = \lambda g(r). \tag{2.45}$$

Hence, we have that we can approximate Φ' as an inhomogeneous PPP with intensity function:

$$\lambda'(r) = \lambda g'(r), \qquad \text{for the PP } \Phi', \tag{2.46}$$

$$\lambda'^{(\Phi)}(r) = \lambda g'^{(\Phi)}(r), \quad \text{how a typical point in } \Phi \text{ observes interfering points in } \Phi'. \tag{2.47}$$

Fig. 2.2 shows the previously derived intensity functions. We see here that for $r \ll 1$, $\lambda'(r) < \lambda$ and $\lambda'^{\Phi}(r) < \lambda$. This result is obtained since for small distances it is less probable (when compared to an homogeneous PPP) for a typical UE to find another active user close to itself and, for a BS, to find an interfering UE close to itself. On the contrary, when the distance is big, i.e., $r \gg 1$, we have that $\lambda'(r) \to \lambda$ and $\lambda'^{\Phi}(r) \to \lambda$. Showing that under this scenario, the PP of active users acts as a homogeneous PPP, and a BS sees the distribution of interfering users located far away, as well as another homogeneous PPP.

Expressions in (2.41), (2.46) and (2.47) allow us to better characterize the interaction between equipment in the network. In particular, we make extensive use of them in Chapter 4. However, it is very important to mention that for simplicity and without loss of generality, throughout most parts of this work we usually assume, on the one hand, that the distance

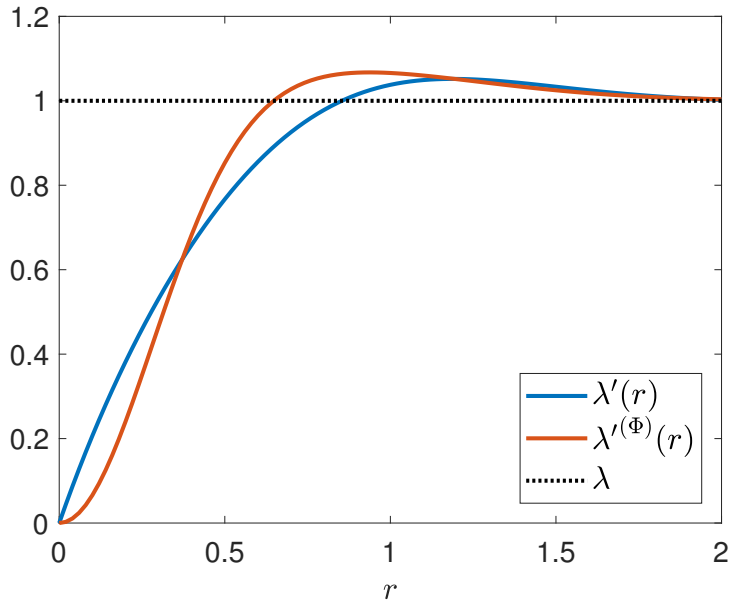

Fig. 2.2 Intensity functions of a homogeneous PPP, Φ, with $\lambda = 1$, of a PP, Φ', formed by uniformly and randomly placing a point in each Voronoi cell of Φ (λ'), and how Φ' is seen from a typical point in Φ ($\lambda'^{(\Phi)}$), according to the development found in [47].

between a user and its serving BS distributes according to the PDF of the contact probability, i.e., $f_R(1,r)$ in (2.20), and on the other hand, that scheduled UEs are distributed along the network as a homogeneous PPPs. These hypothesis are validated each time they are used.

2.5 Cellular networks: a stochastic geometry approach

Let us now analyze the problem introduced in Section 1.3, but by considering a stochastic geometry point of view. To do so, we consider that the positions of BSs, X, are described by a homogeneous PPP, Φ, with intensity function λ. On the other hand, the position of users, Y, is another PPP, Ψ, with intensity λ'. Users are served by their closest BSs. In this regard, the network can be seen as a Voronoi tessellation of the network area, in which the coverage region of each BS is represented by its Voronoi cell (see Fig. 2.1 (a)). We consider that $\lambda' \gg \lambda$, to ensure that there are at least two users per cell[2]. Moreover, we consider that BSs perform random scheduling and the position of scheduled UL and DL users in a RB τ is given by $\Psi_u^{(\tau)}$ and $\Psi_d^{(\tau)}$, respectively (see Y_u and Y_d in Section 1.3). It is highly important to notice that the PP that describes scheduled (UL or DL) users for a given RB, translates to uniformly and randomly drawing a point inside the Voronoi cell of each BS, i.e., served users

[2]This assumption is made in a different context in [48] and [49].

follow the same model as the one introduced in Section 2.4.1. In theory, theses processes are inter-dependent between each other, as they are both drawn from the same PPP, Ψ and depend on their serving BS. However, for the following development we consider that they are independent.

Moreover, we consider that a transmitted signal is affected by path-loss and Rayleigh channel. Then, we write the power received at a location j from a signal coming from i as:

$$P_{i,j}(\tau) = G(i,j)\, P_i\, h(i,j)\, \underbrace{[\kappa(i,j)d(i,j)]^{-\eta(i,j)}}_{L(i,j)^{-1}}, \tag{2.48}$$

where P_i is the power of the signal transmitted by i, $G(i,j)$ is the net antenna gain of the link (i.e., the product between transmitter and receiver antenna gains), h is the fading gain represented by a an exponential RV, such that, $h(i,j) \sim \exp(1)$, $\forall(i,j)$ (given the Rayleigh channels), $\kappa(i,j)$ is the link reference path-loss at 1 meter, $\eta(i,j)$ the path-loss exponent and $d(i,j)$ the distance between the i and j. In the previous expression, $L(i,j)$ is the deterministic distance dependent loss.

Let us notice that even when $P_{i,j}$ is written as a function of τ, i.e., the location of the RB in the spectrum, there is not an explicit dependency on τ in the right-hand side of the expression. Yet, this does not mean that the propagation is independent of the transmission frequency, as this is expressed in different the values of κ and η, according to the system operation frequency.

For this part, we consider that $P_x = P_d$, $\forall x \in \Phi$, $P_y = P_u$, $\forall y \in Y_u$. For the antenna gains we have that:

- $G(i,j) = G$, for all pair (i,j) of BS and served UE,
- $G(i,j) = G'$, for all pair (i,j) of BS and non-scheduled UE,
- $G(i,j) = \breve{G}$, for all pair (i,j) of BSs,
- $G(i,j) = \tilde{G}$, for all pair (i,j) of UEs,
- $G(i,i) = G_{\text{RSI}}$, between the transmitter and receiver of a full-duplex BS.

We consider different gains for the different intended- or interfering-links in the network, to model the ability of equipment to perform beamforming. For instance, if BSs can steer their signal towards their served UEs, then $G > G'$ should generally hold.

Furthermore, for the path-loss we consider that:

- $\kappa(i,j) = \kappa$ and $\eta(i,j) = \eta$, for all pair (i,j) and (j,i) of BS and scheduled UE,

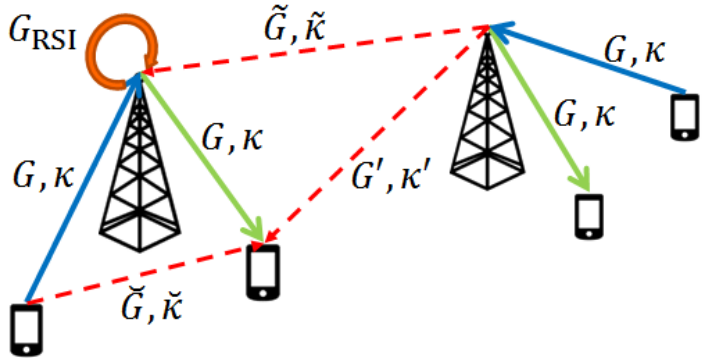

Fig. 2.3 Antenna gains and path-loss variables for BS-BS, UE-UE and BS-UE interactions, where red-dotted lines represent interfering links and the orange loop the self-interference.

- $\kappa(i,j) = \kappa'$ and $\eta(i,j) = \eta'$, for all pair (i,j) and (j,i) of BS and not scheduled UE,
- $\kappa(i,j) = \breve{\kappa}$ and $\eta(i,j) = \breve{\eta}$, for all pair (i,j) of BSs,
- $\kappa(i,j) = \tilde{\kappa}$ and $\eta(i,j) = \tilde{\eta}$, for all pair (i,j) of UEs.

These parameters allow us to model small-cell networks, in which the propagation is different within a cell and across different cells. A graphical representation of the parameters in the model is shown in Fig. 2.3.

Moreover, we assume that the residual self-IC is characterized as:

$$I_{\text{RSI}} = \beta \, G_{\text{RSI}} \, P_d, \tag{2.49}$$

where $\beta \in [0,1]$ is a constant related to the performance of the self-IC used at the BS receiver (see Section 1.2 for recent typical values in dB).

2.5.1 Coverage probability

The *coverage probability* of a link, is defined as the complementary CDF (CCDF) of the SINR, i.e.:

$$\mathbb{P}\left(\gamma_m^{(\text{mode})}(i,j,\tau) > \Gamma\right) \tag{2.50}$$

where $m \in \{u,d\}$, mode $\in \{\text{HD}, \text{FD}\}$ and Γ is a constant. By replacing (2.48) in the previous equation we obtain:

$$\mathbb{P}\left(h(i,j) > \frac{\Gamma\left[\kappa d(i,j)\right]^{\eta}}{G P_m}\left(I_m^{(\text{mode})}(j,\tau) + \sigma^2\right)\right) \tag{2.51a}$$

$$= \mathbb{E}\left[\exp\left(-\frac{\Gamma\left[\kappa d(i,j)\right]^{\eta}}{G P_m}\left(I_m^{(\text{mode})}(j,\tau) + \sigma^2\right)\right)\right] \tag{2.51b}$$

where $I_m^{(\text{mode})}(j)$ is the total interference at j and (2.51b) is due to the fact that all links are subject to a Rayleigh channel. Now, we have that $d(i,j)$ and $I_m^{(\text{mode})}(j,\tau)$ are also RVs. In particular $d(i,j)$, represents the distance between a BS and its scheduled user, i.e., it distributes as R_0 in (2.41). Hence, for any value of m and duplex-mode in (2.50), we can replace $d(i,j)$ by r. Furthermore, the expression $I_m^{(\text{mode})}(j,\tau)$ depends on the value of m and duplex-mode in (2.50), i.e., mode $= \{\text{HD},\ \text{FD}\}$, and we know analyze the behavior of each case.

Half-duplex network

Let us take into account the SINR expressions in Section 1.3.2. For the HD downlink, if we consider a typical user, i.e., $y = \mathscr{O}$, we have that:

$$I_d^{(\text{HD})}(0,\tau) = I_{\text{BS}}^{(d)}(0,\tau) \triangleq I_{\text{BS}}^{(d)}(\tau), \tag{2.52}$$

hence the coverage probability results in:

$$\begin{aligned}\mathbb{P}\left(\gamma_d^{(\text{HD})}(\tau) > \Gamma\right) &= \int_0^\infty f_{R_0}(r) \underbrace{\mathbb{E}_{I_{\text{BS}}^{(d)}}\left[\exp\left(-\frac{\Gamma\,[\kappa r]^\eta}{GP_d} I_{\text{BS}}^{(d)}(\tau)\right)\right]}_{\mathscr{L}\left\{I_{\text{BS}}^{(d)}(\tau)\right\}(r,\Gamma)} \underbrace{\exp\left(-\frac{\Gamma\,[\kappa r]^\eta}{GP_d}\sigma^2\right)}_{N_d(r,\Gamma)} \mathrm{d}r \\ &\triangleq \mathscr{P}_d^{(\text{HD})}(\tau,\Gamma),\end{aligned} \tag{2.53}$$

where $\mathscr{L}\{I_{\text{BS}}^{(d)}\}$ is the Laplace transform of $I_{\text{BS}}^{(d)}$ and comes from the definition of the Laplace transform of a RV, that states that for a general random variable Q, its Laplace transform can be expressed as $\mathscr{L}\{Q\}(s) = \mathbb{E}[\mathrm{e}^{-sQ}]$. We highlight the fact that the last expression refers to the DL coverage probability of a typical user, by omitting to specify the position of the transmitter and receiver (see (i,j) in (2.50)) and by defining it as $\mathscr{P}_d^{(\text{HD})}(\tau,\Gamma)$.

By considering (1.10) we have that:

$$I_{\text{BS}}^{(d)}(\tau) = \sum_{x'\in\Phi\setminus\{x\}} G' P_d\, h(x,y) \left[\kappa' d(x',y)\right]^{-\eta'}, \tag{2.54a}$$

$$= \sum_{x'\in\Phi} G' P_d\, h(x,y) \left[\kappa d(x',y)\right]^{-\eta'} \mathbb{1}\left\{\left[\kappa' d(x',y)\right]^\eta > \left[\kappa d(x,y)\right]^\eta\right\}, \tag{2.54b}$$

$$= \sum_{x'\in\Phi} G' P_d\, h \left[\kappa' r_{x'}\right]^{-\eta'} \mathbb{1}\left\{\left[\kappa r_{x'}\right]^\eta > \left[\kappa r\right]^\eta\right\}, \tag{2.54c}$$

where $d(x',y) = d(x',0) = r_{x'}$ and $h(x,y) = h$ in (2.54c) as all links suffer from Rayleigh fading. Thus, we have that the Laplace transform can be developed as:

$$\mathscr{L}\left\{I_{\mathrm{BS}}^{(d)}(\tau)\right\}(r,\Gamma) = \mathbb{E}_{I_{\mathrm{BS}}^{(d)}}\left[\exp\left(-\frac{\Gamma\left[\kappa r\right]^{\eta}}{GP_d} I_{\mathrm{BS}}^{(d)}(\tau)\right)\right], \tag{2.55a}$$

$$= \mathbb{E}\left[\exp\left(-\frac{\Gamma\left[\kappa r\right]^{\eta}}{GP_d}\sum_{x'\in\Phi} G' P_d\, h\left[\kappa' r_{x'}\right]^{-\eta'} \mathbb{1}\left\{\left[\kappa' r_{x'}\right]^{\eta'} > \left[\kappa r\right]^{\eta}\right\}\right)\right], \tag{2.55b}$$

$$= \mathbb{E}\left[\prod_{x'\in\Phi}\exp\left(-\Gamma\left[\kappa r\right]^{\eta}\frac{G'}{G} h\left[\kappa' r_{x'}\right]^{-\eta'} \mathbb{1}\left\{\left[\kappa' r_{x'}\right]^{\eta'} > \left[\kappa r\right]^{\eta}\right\}\right)\right], \tag{2.55c}$$

$$= \mathbb{E}_{\Phi}\left[\prod_{x'\in\Phi}\mathbb{E}_h\left[\exp\left(-\Gamma\frac{\left[\kappa r\right]^{\eta}}{\left[\kappa' r_{x'}\right]^{-\eta'}}\frac{G'}{G} h \mathbb{1}\left\{\left[\kappa' r_{x'}\right]^{\eta'} > \left[\kappa r\right]^{\eta}\right\}\right)\right]\right], \tag{2.55d}$$

$$= \mathbb{E}_{\Phi}\left[\prod_{x'\in\Phi}\left(1+\Gamma\left[\kappa r\right]^{\eta}\left(G'/G\right)\left[\kappa' r_{x'}\right]^{-\eta'} \mathbb{1}\left\{\left[\kappa' r_{x'}\right]^{\eta'} > \left[\kappa r\right]^{\eta}\right\}\right)^{-1}\right], \tag{2.55e}$$

$$= \exp\left(-2\pi\lambda\Gamma\frac{G'}{G}\frac{1}{\eta'}\left[\kappa r\right]^{\eta}\frac{1}{\kappa'^{2}}\int_{\left[\kappa r\right]^{\eta}}^{\infty}\frac{z^{2/\eta'-1}}{z+\Gamma(G'/G)\left[\kappa r\right]^{\eta}}\,\mathrm{d}z\right), \tag{2.55f}$$

where (2.55f) comes from the definition of the PGFL of a PPP (see (2.21)) and by using the change of variable $z = \left[\kappa' r_{x'}\right]^{\eta'}$. Consequently, we can write the following Lemma.

Lemma 2.5.1 (Half-duplex DL coverage probability)**.**

$$\mathscr{P}_d^{(HD)}(\tau,\Gamma) = \int_0^{\infty} f_{R_0}(r)\mathscr{L}\left\{I_{BS}^{(d)}(\tau)\right\}(r,\Gamma)N_d(r,\Gamma)\mathrm{d}r, \tag{2.56}$$

where

$$\mathscr{L}\left\{I_{BS}^{(d)}(\tau)\right\}(r,\Gamma) = \exp\left(-2\pi\lambda\Gamma\frac{G'}{G}\frac{1}{\eta'}\left[\kappa r\right]^{\eta}\frac{1}{\kappa'^{2}}\int_{\left[\kappa r\right]^{\eta}}^{\infty}\frac{z^{2/\eta'-1}}{z+\Gamma(G'/G)\left[\kappa r\right]^{\eta}}\,\mathrm{d}z\right). \tag{2.57}$$

This result is already found in other works, for instance in [48].

Further, for the HD uplink, if we consider a typical BS located in the origin, i.e., $x = \mathcal{O}$, we have that:

$$I_u^{(\mathrm{HD})}(0,\tau) = I_{\mathrm{UE}}^{(u)}(0,\tau) \triangleq I_{\mathrm{UE}}^{(u)}(\tau), \tag{2.58}$$

and we can proceed similarly as for the DL case, we obtain the following Lemma.

Lemma 2.5.2 (Half-duplex UL coverage probability)**.** *The UL coverage probability is:*

$$\mathscr{P}_u^{(HD)}(\tau,\Gamma) = \int_0^\infty f_{R_0}(r) \underbrace{\mathbb{E}_{I_{UE}^{(u)}}\left[\exp\left(-\frac{\Gamma\left[\kappa r\right]^\eta}{GP_u} I_{UE}^{(u)}(\tau)\right)\right]}_{\mathscr{L}\left\{I_{UE}^{(u)}(\tau)\right\}(r,\Gamma)} \underbrace{\exp\left(-\frac{\Gamma\left[\kappa r\right]^\eta}{GP_u}\sigma^2\right)}_{N_u(r,\Gamma)} \mathrm{d}r, \tag{2.59}$$

where

$$\mathscr{L}\left\{I_{UE}^{(u)}(\tau)\right\}(r,\Gamma) = \exp\left(-2\pi\Gamma\frac{G'}{G}\frac{1}{\eta'}\frac{\left[\kappa r\right]^\eta}{\kappa'^2}\int_{\left[\kappa r\right]^\eta}^\infty \lambda_u^{(BS)}\left(\frac{z^{1/\eta'}}{\kappa'}\right)\frac{z^{2/\eta'-1}}{z+\Gamma(G'/G)\left[\kappa r\right]^\eta}\mathrm{d}z\right). \tag{2.60}$$

As it is the case for the DL, the HD uplink coverage probability expression can also be found elsewhere, e.g. [50].

However, as opposed to the DL case, for a given RB $\tau \in B_u$, the process $Y_u(\tau)$ is not actually a homogeneous PPP, as the position of the scheduled UEs depends on the position of their serving BSs, thus $\lambda_u^{(\mathrm{BS})}(\cdot)$ replaces λ and represents the density of interfering UEs as seen from the typical BS. The previous intensity function can be seen as equivalent to $\lambda'^{(\Phi)}$ derived in Section 2.4.1.

Full-duplex network

For the FD case, there is additional interference in DL and UL as seen in Section 1.3.2, i.e.:

$$I_d^{(\mathrm{FD})}(0,\tau) = I_{\mathrm{BS}}^{(d)}(0,\tau) + I_{\mathrm{UE}}^{(d)}(0,\tau) \triangleq I_{\mathrm{BS}}^{(d)}(\tau) + I_{\mathrm{UE}}^{(d)}(\tau), \tag{2.61}$$

$$I_u^{(\mathrm{FD})}(0,\tau) = I_{\mathrm{BS}}^{(u)}(0,\tau) + I_{\mathrm{UE}}^{(u)}(0,\tau) + I_{\mathrm{RSI}} \triangleq I_{\mathrm{BS}}^{(u)}(\tau) + I_{\mathrm{UE}}^{(u)}(\tau) + I_{\mathrm{RSI}}. \tag{2.62}$$

Now, by following similar steps as for the HD network, we can derive for the FD downlink the following Lemma.

Lemma 2.5.3 (Full-duplex DL coverage probability)**.**

$$\mathscr{P}_d^{(FD)}(\tau,\Gamma)=\int_0^{\infty} f_{R_0}(r)\mathscr{L}\left\{I_{BS}^{(d)}(\tau)\right\}(r,\Gamma)\mathscr{L}\left\{I_{UE}^{(d)}(\tau)\right\}(r,\Gamma)N_d(r,\Gamma)\,\mathrm{d}r, \tag{2.63}$$

where,

$$\mathscr{L}\left\{I_{UE}^{(d)}(\tau)\right\}(r,\Gamma)=\exp\left(-2\pi\Gamma\frac{\tilde{G}}{G}\frac{\mu}{\tilde{\eta}}\left[\kappa r\right]^{\eta}\frac{1}{\tilde{\kappa}^2}\int_0^{\infty}\lambda_u\left(\frac{z^{1/\tilde{\eta}}}{\tilde{\kappa}}\right)\frac{z^{2/\tilde{\eta}-1}}{z+\Gamma(\tilde{G}/G)\mu\left[\kappa r\right]^{\eta}}\,\mathrm{d}z\right) \tag{2.64}$$

is the UE-to-UE interference factor term with $\mu=P_u/P_d$ and $\lambda_u(\cdot)$ represents the density of active UL users as seen from the typical DL user (equivalent to $\lambda'(r)$ in Section 2.4.1).

In (2.64), the integral is evaluated starting from 0, as the closest interfering UL user might be in the same cell as the one in which the typical DL user lies (there is no indicator function when developing the term as we consider all UL users).

Remark 2.5.1. *When $\tilde{G}=0$ or $\tilde{\eta}\to\infty$, i.e., there is a high obstruction between different UEs, we have that $\mathscr{L}\left\{I_{UE}^{(d)}(\tau)\right\}(r,\Gamma)=1$. Hence, there is no UE-to-UE interference and $\mathscr{P}_d^{(FD)}(\tau,\Gamma)=\mathscr{P}_d^{(HD)}(\tau,\Gamma)$.*

Proceeding similarly as for the DL, for the FD uplink we have the following:

Lemma 2.5.4 (Full-duplex UL coverage probability)**.**

$$\begin{aligned}\mathscr{P}_u^{(FD)}(\tau,\Gamma)=\int_0^{\infty} f_{R_0}(r)&\underbrace{\mathbb{E}_{I_{UE}^{(u)}}\left[\exp\left(-\frac{\Gamma\left[\kappa r\right]^{\eta}}{GP_u}I_{UE}^{(u)}(\tau)\right)\right]}_{\mathscr{L}\left\{I_{UE}^{(u)}(\tau)\right\}(r,\Gamma)}\underbrace{\mathbb{E}_{I_{BS}^{(u)}}\left[\exp\left(-\frac{\Gamma\left[\kappa r\right]^{\eta}}{GP_u}I_{BS}^{(u)}(\tau)\right)\right]}_{\mathscr{L}\left\{I_{BS}^{(u)}(\tau)\right\}(r,\Gamma)}\\&N_{\beta}(r,\Gamma)N_u(r,\Gamma)\,\mathrm{d}r,\end{aligned} \tag{2.65}$$

where

$$N_{\beta}(r,\Gamma)=\exp\left(-\frac{\Gamma\left[\kappa r\right]^{\eta}}{GP_u}I_{RSI}\right) \tag{2.66}$$

represents the RSI factor and

$$\mathscr{L}\left\{I_{BS}^{(u)}(\tau)\right\}(r,\Gamma)=\exp\left(-2\pi\lambda\Gamma\frac{\breve{G}}{G}\frac{1}{\mu\breve{\eta}}\left[\kappa r\right]^{\eta}\frac{1}{\breve{\kappa}^{2}}\int_{0}^{\infty}\frac{z^{2/\breve{\eta}-1}}{z+\Gamma(\breve{G}/G)(1/\mu)\left[\kappa r\right]^{\eta}}\mathrm{d}z\right) \tag{2.67}$$

is the BS-to-BS interference factor term.

Particularly, let us notice that in the BS-to-BS interference factor term, the density is just λ as BSs positions are described by a homogeneous PPP. Thus, the integral is evaluated starting from 0, as the closest BS might be arbitrarily close to the typical point under study.

Remark 2.5.2. *When $\breve{G}=0$ or $\breve{\eta}\to\infty$, i.e., there is a high obstruction between different BSs, we have that $\mathscr{L}\left\{I_{BS}^{(u)}(\tau)\right\}(r,\Gamma)=1$. Consequently, there is no BS-to-BS interference. Moreover, we observe that under this condition:*

$$\mathscr{P}_{u}^{(HD)}(\tau,\Gamma)=\frac{\mathscr{P}_{u}^{(FD)}(\tau,\Gamma)}{N_{\beta}(r,\Gamma)}, \tag{2.68a}$$

$$=\frac{\mathscr{P}_{u}^{(FD)}(\tau,\Gamma)}{\exp\left(-\dfrac{\Gamma\left[\kappa r\right]^{\eta}}{GP_{u}}\beta G_{RSI}P_{d}\right)} \tag{2.68b}$$

Thus, in a perfect self-IC scenario, i.e., $\beta=0$, then $\mathscr{P}_{d}^{(FD)}(\tau,\Gamma)=\mathscr{P}_{d}^{(HD)}(\tau,\Gamma)$.

Numerical application

Let us consider a cellular network described by small-cells deployment. This kind of deployments are characterized by having lower BS transmission powers (when compared to their macro-cell counterparts), hence smaller cell ranges are observed. SCs are particularly useful when having high throughput demands in dense networks, because there a fewer users per cell, smaller distances imply higher useful signal power and the deployment below roof tops reduces the interference.

By using the parameters found in Table 2.1, we simulate a HD and three-node FD network under the framework presented in the beginning of Section 2.5. From this, we plot the DL and UL coverage probabilities in Figs. 2.4 and 2.5, respectively. In addition, we also plot the

curves obtained by using the theoretical development found above, where for simplicity we assume that:

$$\lambda_u(r) = \lambda_u^{(\mathrm{BS})}(r) = \lambda, \tag{2.69}$$

$$f_{R_0}(r) = f_R(r) = 2\pi\lambda r \exp(-\pi\lambda r^2). \tag{2.70}$$

We can notice that with (2.69) we consider that active users distribute as an homogeneous PPP (seen from a typical UE or from a typical BS). The same applies for (2.70), in which the distance between a user and its serving BS is equivalent to the nearest neighbor distance, $f_R(r)$, of a homogeneous PPP of intensity λ (see (2.20)).

For the DL case in Fig. 2.4, we remark that theoretical and simulation-based results match well, validating our analytical development and previous assumption concerning λ_u, $\lambda_u^{(\mathrm{BS})}$ and f_{R_0}. Further, we can notice that HD outperforms FD in terms of coverage probability, as the interference is greater in the latter. Yet the different is of only 1.4 dB between the two, which still enables the FD downlink case to rest inside acceptable SINR values.

For the UL case in Fig. 2.5, we also plot the behavior for different levels of RSI (i.e. various values of β). Firstly, we observe again that theory and simulation-based results match well. However, for $\beta = 0$, there is a bigger gap between the curves. This is due to the fact that for $\beta = 0$, only UE-to-BS and BS-to-BS interference (i.e., the network geometry) affects the FD UL performance. Hence, the difference is given by assuming (2.69). Indeed,

Table 2.1 Simulation parameters

	Parameter	Value	Parameter	Value
	B	20 MHz	ω	180 KHz
	Noise figure	8 dB	Noise density	-174 dBm/Hz
	P_u	23 dBm	G_u	0 dBi
	(κ', η')	(κ, η)	G'	G
	β	various	UE height	1.5 m
small-cell	P_d	30 dBm	G_{RSI}	$G_{\max}G_{\min}$
	$G_{\max}$	6 dBi	$G_{\min}$	6 dBi
	(κ, η)	(3.53, 7.67)	$(\breve{\kappa}, \breve{\eta})$	(3.53, 7.67)
	$(\tilde{\kappa}, \tilde{\eta})$	(3.53, 7.67)	Inter site	200 m
	BS height	10 m	distance	
macro-cell	P_d	46 dBm	G_{RSI}	$G_{\min}G_{\min}$
	$G_{\max}$	15 dBi	$G_{\min}$	-5 dBi
	(κ, η)	(3.91, 3.62)	$(\breve{\kappa}, \breve{\eta})$	(2.20, 44.66)
	$(\tilde{\kappa}, \tilde{\eta})$	(2.20, 44.66)	Inter site	500 m
	BS height	25 m	distance	

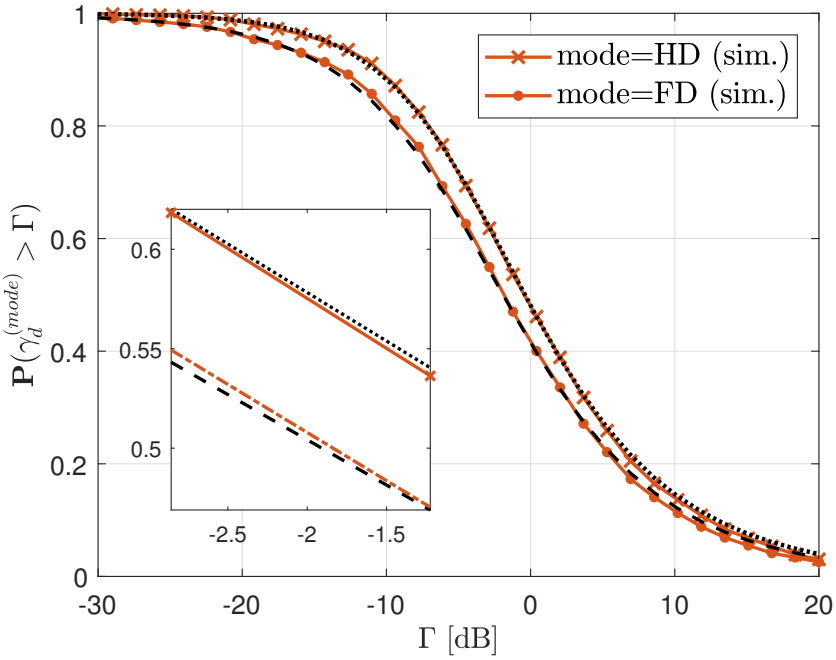

Fig. 2.4 Downlink coverage probability for HD and three-node FD small-cell networks, where "sim." stands for simulation-based results. The black dotted line is obtained by the HD theoretical result in (2.53) and the black dashed line by the FD theoretical result in (2.63).

simulation-based results show higher SINRs than the analytical ones, as λ is mostly greater than $\lambda_u^{(\mathrm{BS})}(r)$ (as seen in Fig. 2.2). Hence, when assuming that $\lambda_u^{(\mathrm{BS})}(r) = \lambda$, we consider in average more interference than the actual one.

Moreover, we can remark the critical impact of the RSI towards the UL performance, as the UL coverage probability decreases with β, i.e., the greater the RSI, the lower the UL coverage probability. Yet, we see that even under a perfect self-IC scenario ($\beta = 0$), there exists a 14 dB gap between the HD and FD models, which is considerably greater than for the DL (of only 1.4 dB), directly limiting the implementation of FD for UL purposes. Moreover, in practical applications, it is not reasonable to consider perfect self-IC, which impairs the UL performance of FD to a greater extent. This shows why FD implementation is not envisioned for high UL coverage requirements.

Let us highlight, that in this particular numerical application, we consider the same channel characteristic for all links (i.e., $\kappa = \breve{\kappa} = \tilde{\kappa}$ and $\eta = \breve{\eta} = \tilde{\eta}$) and omnidirectional antennas for BSs and UEs. Hence, downlinks better tolerate the increased interference due to FD, mainly due to the higher transmission power of BSs (with respect to UL powers).

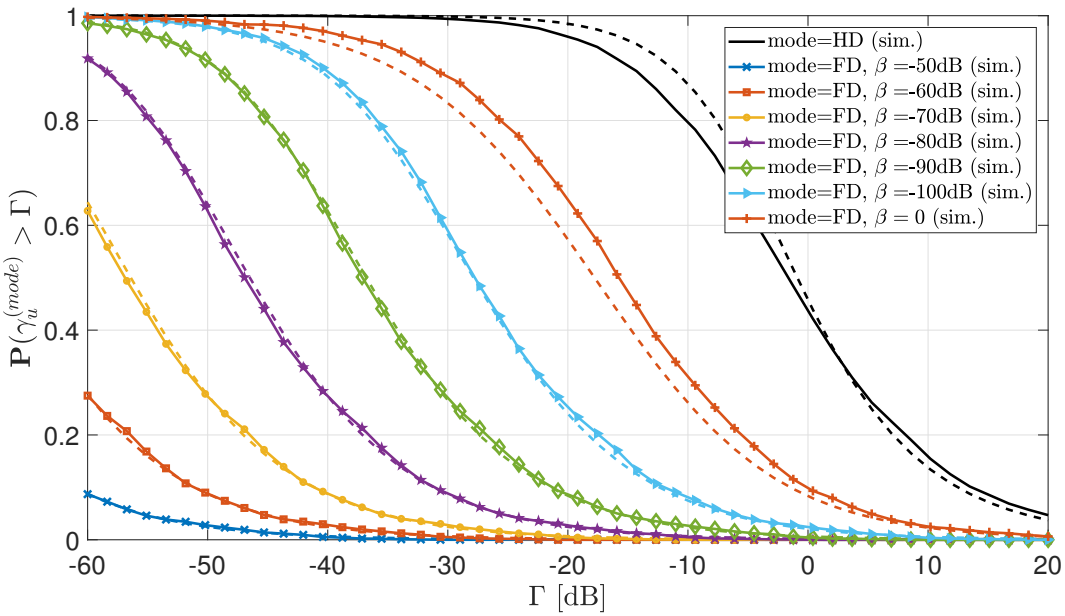

Fig. 2.5 Uplink coverage probability for HD and three-node FD SC-based networks, where "sim." stands for simulation-based results. The dashed lines are obtained by implementing the respective analytical results. Hence, for the HD case we use (2.59) and for the FD cases (2.65).

2.5.2 Capacity and spectral efficiency

Capacity

We define the *instantaneous capacity* (in bits-per-seconds) achieved by a link at a RB τ as:

$$\mathscr{C}_m^{(\text{mode})}(\tau) \triangleq \omega \log_2\left(1+\gamma_m^{(\text{mode})}(\tau)\right), \tag{2.71}$$

where $m \in \{d,u\}$, mode $\in \{\text{HD},\ \text{FD}\}$ and ω is the RB bandwidth.

The previous equation comes from the Shannon capacity and, from it, we define the *ergodic capacity* of the previous link as:

$$\overline{\mathscr{C}}_m^{(\text{mode})}(\tau) \triangleq \mathbb{E}_{\gamma_m^{(\text{mode})}}\left[\mathscr{C}_m^{(\text{mode})}(\tau)\right], \tag{2.72}$$

where the expected value is taken other the SINR distributions.

Lemma 2.5.5 (Capacity as a function of the coverage probability)**.** *As the RV describing the SINR of all different cases is always positive, i.e., $\gamma_m^{(mode)}(\tau) \geq 0$, $\forall \tau \in B$. Thus, we can write*

(2.72) *as:*

$$\overline{\mathscr{C}}_m^{(mode)}(\tau) = \mathbb{E}_{\gamma_m^{(mode)}}\left[\log_2\left(1+\gamma_m^{(mode)}(\tau)\right)\right], \tag{2.73a}$$

$$= \int_0^\infty \mathbb{P}\left(\log_2\left(1+\gamma_m^{(mode)}(\tau)\right) > \Gamma\right) \mathrm{d}\Gamma \tag{2.73b}$$

$$= \int_0^\infty \frac{\mathbb{P}\left(\gamma_m^{(mode)}(\tau) > \Gamma\right)}{\ln(2)(1+\Gamma)} \mathrm{d}\Gamma, \tag{2.73c}$$

$$= \int_0^\infty \frac{\mathscr{P}_m^{(mode)}(\tau,\Gamma)}{\ln(2)(1+\Gamma)} \mathrm{d}\Gamma. \tag{2.73d}$$

Notice that Lemma 2.5.5 allows us to express the ergodic capacity in terms of the coverage probability, which we already derive in Section 2.5.1.

From what we have already seen, the interference in FD cellular networks is higher. Thus, both instantaneous and ergodic capacities (at specific RBs) are always upper-bounded by the performance of their HD counterpart. This motivates as to introduce the *throughput* of the link m, which is given by:

$$\mathscr{T}_m^{(\mathrm{mode})} \triangleq \sum_{\tau \in B_m} \overline{\mathscr{C}}_m^{(\mathrm{mode})}(\tau), \tag{2.74}$$

where we recall that B is the total available bandwidth of the system (see Fig. 1.9). In this regard, we observe that, even though locally (in a RB) FD performance is surpassed by HD, what an operator is interested in is global performance, i.e., the net (or total) capacity given by the throughput. In fact, let us analyze the problem according to the spectrum utilization of the different duplex modes, introduced in Section1.3.1.

Firstly, for the case in which the FD system uses the total available bandwidth to perform DL and UL, and as seen in the numerical application of Section 2.5.1, the FD DL performance is close to its HD counterpart. Hence, even without implementing an interference reduction procedure, we have a high probability that the throughput of FD outperforms the one of HD. On the other side, for the UL, the SINR degradation is considerably greater, as $\gamma_u^{(\mathrm{FD})} \ll \gamma_u^{(\mathrm{HD})}$. Then, even when ULs have access to double the bandwidth (with respect to HD), without efficient interference management, it is highly likely that there is also going to be a critical degradation in the UL throughput.

Furthermore, for the option in which some spectrum is freed by adopting FD, the throughput performance of links strictly depends on the strategy adopted to allocate the RBs. On this subject, let us consider 'FD (case 2)' in Fig. 1.9, in which the FD system uses half of

the total available bandwidth of the HD system. In this case, the only way of achieving the same throughput as in HD, is by totally cancelling the additional interference. Hence, for the DLs, the UE-to-UE interference and, for the ULs, the BS-to-BS and RSI. But, if we consider again the fact that the SINR of FD DLs are only slightly surpassed by their HD analogue, then it is arguably simpler to maintain a reasonable close throughput performance level, even when the system bandwidth is halved. For the UL the panorama is completely different, as we have seen that the SINR is critically degraded. Hence, reducing available bandwidth for ULs is not recommended, when no interference management is introduced.

Spectral efficiency

The *average spectral efficiency* (ASE), is defined as the ratio between the average capacity and bandwidth. When focusing on a given RB τ, the ASE is simply a normalized version of the instantaneous capacity: $\mathbb{E}_{\gamma_m^{(\text{mode})}}[\mathscr{C}_m^{(\text{mode})}(\tau)]/\omega$. System wise though, the importance does not lies in an specific RB and we write the ASE as:

$$\mathscr{A}_m^{(\text{mode})} \triangleq \frac{\mathscr{T}_m^{(\text{mode})}}{B_T^{(\text{mode})}}, \tag{2.75}$$

where $B_T^{(\text{mode})}$ is the total system bandwidth for the corresponding mode and is found in (1.6). Moreover, we define the *cell average spectral efficiency* as:

$$\mathscr{A}_c^{(\text{mode})} \triangleq \mathscr{A}_u^{(\text{mode})} + \mathscr{A}_d^{(\text{mode})}. \tag{2.76}$$

If we assume that all the RBs are statistically equivalent, then, we have that $\overline{\mathscr{C}}_m^{(\text{mode})}(\tau) = \overline{\mathscr{C}}_m^{(\text{mode})}(\tau') = \overline{\mathscr{C}}_m^{(\text{mode})}$, $\forall(\tau,\tau') \in B_T^{(\text{mode})}$. Hence, (2.75) reduces to:

$$\mathscr{A}_m^{(\text{mode})} = \alpha_m^{(\text{mode})} \overline{\mathscr{C}}_m^{(\text{mode})}, \tag{2.77}$$

where $\alpha_m^{(\text{mode})}$ is the resource utilization ratio in (1.2).

Finally, we define the *FD-to-HD average spectral efficiency ratio*, ϑ, as:

$$\vartheta_m \triangleq \frac{\mathscr{A}_m^{(\text{mode})}}{\mathscr{A}_m^{(\text{HD})}}. \tag{2.78}$$

Table 2.2 Simulation- and analytical-based results for normalized link capacities (i.e., quantities in bps/Hz) and ASEs, when considering HD and three-node FD small-cell networks according to parameters in Table 2.1. The total bandwidth of FD and HD systems are equal and for the FD system, we consider that $\beta = -100$ dB. In the Table, "cell" represents the net cell performance, i.e., UL + DL, "simu." for simulation-based results and "theo." for the theoretical ones.

	Link (m)	Half-duplex		Full-duplex		
		$\mathscr{T}_m^{(\mathrm{HD})}$	$\mathscr{A}_m^{(\mathrm{HD})}$	$\mathscr{T}_m^{(\mathrm{FD})}$	$\mathscr{A}_m^{(\mathrm{FD})}$	ϑ_m
simu.	DL	1.65	0.83	2.88	1.44	1.73
	UL	1.67	0.83	0.17	0.09	0.11
	cell	3.32	1.66	3.05	1.53	0.92
theo.	DL	1.71	0.85	2.99	1.49	1.75
	UL	1.64	0.82	0.18	0.09	0.11
	cell	3.35	1.67	3.17	1.58	0.95

Numerical application

Let us consider the same setting as the one in the numerical application of Section 2.5.1, where the parameter values are found in Table 2.1. Nevertheless, now we are interested in analyzing the capacity and ASE performance of HD and FD small-cell deployments.

Table 2.2 shows the simulation- and theoretically-based results for both HD and FD networks, when for the latter $\beta = -100$ dB. Moreover, for both systems we consider the same total bandwidth, thus we have the scenarios 'FDD HD' and 'FD (case 1)' depicted in Fig. 1.9. Firstly, we observe that simulations and analytical equations results match well. When focusing in the DL, we see that FD achieves approximately a 75% increase with respect to HD, in terms of throughput and ASE.

Regarding the UL, we observe that FD implementation critically degrades the performance of the system. In fact, even when doubling the available bandwidth of ULs, the throughput and ASE achieved only represent a 10% of the HD performance. Hence, even though we have a high enhancement of the DLs, the FD cell performance is lower than the one of HD, given the extremely high UL degradation. However, as we will see in the following Chapter (see Section 3.4), different path-loss and antenna gain parameters might actually enable FD to outperform its HD counterpart for the cell performance as well.

Further, we plot in Fig. 2.6 the characteristics of ϑ_u as a function of the RSI level (i.e., β values). We observe that the performance is degraded for higher values of β, i.e., for higher RSI levels. Interestingly, we observe that even for a $\beta = -120$ dB, the FD ASE still only represents roughly 40% of the one achieved by HD.

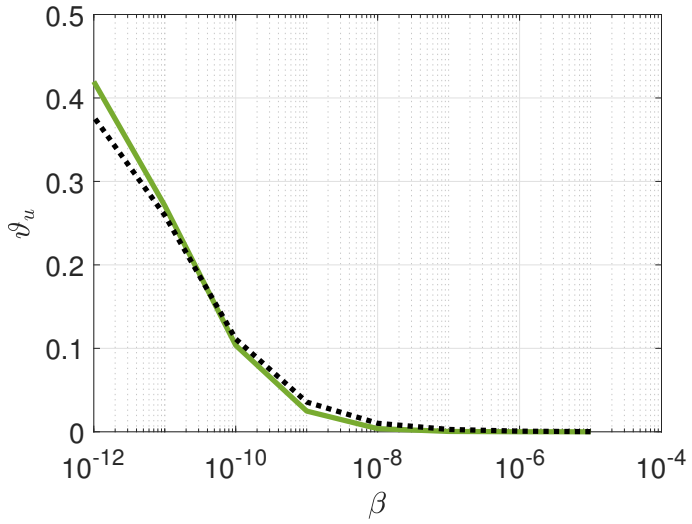

Fig. 2.6 Uplink FD-to-HD ASE ratio, where the continuous line is for simulation-based results and the black dotted line given by (2.78).

2.5.3 Transmission power and cell coverage range

Until now we have only analyzed the small-cell scenario. Yet macro-cell (MC) deployments are also fundamental for mobile network operators as they represent a cost-effective solution to cover the demand of larger areas of users by using less equipment. To do so, macro BSs transmit at a higher power. In this regard, HD networks performance should not be impaired by the previous consideration, as the higher interference power is proportional to the higher received signal for the intended links. On the other hand, for the UL case, UEs might be farther away from their serving BSs, but the interfering active UL users are as well. Hence, we should again observe a similar behavior as the one in SC deployments.

Yet, having higher DL powers is in fact a direct impairment for FD networks, as completely cancelling the RSI is unfeasible in practice and also, because higher DL powers, directly increases the interference in the network (higher BS-to-BS and BS-to-UE interference). In the next numerical application we compare the performance of SC and MC deployments when having HD and FD base stations.

Numerical application

Let us consider the same model as the one in Section 2.5.1 and the MC parameters found in Table 2.1, where $\beta = -100$ dB is considered for the FD cases. In contrast to the SC case, in the MC deployment we consider that BS antennas are not omnidirectional. In fact, we consider the model shown in Fig. 2.7, where each BS has a maximum and a

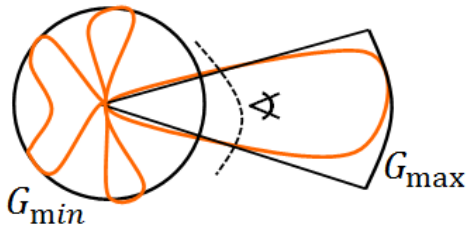

Fig. 2.7 Antenna gain pattern model used for MC deployments consisting of a main lobe of gain $G_{\max}$, that is considered for the intended links, and a secondary lobe of gain $G_{\min}$ that affects interfering links. The orange line represents a more realistic antenna model and the bold-black line the approximation considered.

minimum gain. The first corresponds to the gain towards intended links, i.e., between the BS and its served UE, and the latter for the interfering links, i.e., BS-to-BS and BS-to-UE interference. This model is considered, as operators usually deploy sectorized antenna models that enable to reduce the interaction between non-intended links. Moreover, we consider that for MC, the net self-interference antenna gain is given by, $G_{\text{RSI}} = G_{\min}G_{\min}$, instead of the $G_{\text{RSI}} = G_{\min}G_{\max}$ used in SC. This is done as it is easier to isolate the transmitter- and receiving-end of MC base stations and, also, because as there is less space, cost and energy constraints in MCs.

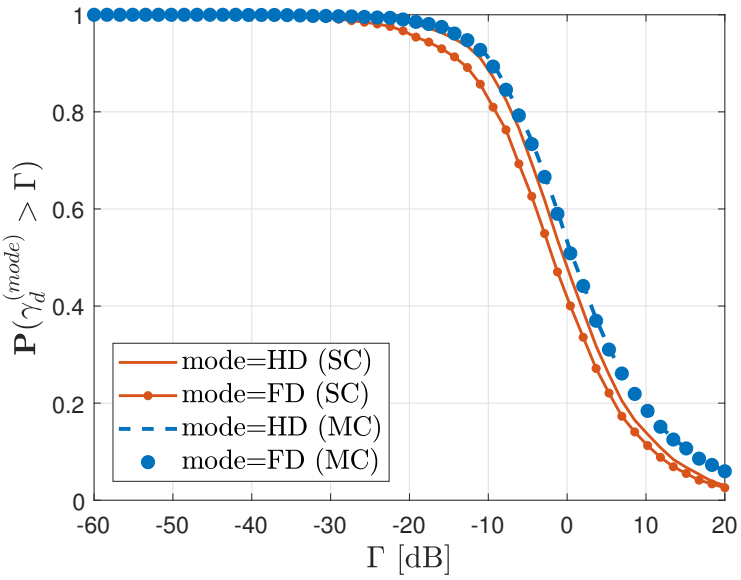

Fig. 2.8 Simulation-based results for the DL coverage probability in small-cells and macro-cells HD and three-node FD networks.

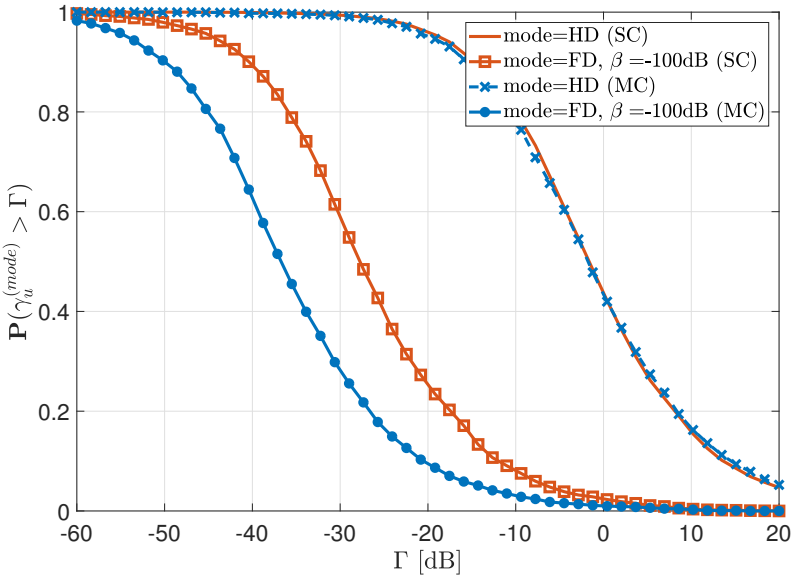

Fig. 2.9 Simulation-based results for the UL coverage probability in small-cells and macro-cells HD and three-node FD networks.

Fig. 2.8 shows the DL coverage probability for both types of deployments. As previously discussed, we see that SC and MC performances are similar for the HD case. In fact, the macro-cell deployment outperforms its SC counterpart, as the mean received power in this particular scenario is higher. The same behavior is observed for FD, yet let us notice that in MC, FD is only slightly outperformed by the HD. This demonstrates that under this regime, i.e., $P_d \gg P_u$, the order of magnitude of the interference generated by UL users is not comparable with the one of the received signal from the serving BS.

Further, Fig. 2.9 shows the UL coverage probability for both cases. Here we observe again that when considering a HD network, SC and MC perform similarly. Yet, it is possible to notice that even when considering a favourable antenna model for BSs and a more robust self-IC characterization ($G_{\text{RSI}} = G_{\text{min}}G_{\text{min}}$), the UL is even more degraded in FD when implementing MC base stations. This demonstrates that considering a more favourable self-IC or antenna model to reduce the BS-to-BS interference, are not enough to address the higher DL power levels experienced in MC deployments.

2.6 Summary and final remarks

The stochastic geometry tools introduced in this Chapter allow us, firstly, to model in a more realistic way the distribution of equipment in cellular networks. Secondly, to characterize and quantify key performance indicators to further study the impact of implementing FD.

In this regard, we see that even when FD increases the interference with respect to HD, the DL throughput performance is still enhanced, since, the lower SINR levels experienced by UEs is compensated by the additional radio resources that are available due to FD. However, the picture is completely different for ULs. In the first place, we observe how critical the effectiveness of the self-interference cancellation system is towards the UL performance. Indeed, we clearly remark that no self-IC, means that the simple idea of thinking about FD is not practical. Nevertheless, we notice that even with perfect self-IC, the UL SINR reduction due to FD is not proportional (at all) to the one experienced by DLs. In fact, this show us two main things. First, that the higher transmission power of BSs (compared to UEs) enables the DL to combat more effectively the increase in interference. And secondly, that the BS-to-BS interference is another limiting factor when it comes to thinking of equally performing DL and UL FD systems. Therefore, if we already see that with small-cells the panorama of ULs is challenging, it is hard to imagine that the implementation of FD in macro-cells can be effectively carried out. As with this last type of deployments, there is generally a more favourable propagation between BSs and, on top of that, higher levels of self-interference must be cancelled.

In the following Chapter, we present a duplex-switching policy that seeks to enhance the UL degradation by enabling BSs to chose the FD-mode only when the conditions are favourable, while still trying to profit from the beneficial performance gains of FD in the DLs.

Chapter 3

Full and half duplex-switching policy for cellular networks

By using the same RB for uplink and downlink, FD promises to double the spectral efficiency or throughput of NGWNs. However, as previously studied, under a cellular context, FD transmissions are degraded by co-channel interference coming from either base stations or user terminals employing the same radio resource. As a consequence, FD implementation does not allow to double the performance of networks, when compared to their traditional HD counterpart. Nevertheless, we observe that under traditional network parameters, even when not doubled, FD enhances the performance of DLs. Yet, on the other hand, ULs are critically degraded, not even allowing a slight performance enhancement with respect to HD.

In this chapter, we propose a duplex-switching policy that can be implemented by operators in their BSs, in which these latter can adopt FD- or HD-mode as a function of the position of their scheduled users. The goal is to reduce the UL degradation present in FD, while still benefiting from the DL performance improvement.

3.1 Related works

A set of papers in the literature try to tackle the FD uplink degradation problem by proposing solutions that combine half-duplex and full-duplex transmissions depending on radio conditions and the locations of the interferers [13, 14, 51]. In [13], users in an heterogeneous network decide the duplex-mode based on the received power from their serving BSs. The SINR and SE are analyzed for both DL and UL by using inhomogeneous PPP tools. Results show that the network sum data rate can be improved with respect to both FD- and HD-systems by adopting a scheme in which BSs can operate in any of the two duplex-modes. In

[14], authors consider a multi-tier cellular network, in which access points are either FD or HD capable. There is however no policy explaining how the duplex-mode should be chosen and only the DL performance is studied. Reference [51] proposes a joint UL and DL power control scheme and the notion of FD reuse factor to mitigate interference. However, only the UL is studied and the model neglects the interference created by users.

On the other hand, in [17, 18, 52], authors propose and study the effect of implementing an adjustable partial overlap between UL and DL channels, by using adapted pulse-shaping and matched filtering. Only a specific value of the overlap factor allows an UL improvement. However, the performance is very sensitive to this optimal value and a slight deviation leads to significant performance losses on the UL. Even if this principle is, nevertheless, different from the previously mentioned hybrid models, the results turn to be similar, as in all cases the idea is to balance the trade-off between favorable DL gains and severely degraded ULs.

3.2 System model

Let us take into account the model presented in Section 2.5, where the location of BSs in the cellular network is modeled by a homogeneous Poisson Point Process, Φ, of spatial density λ on $\mathbb{R}^2$. UEs are attached to their closest BS. Once more, the density of UEs is large with respect to λ to ensure that there are at least two users per cell.

Further, and as also done in Section 2.5, we assume that all users and BSs transmit at their maximum power capabilities, i.e., P_u and P_d, respectively. Small-scale Rayleigh fading with unit power between all the elements of the network is again considered. However, for the purpose of this Chapter we consider that:

- All links reference path-losses at 1 meter (i.e., $\kappa(i,j)$ in (2.48)) are fixed to 1, and that
- Path-loss exponents are the same for all possible interactions between equipment in the network, i.e., $\eta(i,j)$ in (2.48) is such that $\eta(i,j) = \eta > 2, \forall(i,j)$.

The cellular network is composed of HD users (i.e., they can only receive or send information in each RB). Nevertheless, and differently from what we presented in the previous Chapter, BSs can opt whether to work under HD- or FD-mode. Therefore, when BSs adopt FD, we have the three-node FD model previously introduced (check Section 1.3 for more details) and in each time instant it can simultaneously serve one DL and one UL transmission in the same RB. On the other hand, when a BS adopts HD, it serves users in a FDD-manner, where the DL will take place in a RB and the UL in another without interfering between each other.

For HD BSs, the set of RBs, Ω, is partitioned such that the resource utilization ratio of ULs and DLs is the same, i.e., $\alpha_u^{(\mathrm{HD})} = \alpha_d^{(\mathrm{HD})} = 1/2$, as seen in the 'FDD HD' case in Fig. 1.9. In this regard, we have an UL and DL part of the spectrum which we write as B_u and B_d, respectively, where $\|\Omega\| = \|B_u \cup B_d\|$ and $B_u \cap B_d = \emptyset$. For the FD scenario, $\alpha_u^{(\mathrm{HD})} = \alpha_d^{(\mathrm{HD})} = 1$ and the whole system bandwidth (equivalent to one used by its HD counterpart) is used for UL and DL (see 'FD (case 1)' in Fig. 1.9). So we do not particularly differentiate between any UL or DL part of the spectrum for the FD case.

Hence, the configuration of the network can be characterized by the marked PPP:

$$\hat{\Phi} = \{x, y_d(x), y_u(x), s(y_d(x), y_u(x))\} \in \mathbb{R}^2 \times \mathbb{R}^2 \cup \{\emptyset\} \times \mathbb{R}^2 \cup \{\emptyset\} \times \{0,1\}, \tag{3.1}$$

where $\emptyset$ is the empty set, i.e., no user is scheduled on this link. The set $\{x\}$ represents the locations of the BSs (Φ) and, $y_d(x)$ and $y_u(x)$ are independent marks depicting the position of the scheduled DL and UL users inside the area covered by the BS $x \in \Phi$. Furthermore, $s(\cdot)$ is the duplex-switching function which is equal to 0 when BS in x is operating in HD-mode and equal to 1 if it works in FD-mode.

As in Section 2.5, BSs perform random scheduling and full buffer traffic model is assumed, i.e., there is always data to be sent in all directions (UL and DL). Hence, since a BS always has at least two users attached, it randomly chooses one for UL and the other for DL purposes, on every available RB $\tau \in \Omega$. We thus have that two point processes of scheduled UL and DL users, i.e., $\Psi_u^{(\tau)}$ and $\Psi_d^{(\tau)}$, respectively, are dependent on Φ and a realization can be obtained by drawing uniformly two points in every Voronoi cell of the network. Therefore, by construction, each of these processes has the same density as Φ. Further, we consider that all RBs are statistically equivalent, therefore we now omit in the notation the dependence on τ and we write $\Psi_m^{(\tau)}$, simply as Ψ_m, for $m \in \{u,d\}$.

Finally, let us define the point processes $\Phi^{(\mathrm{FD})} \subset \Phi$ and $\Phi^{(\mathrm{HD})} \subset \Phi$ as the processes of BSs operating in FD- and HD-mode, respectively. And, $\Psi_u^{(\mathrm{FD})} \subset \Psi_u$ and $\Psi_u^{(\mathrm{HD})} \subset \Psi_u$ as the processes of UL users linked to FD- and HD-enabled BSs, correspondingly. As DL users do not interfere others, we avoid making the distinction between HD and FD processes.

3.2.1 Duplex-switching policy

We propose the following DS policy. Each BS x has a "FD zone" $\mathscr{Z}_x$. For tractability reasons, we will assume in this paper that $\mathscr{Z}_x$ is a disk of fixed radius, r_x, centered on x, i.e., $r_x = r_f$,

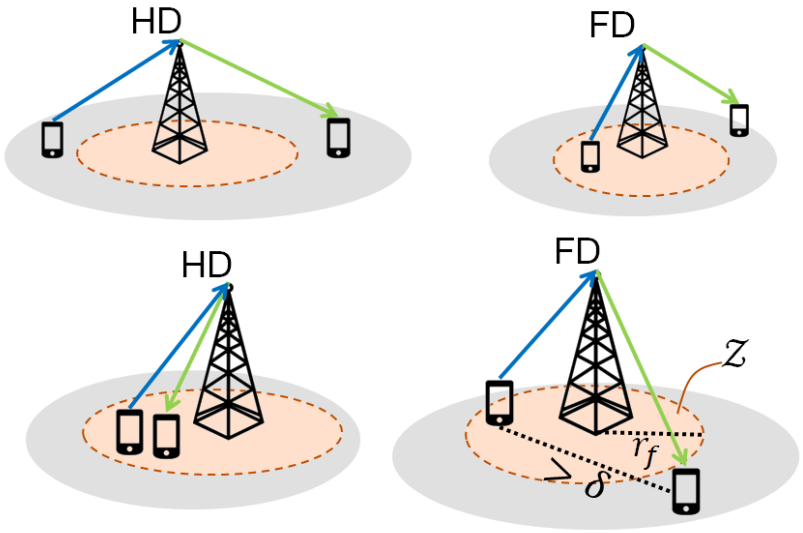

Fig. 3.1 Representation of a cellular network based on the proposed DS policy.

$\forall x \in \Phi$. Then, $s(\cdot)$ is defined as:

$$s(y_d(x), y_u(x)) = \begin{cases} 1, & \text{if } y_u(x) \in \mathscr{Z}_x \text{ and } d(y_d(x), y_u(x)) > \delta, \\ 0, & \text{otherwise,} \end{cases} \tag{3.2}$$

where δ is another network parameter. A representation of this model is depicted in Fig. 3.1.

From (3.2), we can firstly notice that with the proposed policy, a BS adopts FD only when its scheduled UL user is at most r_f meters apart. Hence, the received signal power coming from an active user towards its linked FD BS is increased and, consequently, the UL SINR as well. Secondly, when the BS is in FD-mode, the policy restrains the UL user to be at least δ meters away from the DL user in its same cell, allowing to manage the intra-cell interference and thus, providing higher DL SINR values.

However, as we have previously studied, FD is not always convenient as having more FD-enabled BSs in the network, also increases the BS-to-BS co-channel interference. Hence, let us notice that not only the the two parameters defining the DS policy (i.e., r_f a δ) can control the UL and DL performances. But also, the amount of FD-enabled BSs in the network. On the one hand, for a fixed value of δ, the probability of having a FD BS increases with r_f, as the area of $\mathscr{Z}_x$ also increases. Hence, the chances of having the scheduled UL user inside the FD zone as well. On the other hand, for a fixed value of r_f, when δ increases, the distance constraint between scheduled users in a cell is relaxed, increasing the probability for BSs to be in FD-mode.

We would, thus, like to find optimal values of r_f and δ, according to the QoS constraints imposed by the system, to achieve the best possible UL, DL or cell performances.

3.3 Analytical performance evaluation

3.3.1 Preliminaries

Given our DS policy, the probability that a BS is in FD-mode, p, is:

$$p(x, r_f, \delta) = \mathbb{P}\left(d(x, y_u(x)) \leq r_f \wedge d(y_d(x), y_u(x)) > \delta\right), \ \forall x \in \Phi. \tag{3.3}$$

Hence, point processes $\Phi^{(\mathrm{FD})}$ and $\Phi^{(\mathrm{HD})}$ can be characterized by applying the $p(x, r_f, \delta)$- and $[1 - p(x, r_f, \delta)]$-thinning rule to Φ, respectively.

We observe that the position of scheduled UL and DL users depend on the position of their serving BS, since it is the latter which actually decides to serve these particular users in a given set of RBs. Moreover, Ψ_u and Ψ_d are drawn from the same point process of users, Ψ. Thus, they are also inter-dependent. However, let us adopt the same approach as in the Numerical Application of Section 2.5.1 (which can also be found in [14, 17, 49, 51, 53]) and assume that the positions of scheduled UL and DL UEs are independent PPPs of intensity λ. Notice that by doing so, then:

- The distance between a typical user and its serving BS, and
- The distance between a typical DL user and its closest UL UE interferer,

are given by $f_R(r)$ in (2.20), i.e., the PDF of the distance from a typical point to its nearest neighbor.

Furthermore, we consider that the distance between scheduled (UL and DL) users in a given cell, is equivalent to the distance between a typical DL user and its closest UL UE interferer. The previous simplifying assumptions enable us to write p as:

$$p(r_f, \delta) = \exp(-\pi\lambda\delta^2)(1 - \exp(-\pi\lambda r_f^2)). \tag{3.4}$$

Let us notice that (3.4) respects the idea behind the proposed DS policy, i.e., $p \to 1$ when $\delta \to 0$ and $r_f \to \infty$, whereas $p \to 0$ either when $r_f = 0$ or when $\delta \to \infty$. Moreover, let us highlight the fact that $p(r_f, \delta)$ in (3.4) acts now a p-thinning rule, from which we define:

$$\lambda^{(\mathrm{FD})}(r_f, \delta) = p(r_f, \delta)\lambda, \tag{3.5}$$

$$\lambda^{(\mathrm{HD})}(r_f, \delta) = (1 - p(r_f, \delta))\lambda, \tag{3.6}$$

as the intensities of the new PPPs $\Phi^{(\mathrm{FD})}$ and $\Psi_u^{(\mathrm{FD})}$, and $\Phi^{(\mathrm{HD})}$ and $\Psi_u^{(\mathrm{HD})}$, respectively.

We insist in the fact that (3.4) is only an approximation and we validate all previous assumptions by simulations in Section 3.4.

3.3.2 SINR analysis

For a user located in y and served by a BS in x, we denote $L_0(r) = (\kappa r)^\eta$ as the deterministic path-loss to its serving BS and $h(x,y) = h(r)$, where $r = ||x-y||$. Moreover, when we refer to a typical user or a typical BS and when the context is clear, we write for simplicity $d(i) = d(0,i)$, $h(0,i) = h(i)$ and $L(0,i) = L(i)$, where i is the position of the element to from which they are receiving or transmitting.

Downlink SINR

Under the DS policy setting, the SINR at RB $\tau \in \Omega$, of a typical DL user served by a FD BS, i.e., $x \in \Phi^{(\mathrm{FD})}$ is given by:

$$\gamma_d^{(\mathrm{FD})}(\tau) = \frac{P_d h(r) L_0^{-1}}{I_d^{(\mathrm{FD})}(\tau) + \sigma^2}, \tag{3.7}$$

where

$$\begin{aligned} I_d^{(\mathrm{FD})}(\tau) &= \mathbb{1}[\tau \in B_d] \sum_{x'' \in \Phi^{(\mathrm{HD})}} P_d h(x'') L(x'')^{-1} + \mathbb{1}[\tau \in B_u] \sum_{y'' \in \Psi_u^{(\mathrm{HD})}} P_u h(y'') L(y'')^{-1} \\ &\quad + \sum_{x' \in \Phi^{(\mathrm{FD})} \setminus \{x\}} P_d h(x') L(x')^{-1} + \sum_{y' \in \Psi_u^{(\mathrm{FD})}} P_u h(y') L(y')^{-1} \end{aligned} \tag{3.8}$$

The terms in the first line of (3.8) represent the interference coming from HD equipment, which depends on the random position of τ along Ω. Resulting, in either the interference generated by the HD BSs, or the one by their associated UL users. The terms in the second line represent the interference generated by the FD BSs and their associated UL users. These are always present as we consider the FD case in which $\alpha_m^{(\mathrm{FD})} = 1$ and there is no system bandwidth reduction with respect to HD. With this we can proceed to establish the following Theorem.

Theorem 3.3.1 (CDF of the DL SINR for a FD-enabled BS)**.** *The probability that* $\mathbb{P}(\gamma_d^{(FD)} \leq \Gamma)$ *is given by:*

$$\mathbb{P}(\gamma_d^{(FD)} \leq \Gamma) = \int_0^\infty f_R(r) \left[1 - \mathscr{L}\left\{I_d^{(FD)}\right\}(r,T) N_d(r,\Gamma)\right] \mathrm{d}r, \tag{3.9}$$

where $N_d(r,\Gamma) = \exp\left(-\Gamma L_0(r)\sigma^2/P_d\right)$ *and*

$$\mathscr{L}\left\{I_d^{(FD)}\right\}(r,\Gamma) = \exp\left(-2\pi\lambda^{(FD)}(r_f,\delta)\left[\int_r^\infty \frac{\Gamma r^\eta}{z^\eta+\Gamma r^\eta} z\mathrm{d}z + \int_\delta^\infty \frac{\mu\Gamma r^\eta}{z'^\eta+\mu\Gamma r^\eta} z'\mathrm{d}z'\right]\right) \cdot \exp\left(-\pi\lambda^{(HD)}(r_f,\delta)\left[\int_r^\infty \frac{\Gamma r^\eta}{z^\eta+\Gamma r^\eta} z\mathrm{d}z + \int_0^\infty \frac{\mu\Gamma r^\eta}{z'^\eta+\mu\Gamma r^\eta} z'\mathrm{d}z'\right]\right). \tag{3.10}$$

Proof. Follows from the same reasoning as for the development of the coverage probability expressions for HD and FD networks in Section 2.5.1. Since, we notice that the CDF of the SINR is simply the complement of the coverage probability. □

On the other hand, if the typical user is served by a HD BS, $x \in \Phi^{(\mathrm{HD})}$, then the DL SINR at a RB $\tau \in B_d$ is:

$$\gamma_d^{(\mathrm{HD})}(\tau) = \frac{P_d h(r) L_0^{-1}}{I_d^{(\mathrm{HD})}(\tau) + \sigma^2}, \tag{3.11}$$

where

$$I_d^{(\mathrm{HD})}(\tau) = \sum_{x''\in\Phi^{(\mathrm{HD})}\setminus\{x\}} P_d h(x'') L(x'')^{-1} + \sum_{x'\in\Phi^{(\mathrm{FD})}} P_d h(x') L(x')^{-1} + \sum_{y'\in\Psi_u^{(\mathrm{FD})}} P_u h(y') L(y')^{-1}. \tag{3.12}$$

The first term in (3.12) represents the interference coming from the HD BSs and the other two from the FD BSs and their scheduled UL users. We then write the following Theorem.

Theorem 3.3.2 (CDF of the DL SINR for a HD-enabled BS)**.** *The probability that* $\mathbb{P}(\gamma_d^{(HD)} \leq T)$ *is:*

$$\mathbb{P}(\gamma_d^{(HD)} \leq \Gamma) = \int_0^\infty f_R(r)\left[1 - \mathscr{L}\left\{I_d^{(HD)}\right\}(r,\Gamma) N_d(r,\Gamma)\right]\mathrm{d}r, \tag{3.13}$$

where

$$\begin{aligned}\mathscr{L}\left\{I_d^{(HD)}\right\}(r,\Gamma) &= \exp\left(-2\pi\lambda^{(FD)}(r_f,\delta)\left[\int_r^\infty \frac{\Gamma r^\eta}{z^\eta+\Gamma r^\eta} z\mathrm{d}z + \int_0^\infty \frac{\mu\Gamma r^\eta}{z'^\eta+\mu\Gamma r^\eta} z'\mathrm{d}z'\right]\right) \\ &\quad \cdot \exp\left(-2\pi\lambda^{(HD)}(r_f,\delta)\int_r^\infty \frac{\Gamma r^\eta}{z^\eta+\Gamma r^\eta} z\mathrm{d}z\right).\end{aligned} \tag{3.14}$$

Proof. Similar to Theorem 3.3.1. □

Notice that the first line in $\mathscr{L}\{I_d^{(\mathrm{HD})}\}$ differs from the first line in $\mathscr{L}\{I_d^{(\mathrm{FD})}\}$, as in the latter the interference generated by the scheduled UL users is evaluated from δ, given the DS policy constraint regarding the distance between scheduled users in a FD cell.

Uplink SINR

When the typical BS is in FD, i.e., $x \in \Phi^{(\mathrm{FD})}$, and its scheduled UL user at a RB $\tau \in \Omega$ is in y, we have that the UL SINR is:

$$\gamma_u^{(\mathrm{FD})}(\tau) = \frac{P_u h(r) L_0^{-1}}{I_u^{(\mathrm{FD})}(\tau) + \sigma^2}, \tag{3.15}$$

where

$$\begin{aligned} I_u^{(\mathrm{FD})}(\tau) &= \mathbb{1}[\tau \in B_d] \sum_{x'' \in \Phi^{(\mathrm{HD})}} P_d h(x'') L(x'')^{-1} + \mathbb{1}[\tau \in B_u] \sum_{y'' \in \Psi_u^{(\mathrm{HD})}} P_u h(y'') L(y'')^{-1} \\ &+ \sum_{x' \in \Phi^{(\mathrm{FD})} \setminus \{x\}} P_d h(x') L(x')^{-1} + \sum_{y' \in \Psi_u^{(\mathrm{FD})}} P_u h(y') L(y')^{-1} + I_{\mathrm{RSI}}. \end{aligned} \tag{3.16}$$

Notice that when comparing $I_d^{(\mathrm{FD})}$ with $I_u^{(\mathrm{FD})}$, the only difference is that in the latter the self-IC term appears[1]. We use the same model as the one shown in (2.49) to model the RSI, i.e., for the DS-policy model here presented $I_{RSI} = \beta P_d$.

Theorem 3.3.3 (CDF of the UL SINR for a FD-enabled BS)**.** *The probability that* $\mathbb{P}(\gamma_u^{(FD)} \leq \Gamma)$ *is:*

$$\mathbb{P}(\gamma_u^{(FD)} \leq \Gamma) = \int_0^{r_f} \tilde{f}_R(r) \left[1 - \mathscr{L}\left\{I_u^{(FD)}\right\}(r,\Gamma) N_u(r,\Gamma) N_\beta(r,\Gamma)\right] \mathrm{d}r, \tag{3.17}$$

where

$$\tilde{f}_R(r) = \frac{2\pi\lambda r \mathrm{e}^{-\pi\lambda r^2}}{1 - \mathrm{e}^{-\pi\lambda r_f^2}}, \tag{3.18}$$

[1] Obviously the first is the interference at a typical user and the other at a typical BS.

$N_u(r,T) = \exp\left(-TL_0(r)\sigma^2/P_u\right)$, $N_\beta(r,T) = \exp\left(-TL_0(r)\beta/\mu\right)$ *and*

$$\mathscr{L}\left\{I_u^{(FD)}\right\}(r,\Gamma) = \exp\left(-2\pi\lambda^{(FD)}(r_f,\delta)\left[\int_0^\infty \frac{\Gamma r^\eta}{\mu y^\eta + \Gamma r^\eta} y\mathrm{d}y + \int_r^\infty \frac{\Gamma r^\eta}{x^\eta + \Gamma r^\eta} x\,\mathrm{d}x\right]\right)$$
$$\exp\left(-2\pi\lambda^{(HD)}(r_f,\delta)\left[\int_0^\infty \frac{\Gamma r^\eta}{\mu y^\eta + \Gamma r^\eta} y\mathrm{d}y + \int_r^\infty \frac{\Gamma r^\eta}{x^\eta + \Gamma r^\eta} x\mathrm{d}x\right]\right). \tag{3.19}$$

Proof. Let us consider an UL user $y \in \Psi_u^{(\mathrm{FD})}$ linked to a BS in x, i.e., we have $y = y_u(x)$. Given the DS policy in (3.2), $d(y_u(x),x) \le r_f$. Hence, we can write the CDF of the RV $d(y_u(x),x)$, such that the latter condition holds as:

$$\mathbb{P}\left(d(y_u(x),x) \le r \,|\, d(y_u(x),x) \le r_f\right) = \phi(r) = \frac{1-\mathrm{e}^{-\pi\lambda r^2}}{1-\mathrm{e}^{-\pi\lambda r_f^2}}. \tag{3.20}$$

Now, by taking the derivative of (3.20), we obtain the PDF, $\tilde{f}_R(r)$:

$$\frac{\mathrm{d}\phi(r)}{\mathrm{d}r} = \tilde{f}_R(r) = \frac{2\pi\lambda r\mathrm{e}^{-\pi\lambda r^2}}{1-\mathrm{e}^{-\pi\lambda r_f^2}}. \tag{3.21}$$

The rest of the proof is similar to Theorem 3.3.1. □

Furthermore, when the typical BS is in HD, i.e., $x \in \Phi^{(\mathrm{HD})}$, the UL SINR at a RB $\tau \in \Omega$ when its serving UL user is in y is:

$$\gamma_u^{(\mathrm{HD})}(\tau) = \frac{P_u h(r) L_0^{-1}}{I_u^{(\mathrm{HD})}(\tau) + \sigma^2}, \tag{3.22}$$

where

$$\begin{aligned} I_u^{(\mathrm{HD})}(\tau) \;=\; & \sum_{x' \in \Phi^{(\mathrm{FD})}} P_d h(x') L(x')^{-1} + \sum_{y' \in \Psi_u^{(\mathrm{FD})}} P_u h(y') L(y')^{-1} \\ & + \sum_{y'' \in \Psi_u^{(\mathrm{HD})} \setminus \{y\}} P_u h(y'') L(y'')^{-1}. \end{aligned} \tag{3.23}$$

Theorem 3.3.4 (CDF of the UL SINR for a HD-enabled BS)**.** *The probability that* $\mathbb{P}(\gamma_u^{(HD)} \leq \Gamma)$ *is given by:*

$$\mathbb{P}(\gamma_u^{(HD)} \leq \Gamma) = \int_0^\infty f_R(r) \left[1 - \mathscr{L}\left\{I_u^{(HD)}\right\}(r,\Gamma) N_u(r,\Gamma)\right] \mathrm{d}r, \tag{3.24}$$

where

$$\begin{aligned} \mathscr{L}\left\{I_u^{(HD)}\right\}(r,\Gamma) &= \exp\left(-2\pi\lambda^{(FD)}(r_f,\delta)\left[\int_0^\infty \frac{\Gamma r^\eta}{\mu z^\eta + \Gamma r^\eta} z \mathrm{d}z + \int_r^\infty \frac{\Gamma r^\eta}{z'^\eta + \Gamma r^\eta} z' \mathrm{d}z'\right]\right) \\ &\quad \cdot \exp\left(-\pi\lambda^{(HD)}(r_f,\delta) \int_r^\infty \frac{\Gamma r^\eta}{z'^\eta + \Gamma r^\eta} z' \mathrm{d}z'\right). \end{aligned} \tag{3.25}$$

Proof. Similar to Theorem 3.3.1. □

3.3.3 Reference models

From the previous expressions, we can directly derive the SINR CDF expressions for reference schemes in which all BSs work under FD (or HD), while users use the HD-mode (analog to the ones shown in Section 2.5). We call these the "reference FD" and "reference HD" systems.

Corollary 3.3.1 (Reference FD network)**.** *Let us consider the case in which* $r_f \to \infty$ *and* $\delta = 0$*. This implies that* $p(r_f,\delta) \to 1$*. Consequently, by* (3.5) *and* (3.6)*,* $\lambda^{(HD)} = 0$ *and* $\lambda^{(FD)} = \lambda$*. Therefore, the network is only characterized by FD-enabled BSs, since* $\Phi = \Phi^{(FD)}$*. Thus, under this scenario we have a general expression for the CDF of the DL SINR,* $\mathbb{P}(\gamma_d \leq \Gamma)$*, given by:*

$$\int_0^\infty f_R(r) \left[1 - \exp\left(-2\pi\lambda \left[\int_r^\infty \frac{\Gamma r^\eta}{z^\eta + \Gamma r^\eta} z \mathrm{d}z + \int_0^\infty \frac{\mu\Gamma r^\eta}{z'^\eta + \mu\Gamma r^\eta} z' \mathrm{d}z'\right]\right) N_d(r,\Gamma)\right] \mathrm{d}r, \tag{3.26}$$

which is equivalent to the complement of the DL coverage probability in (2.63)*, i.e.,* $(1 - \mathscr{P}_d^{(FD)}(\tau,\Gamma))$*.*

Furthermore, for the UL we observe that as $r_f \to \infty$ $\tilde{f}_R(r) \to f_R(r)$. *Hence, again we have a general expression for the CDF of the SINR,* $\mathbb{P}(\gamma_u \leq \Gamma)$, *given by:*

$$\int_0^\infty f_R(r)\left[1-\exp\left(-2\pi\lambda\left[\int_0^\infty \frac{\Gamma r^\eta}{\mu z^\eta+\Gamma r^\eta}z\mathrm{d}z+\int_r^\infty \frac{\Gamma r^\eta}{z'^\eta+\Gamma r^\eta}z'\mathrm{d}z'\right]\right)N_u(r,\Gamma)N_\beta(r,\Gamma)\right]\mathrm{d}r, \tag{3.27}$$

which, as well, is equivalent to the complement of the UL coverage probability in (2.65)*, i.e.,* $(1-\mathscr{P}_u^{(FD)}(\tau,\Gamma))$.

Corollary 3.3.2 (Reference HD network)**.** *Let us consider the scenario in which,* $r_f \to 0$ *and* $\delta \to \infty$. *Then,* $p(r_f,\delta)=0$ *and as a consequence,* $\lambda^{(HD)}=\lambda$ *and* $\lambda^{(FD)}=0$. *Therefore, the cellular network is only characterized by HD-enabled BSs, since* $\Phi=\Phi^{(HD)}$. *Thus, under this scenario we have a general expression for the CDF of the DL SINR,* $\mathbb{P}(\gamma_d \leq \Gamma)$, *given by:*

$$\int_0^\infty f_R(r)\left[1-\exp\left(-2\pi\lambda\int_r^\infty \frac{\Gamma r^\eta}{z^\eta+\Gamma r^\eta}z\mathrm{d}z\right)N_d(r,\Gamma)\right]\mathrm{d}r, \tag{3.28}$$

which is equivalent to the complement of the DL coverage probability in (2.53)*, i.e.,* $(1-\mathscr{P}_d^{(HD)}(\tau,\Gamma))$.

For the UL, we have again a general expression for the CDF of the UL SINR, $\mathbb{P}(\gamma_u \leq \Gamma)$, *given by:*

$$\int_0^\infty f_R(r)\left[1-\exp\left(-2\pi\lambda\int_r^\infty \frac{\Gamma r^\eta}{z'^\eta+\Gamma r^\eta}z'\mathrm{d}z'\right)N_u(r,\Gamma)\right]\mathrm{d}r, \tag{3.29}$$

which, as well, is equivalent to the complement of the UL coverage probability in (2.59)*, i.e.,* $(1-\mathscr{P}_u^{(HD)}(\tau,\Gamma))$.

3.3.4 Spectral efficiency

Let us take into account the definition of the average spectral efficiency introduced in Section 2.5.2.

For our model, we assume that all RBs are statistically equivalent. Hence, we can write the ASE of each link $m \in \{u,d\}$ as:

$$\mathscr{A}_m^{(\mathrm{mode})} = \alpha_m^{(\mathrm{mode})}\overline{\mathscr{C}}_m^{(\mathrm{mode})}, \tag{3.30}$$

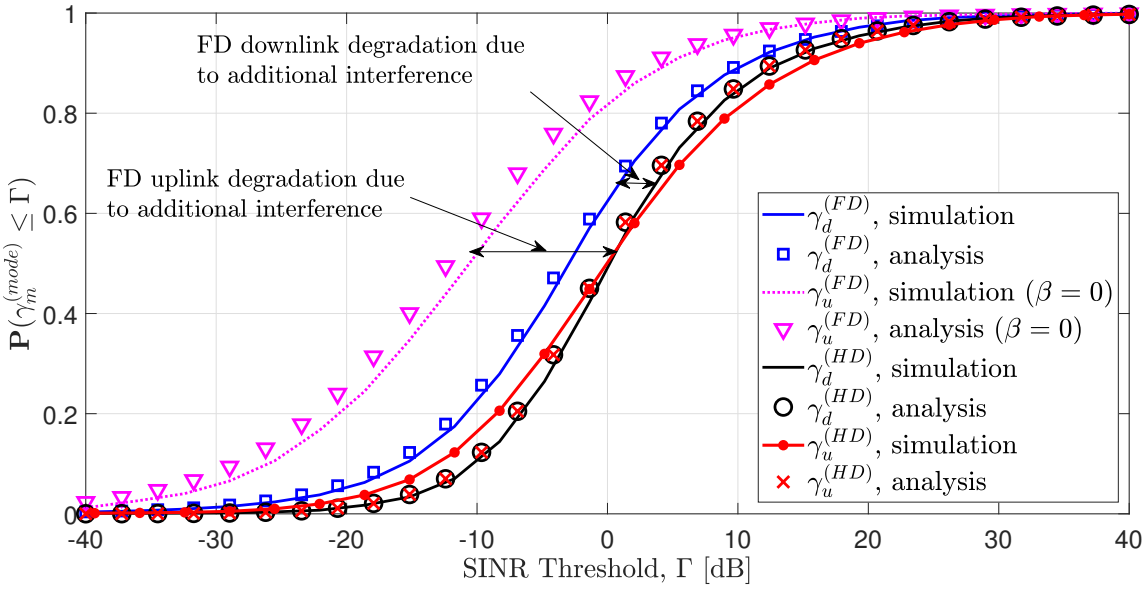

Fig. 3.2 CDF of SINRs for reference HD and FD networks with $\beta = 0$.

where $\overline{\mathscr{C}}_m^{(\text{mode})}$ is the ergodic capacity in (2.72). Therefore, by considering that $\alpha_u^{(\text{HD})} = \alpha_d^{(\text{HD})} = 1/2$ and $\alpha_u^{(\text{FD})} = \alpha_d^{(\text{FD})} = 1$, we have that the ASE for FD- and HD-enabled BSs can be written as:

$$\mathscr{A}_m^{(\text{FD})} = \int_0^{\infty} \frac{1 - \mathbb{P}(\gamma_m^{(\text{FD})} \leq \Gamma)}{\ln(2)(1+\Gamma)} \mathrm{d}\Gamma, \tag{3.31}$$

$$\mathscr{A}_m^{(\text{HD})} = \frac{1}{2} \int_0^{\infty} \frac{1 - \mathbb{P}(\gamma_m^{(\text{HD})} \leq \Gamma)}{\ln(2)(1+\Gamma)} \mathrm{d}\Gamma. \tag{3.32}$$

However, as the network is hybrid (in the sense that BSs can be operating in FD or HD depending on the position of their scheduled users), it holds that the ASE of ULs and DLs is given by the following equation:

$$\mathscr{A}_m = p(r_f, \delta)\mathscr{A}_m^{(\text{FD})} + (1 - p(r_f, \delta))\mathscr{A}_m^{(\text{HD})}. \tag{3.33}$$

Moreover, as the cell performance is defined as the sum between the UL and DL parts, we have that the cell ASE achieved by a random cell in the proposed DS environment is:

$$\mathscr{A}_c = p(r_f, \delta)\left(\mathscr{A}_u^{(\text{FD})} + \mathscr{A}_d^{(\text{FD})}\right) + (1 - p(r_f, \delta))\left(\mathscr{A}_u^{(\text{HD})} + \mathscr{A}_d^{(\text{HD})}\right). \tag{3.34}$$

Table 3.1 Simulated (Sim.) and analytical (An.) ASE performances in bps/Hz.

Network Configuration	DL		UL		cell	
	Sim.	An.	Sim.	An.	Sim.	An.
Reference HD	0.87	0.86	0.93	0.86	1.80	1.72
Reference FD	1.28	1.29	0.66	0.58	1.94	1.87
DS $(r_f, \delta) = (500, 100)$ m	1.35	1.36	0.68	0.57	2.03	1.93
DS $(r_f, \delta) = (85, 0)$ m	0.95	0.96	0.97	1.07	1.92	2.03
DS $(r_f, \delta) = (125, 0)$ m	1.03	1.04	0.91	1.03	1.94	2.07
DS $(r_f, \delta) = (182, 100)$ m	1.13	1.15	0.81	0.86	1.94	2.01

3.4 Simulation and performance evaluation

The system is simulated according to the small-cell parameters in Table 2.1, which were chosen to be consistent with related works (e.g. [13, 14, 16]) and 3GPP parameters [54]. Particularly, we set $\eta = 3.5$ and omnidirectional antennas with gain 1 for BSs and UEs. Moreover, let us recall that in a PPP-based network, the average inter-site distance (ISD), can be calculated by computing $\mathbb{E}_R[r] = 1/(2\sqrt{\lambda})$. We fix the ISD to 200 m.

Fig. 3.2 shows the simulated and analytical CDFs of the SINR for the reference HD and FD systems (in the ideal case of $\beta = 0$) for UL and DL. Results match well, hence we validate the assumption regarding the fact that the position of scheduled UL users is described by a homogeneous PPP. Further, we observe that even when some of the network parameters are different (particularly the antenna gains and parameters that describe the path-loss), the Numerical Application in Section 2.5.1 can be considered as equivalent to the curves plotted in Fig. 3.2. Indeed, we see a slight shift in the curves with respect to the ones shown in the Numerical Application in Section 2.5.1, but the results and conclusions for the previous figure are equivalent to the ones shown Figs. 2.4 and 2.5. In other words, we firstly observe that in spite of the perfect self-IC, FD UL is highly surpassed by HD. And secondly, that the CDF curve for the DL in FD is, arguably, not that far from the one of HD, as DLs can cope better the increase of interference due to higher transmission powers of BSs. We will further notice though, that the small difference between the simulated and analytical CDF results may result in a slight difference in the ASE performance. However, this does not alter the conclusions of the proposed DS policy.

Table 3.1 shows the DL, UL and cell ASE performances, with imperfect self-IC ($\beta = -100$ dB), for the different network configurations, i.e., values of r_f and δ. We can firstly note that analytical and simulated results match well. Nevertheless, there is slightly higher difference for the ULs, as the gap between SINR curves in Fig. 3.2 is to some degree bigger. In addition, we have again, that although FD outperforms HD in terms of DL ASE

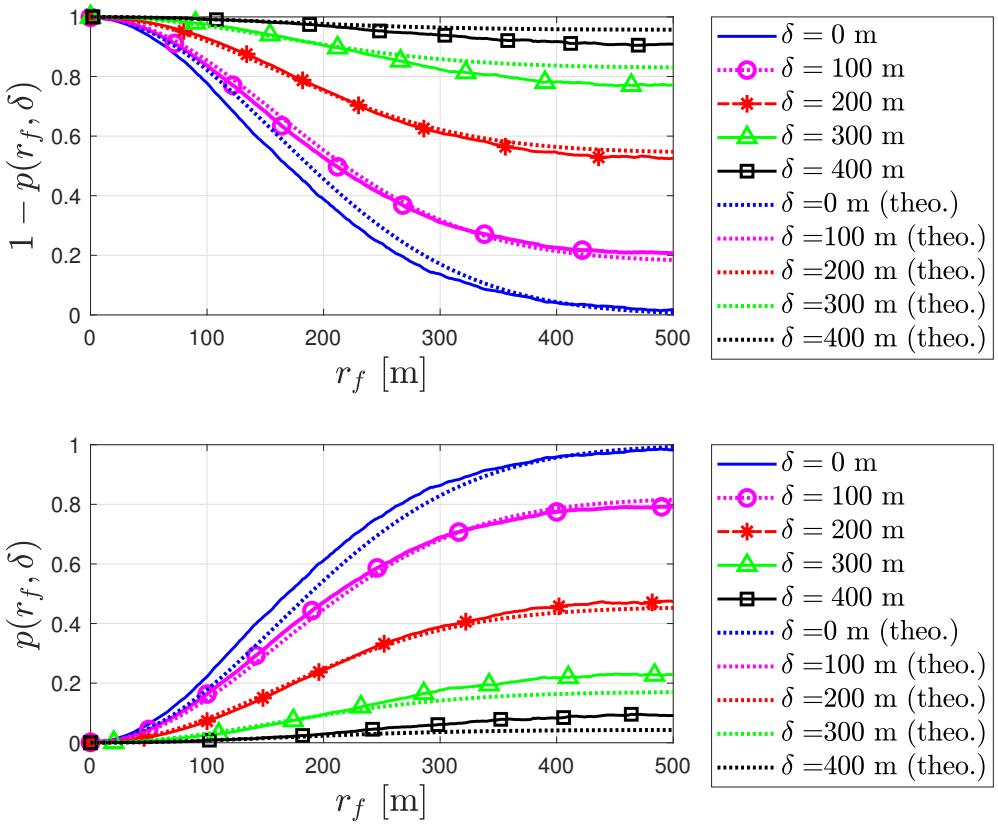

Fig. 3.3 Probability of having HD and FD BSs for different values of r_f and δ, i.e., characteristic of $p(r_f,\delta)$, where bold lines are for simulations and dotted ones for the analytical expression in (3.4)

performance, the UL is critically degraded. However, with this new network parameters (for path-losses and antenna gains), the FD cell performance is higher than the one of HD, differently to what is obtained in the results of the Numerical Application of Section 2.5.2 (see Table 2.2). This is mostly due to the fact that with lower net antenna gains between BSs (see $\breve{G}$ in Fig. 2.3), the BS-to-BS interference is reduced, allowing the UL performance to be less impacted. Hence, obtaining a higher cell performance. We thus see that the relative performance of FD with respect to HD is extremely sensitive to network conditions.

We plot in Fig. 3.3 the probability that a BS in the network is in FD-mode for diverse values of r_f and δ. The simulation-based results do not consider the approximation made in (3.4). However, we notice that results match well, even when in our analytical expression for p we assume that the distance between scheduled users in a same cell is equivalent to the distance between a typical DL user and its closest UL users (which is not always the case in reality). This validates our simplification assumption for $p(r_f,\delta)$.

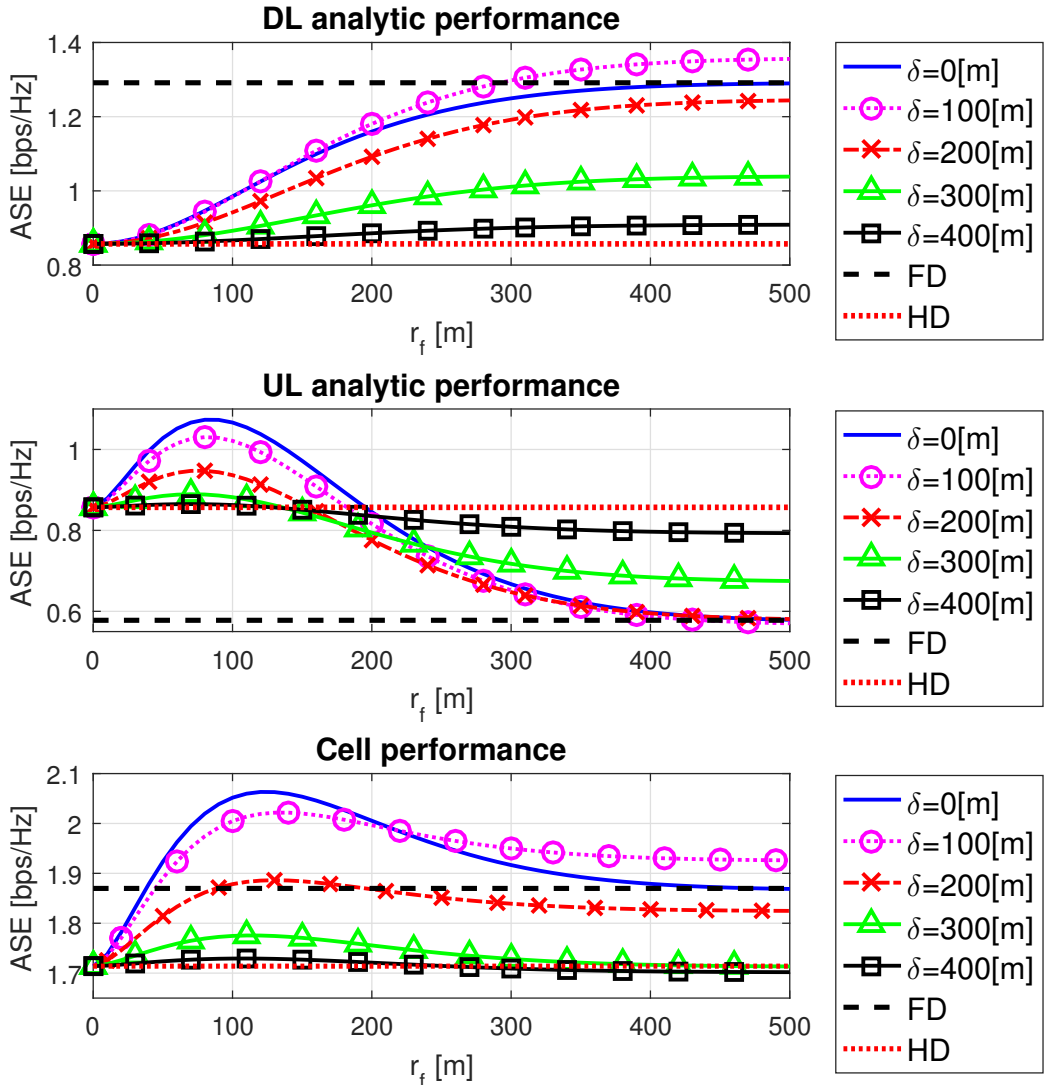

Fig. 3.4 Analytical ASE performance with $\beta = -100$ dB.

The analytical ASE performance of the DS system for $\beta = -100$ dB and different values of $\{r_f, \delta\}$ is depicted in Fig. 3.4. Regarding the DL performance, we can observe that the ASE level achieved by a reference HD network acts as a lower bound, reassuring the fact that FD increases the DL performance. For all (r_f, δ) values, the DS policy outperforms the HD lower bound. Additionally, for a given δ, the DL performance increases with r_f, yet the maximum ASE level is reached when the percentage of FD BSs can not be further increased. If δ decreases, the number of FD BSs grows; however the intra-cell interference gets larger as well. There is thus an optimal value for δ, which is approximately $\delta = 100$ m in our setting.

In contrast, when analyzing the UL ASE, the results show that the DS policy outperforms the reference FD model for almost all (r_f, δ) values, except for a nearly negligible loss seen for $\delta = 100$ m and $r_f > 440$ m. Moreover, for $r_f < 200$ m and $\delta = \{0, 100, 200, 300\}$ m, the DS system can even outperform the reference HD performance, with maximum value at $\{r_f, \delta\} = \{85, 0\}$ m. This is due to the fact that there are few FD BSs and in every FD cell the UL distance is small.

While considering both UL and DL, the cell performance is maximized for $\{r_f, \delta\} = \{125, 0\}$ m, where DS outperforms both FD (+11%) and HD (+20%) reference systems. In this case, UL and DL surpass the reference HD ASE, while the DL performance is 19% lower than the ASE achieved by the reference FD system, as seen in Table 3.1.

As a conclusion, the operator can tune the parameters (r_f and δ) to favor more or less the DL vs. UL. In Table 3.1, the values $\{r_f, \delta\} = \{182, 100\}$ m provide a good trade-off between DL and UL: DS exhibits a gain of 48% compared to FD and no loss compared to HD on the UL. The loss is 11% compared to FD and the gain is 34% compared to HD on the DL. This demonstrates the interest of the proposed scheme.

3.5 Summary and final remarks

In this Chapter we propose a duplex-switching policy for cellular networks, where BSs are FD- and HD- capable. The objective is to solve the problem of UL performance degradation observed in FD systems where all BSs adopt FD. In the proposed policy, a BS adopts FD only if its UL scheduled user is close, and the scheduled DL user is far from the UL user. These distances are controlled by two parameters r_f and δ. An analytical study using tools from stochastic geometry shows that our scheme is able to improve the UL performance at the cost of slightly reducing the performance gains obtained by FD in the DLs. The DS policy offers thus a flexible tool for the operator to favor more or less one link against the other. Though, when δ and r_f are optimized, our DS policy outperforms both HD and FD in terms of cell average spectral efficiency.

In this sense, the hybrid HD/FD network model that is generated by implementing our DS policy, seeks (as the other related works) to limit the number of FD-enabled BSs for those cases in which good conditions are met, e.g. favorable UL radio propagation or reduced co-channel interference scenarios. Hence, that is why we observe a reduction in the global interference level and, thus, an enhancement in the sum data rate. In all these works though, FD technique is restrained with the goal of reducing interference, so that its potential is not fully exploited.

Moreover, the implementation of the proposed DS policy in practice remains as a big question mark, since even though a BS may eventually measure the distance that separates itself from one of its scheduled users (r_f), e.g. by knowing the channel characteristics and measuring the SINR from a pilot tone received from the latter, it is not a direct operation to accurately measure the distance between scheduled user in a same cell. In this regard, we can think of solutions concerning Global Positioning System (GPS), in which UEs can communicate their locations to their serving BSs. However, in any case, additional capabilities must be implemented in the BSs and delays might be expected due to further signalization or data processing, in order to deploy the proposed DS policy.

Chapter 4

Millimeter wave full-duplex cellular networks

5G will exploit mmWave bands due to the larger bandwidths that they offer, which allows at the same time to increase data rates and many of the expected use cases for 5G. In this sense, mmWaves enable to perform beamforming, since given the smaller wavelengths, a higher number of antennas can be introduced in transceivers. Hence, using mmWave bands may, on the one hand, helps to offload the currently saturated spectrum and on the other hand, to increase systems bandwidths. In this regard, MIMO and 3D beamforming technologies can directly cope the degradation experienced in mmWaves propagation by steering the signals towards the intended receiver. Simultaneously, mmWave adoption can improve the feasibility of massive MIMO systems, as smaller wavelengths enable the utilization of smaller antennas, allowing to place bigger antenna arrays in smaller surfaces. Thus, the idea of implementing FD under a mmWave context can be jointly beneficial, as FD may enhance the spectral efficiency of mmWave systems, and on the other hand, a beamforming-based mmWave model can help to reduce the interference of FD in sub-6 GHz networks, which can be directly advantageous for the improvement of the FD UL performance.

In this Chapter, we are interested in studying whether hybrid FD/HD networks in which BSs can opt to operate rather in HD or FD (as the one presented in the previous Chapter) are necessary in the mmWave context. Additionally, a novel way of modeling the residual self-interference of FD-enabled BSs in this new beamforming-based scenario is proposed. In this regard, we study the optimal proportion of FD and HD BSs in the network and, finally, we investigate a power control scheme for FD BSs which enables to further improve the UL performance of the system.

4.1 Related works

Several publications have studied the performance of mmWave cellular networks using stochastic geometry. In all these papers, channel modeling plays an important role. Regarding the use of stochastic geometry to analyze HD-based mmWave cellular systems, authors in [55] use a distance-dependent line-of-sight (LOS) probability function and propose to model the locations of the LOS and non-LOS (NLOS) BSs as PPPs. Similarly, in [56] a LOS ball approximation is used, yet larger transmission bandwidths and Log-Normal shadowing are considered. Actual building locations are used to validate the results. In [57], a blockage model is also considered. Closed-form expressions are obtained thanks to a two ball approximation. Further, in [58] an overview of mathematical models is provided. Results show that mmWave systems are in general significantly more noise-limited than sub-6 GHz ones, that self-backhauling is more viable and that operators can benefit from sharing their spectrum.

The potential and applicability of FD mmWave-based cellular networks has been addressed in recent works [59–63]. Particularly, in [59], results show that an antenna with separate arrays for transmission and reception favors the self-interference cancellation, when compared to a single array model. In [63], several sub-optimal solutions are proposed for the joint transmission and reception beamforming problem, to maximize the achievable rate. Results show the feasibility of FD mmWave communications, since the geometry of antenna arrays are robust against channel estimation errors. As just mentioned, these works mostly analyze the feasibility of FD in mmWave scenarios, however none analyzes mmWave-FD by using stochastic geometry. By drawing inspiration from the mathematical development carried out by the author in [57], in this chapter we adapt the HD-based mmWave cellular model presented here, to meet with hybrid FD/HD capabilities. In this sense, we firstly seek to study the need of having, in mmWave scenarios, BSs that can switch between FD and HD (as done in the previous chapter). For this, we propose a novel way of modeling the residual self-interference in FD-enabled BSs, by considering the geometry of the transmitted and received beams and, additionally, we investigate the advantage of performing power control at FD BSs, which is not currently done by 4G networks.

4.2 System model

Let us consider the same stochastic geometry-based model as in Chapter 3, where BS locations are modeled as a homogeneous PPP, Φ, on $\mathbb{R}^2$, with spatial density λ. The average cell radius is $R_c = 1/\sqrt{\pi\lambda}$. The location of all users in the network is modeled by another

PPP, Ψ, with density large, when compared to λ. But, as opposed to what we have previously considered, users are connected to base stations with the minimum path-loss. This choice will be discussed later.

We stick to the fact that UEs are strictly HD elements. For the mmWave context, this idea is again supported by the findings in [59], where results show that a network can still benefit from FD gains even without FD users. Base stations are once again capable of operating both in HD- and FD-mode, with p being the probability that a BS adopts FD-mode. In this Chapter though, we do not focus in any specify duplex-switching policy and we directly assume that p is independent of the position of the BS. Consequently, the point processes of HD- and FD- BSs can be directly characterized by the $(1-p)$-thinning and p-thinning of Φ, respectively. In this regard, $\Phi^{(\mathrm{HD})}$ is the homogeneous PPP of density $(1-p)\lambda$ which describes the position of HD BSs and $\Phi^{(\mathrm{FD})}$ the homogeneous PPP of density $p\lambda$ for FD BSs.

As in Chapter 3, on the one hand we have that for HD BSs the set of RBs, Ω, is partitioned such that $\alpha_u^{(\mathrm{HD})} = \alpha_d^{(\mathrm{HD})} = 1/2$. In this regard for HD, we have an UL and DL part of the spectrum which we write as B_u and B_d, respectively, where $\Omega = B_u \cup B_d$ and $B_u \cap B_d = \emptyset$. On the other hand, for FD BSs, $\alpha_u^{(\mathrm{HD})} = \alpha_d^{(\mathrm{HD})} = 1$ and the FD system bandwidth is equivalent to the one used by its HD counterpart. Since there is no UL or DL parts for FD, when referring to B_u or B_d, we strictly refer to the DL and UL parts described by the partition of the HD-based spectrum (see the 'FDD HD' and 'FD (case 1)' examples in Fig. 1.9).

As opposed to Chapter 3, in this chapter we are particularly interested in analyzing the performance of generic RBs located in each part of the spectrum, i.e., RBs located in B_u and B_d. We hence describe the scheduling process as follows. BSs perform random scheduling and full buffer traffic model is assumed. Hence, since a BS always has at least two users attached, it randomly chooses one on the UL and one on the DL, on every available RB in Ω. Particularly, when a BS adopts the HD-mode, in every instant it serves two of its users in an orthogonal manner, where the UL takes place in $\tau_u \in B_u$ and the DL in $\tau_d \in B_d$, without interfering between each other. On the other hand, when FD is adopted, the same RBs as before, i.e., τ_u and τ_d, can be used simultaneously for UL and DL. Thus, the BS informs its users that they can operate in both RBs, immediately doubling the available transmission bandwidth if compared to the HD-mode.

As opposed to what we have seen in the previous chapters, given the fact that UEs are not necessarily attached to their closest BS, now the two point processes of scheduled UL and DL users, i.e., $\Psi_u^{(\tau)}$ and $\Psi_d^{(\tau)}$, respectively, are not only dependent on Φ, but also on the

propagation conditions. However, as we still have one UL and one DL user per RB[1], we can, nevertheless, consider by construction that each of these processes has the same density as Φ.

Further, we consider that all RBs are statistically equivalent, therefore we now omit in the notation the dependence on τ and we write $\Psi_m^{(\tau)}$, simply as Ψ_m, for $m \in \{u,d\}$. Then, as done as well for base stations, let us define point processes $\Psi_u^{(\mathrm{FD})} \subset \Psi_u$ and $\Psi_u^{(\mathrm{HD})} \subset \Psi_u$ as the processes of UL users linked to FD- and HD-enabled BSs, correspondingly. As DL users do not interfere others, we avoid making the distinction between HD and FD processes for them.

4.2.1 Transmission model

We assume that all users transmit at their maximum power capabilities, P_u, while, a BS transmission power is given by:

$$P^{(\mathrm{mode})} = \begin{cases} \rho P_d, & \forall x \in \Phi^{(\mathrm{FD})}, \\ P_d, & \text{otherwise}, \end{cases} \tag{4.1}$$

where P_d is the maximum transmission power and $\rho \in (0,1]$ serves as power control parameter to FD-enabled BSs.

Given the nature of mmWave transmissions we use directional beamforming to cope with the larger path-loss degradation dependency. In this case, beamforming aims as well to reduce the intra- and inter-cell interference observed in FD-based networks. We implement directional antennas both in BSs and UEs and the antenna gain is given by [55–58]:

$$G_m(\theta) = \begin{cases} G_m^{(\max)}, & \text{if } |\theta| \leq \Theta_m, \\ G_m^{(\min)}, & \text{otherwise}, \end{cases} \tag{4.2}$$

where $m \in \{d,u\}$[2], $\theta \in [-\pi,\pi)$ is the angle of the boresight direction, Θ_m is the beamwidth of the main lobe, $G_m^{(\max)}$ and $G_m^{(\min)}$ are the array gains of the main and side lobes, respectively. Notice that in this case, d and u also refer to the transmission characteristic of BSs and UEs, respectively. Moreover, we assume that every equipment (BS or UE) is able to perfectly estimate its steering angles. Hence, for an intended link, i.e., between BS and scheduled UE, the antenna gain is $G^{(\max)} = G_d^{(\max)} G_u^{(\max)}$. Furthermore, let $G(i,j)$ be the antenna gain product between a network equipment (BS or UE) in i and any interferer in j. We assume

[1] In the FD case we simultaneously serve one UL and one DL user with the same RB, but never two UL or two DL users in the same RB.

[2] This notation must be taken without loss of generality, since DL, d, represents the gain of the BSs that is transmitting and the ULs, u, for the users equipment that is transmitting towards its BS.

that the beams of interfering links are uniformly distributed with respect to each other in $[-\pi, \pi)$. Hence, the gain $G(i, j)$ is randomly distributed [57].

Given the fact that BSs operating in FD simultaneously receive and transmit signals, their antenna patterns can be described by two lobes; one pointing towards the DL user and the other in the direction of the UL as seen in Fig. 4.1. This can be achieved by implementing separated antennas in the BS FD transceiver (check Fig. 1.5). Thus, from (4.2) we can measure the angle between these two lobes for any BS $x \in \Phi^{(\mathrm{FD})}$ as:

$$\Delta\theta(x) = |\theta_u(x) - \theta_d(x)|, \tag{4.3}$$

where θ_u and θ_d are the UL and DL angles of the boresight directions, respectively. By considering (4.2) and (4.3), we are able to write the RSI of a FD-enabled BS as:

$$I_{\mathrm{RSI}} = \begin{cases} \underbrace{\beta G_d^{(\min)} G_d^{(\max)}}_{\alpha} \rho P_d, & \text{if } \Delta\theta(x) > \Theta_d, \\ \underbrace{\beta (G_d^{(\max)})^2}_{\tilde{\beta}} \rho P_d, & \text{otherwise,} \end{cases} \tag{4.4}$$

where $\beta \geq 0$ is the same constant used in (2.49) to model the residual serf-interference after the self-IC technique. From (4.4), we can firstly notice that the term $\beta\rho P_d$ corresponds to the same RSI model used in the previous Chapters[3]. Secondly, that $\tilde{\beta} \geq \alpha \geq 0$, thus the RSI is further reduced at those BSs that have non-interfering beams. And, lastly, that $\tilde{\beta} \geq \alpha \geq \beta$. Hence, due to the antenna gains, mmWave FD-enabled BSs may experience higher RSI values when compared to a sub-6 GHz case, this is the reason why we introduce the power control factor, ρ, for FD BSs.

4.2.2 Channel model

Given the nature of mmWaves propagation, we consider that links can be in LOS, NLOS or outage (OUT) state. LOS happens when there is a direct and unobstructed path between transmitter and receiver. NLOS occurs when the direct path is obstructed, and finally, an outage state refers to the case in which the link can not actually be set. It is due to these three possible link states that we consider that users are attached to the BSs that provide the smallest path-loss.

Let us take into account once again the deterministic distance dependent loss expression, $L(\cdot)$, in (2.48). For this Chapter though, instead of considering values of κ and η according to

[3]The term, ρP_d, simply represents the total transmitted power for the current model.

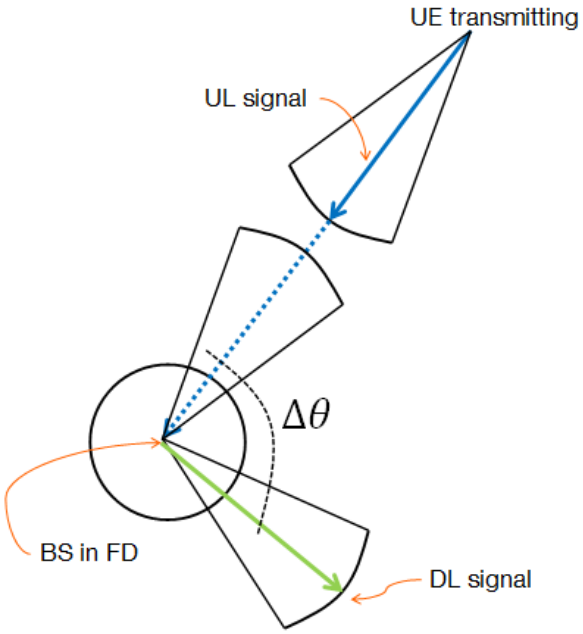

Fig. 4.1 Representation of the receiving and transmitting lobes of a beamforming-enabled FD BS.

the type of links that they describe (see Fig. 2.3), i.e., whether if it is a link between a BS and a user, between UEs or between BSs, here we write them according to their states [57, 64]:

$$L_s(r) = (\kappa_s\, r)^{\eta_s}, \tag{4.5}$$

where 's' is the link state, i.e., $s \in \{\text{LOS, NLOS}\}$ and r is the link distance. Moreover, κ_s and η_s are still the links reference path-loss at 1 meter and the path-loss exponent, respectively. Particularly, for an OUT link state, the path-loss is equal to $+\infty$. In the sequel, we use a plain '$L(\cdot)$' without referring to a particular link state, i.e., LOS, NLOS or OUT, to refer to any possible link state and $L(i, j)$ to define the path-loss between locations i and j.

The probability of occurrence of each link state is given by [57, 65]:

$$\begin{aligned} p_{\text{OUT}}(r) &= \max\{0, 1 - \mathfrak{a}_{\text{OUT}} \exp(-\mathfrak{b}_{\text{OUT}} r)\}, \\ p_{\text{LOS}}(r) &= (1 - p_{\text{OUT}}(r))\mathfrak{a}_{\text{LOS}} \exp(-\mathfrak{b}_{\text{LOS}} r), \\ p_{\text{NLOS}}(r) &= (1 - p_{\text{OUT}}(r))(1 - \mathfrak{a}_{\text{LOS}} \exp(-\mathfrak{b}_{\text{LOS}} r)), \end{aligned} \tag{4.6}$$

where $(\mathfrak{a}_{\text{OUT}}, \mathfrak{b}_{\text{OUT}})$ and $(\mathfrak{a}_{\text{LOS}}, \mathfrak{b}_{\text{LOS}})$ are variables that depend on the environment and on the system operation frequency.

Additionally, shadowing is considered and the channel power variations follow a Log-Normal distribution with means μ_s and standard deviations σ_s, where $s \in \{\text{LOS, NLOS}\}$.

We refer to h_s as the channel gain of an intended link and, as previously, we use $h(i,j)$ to define the channel gain between i and j.

4.2.3 Cell attachment

From the perspective of a typical UE, at the moment of deciding to which particular BS it has to attach and given the three possible link states, the process of BSs is seen as if three different thinning rules were applied to the original PPP, Φ. The three processes for the LOS, NLOS and OUT BSs are defined as Φ_{LOS}, Φ_{NLOS} and Φ_{OUT}, where their intensities are $\lambda_{\text{LOS}}(r) = p_{\text{LOS}}(r)\lambda$, $\lambda_{\text{NLOS}}(r) = p_{\text{NLOS}}(r)\lambda$ and $\lambda_{\text{OUT}}(r) = p_{\text{OUT}}(r)\lambda$, respectively. In this regard, the process of path-losses experienced by the typical user with respect to the BSs in Φ is given by:

$$L = \{\{L_{\text{LOS}}(x,0),\, x \in \Phi_{\text{LOS}}\}, \{L_{\text{NLOS}}(x,0),\, x \in \Phi_{\text{NLOS}}\}, \{L_{\text{OUT}}(x,0),\, x \in \Phi_{\text{OUT}}\}\}. \tag{4.7}$$

The previous process can be seen indeed as a random transformation of Φ and from Definition 2.1.9 we observe that it represents a mapping of the propagation losses of the typical user in $\mathbb{R}^2$, into another point process in $\mathbb{R}^+$. Particularly, we have that $\Phi = \Phi_{\text{LOS}} \cup \Phi_{\text{NLOS}} \cup \Phi_{\text{OUT}}$ and the point process Φ is Poisson. Thus, by using Theorem 2.3.1 we know that the displaced point process, L, is in fact another PPP on $\mathbb{R}^+$.

By adapting the the result found in [64, Section II A] for the current model we can write the following Lemma.

Lemma 4.2.1. *The intensity measure of L, $\Lambda_L([0,x))$, is $\Lambda_L([0,t)) = \Lambda_{\text{LOS}}([0,t)) + \Lambda_{\text{NLOS}}([0,t))$ where $\Lambda_{\text{LOS}}([0,t)) = \Upsilon_0(t;\text{LOS})$ and $\Lambda_{\text{NLOS}}([0,t)) = \Upsilon_1(t;\text{NLOS}) - \Upsilon_0(t;\text{NLOS})$, with*

$$\begin{aligned}\Upsilon_0(t;s) =& \mathscr{K}_2\left(\mathrm{e}^{-W} + W\mathrm{e}^{-W} - \mathrm{e}^{-V_s t^{1/\eta_s}} - V_s t^{1/\eta_s}\mathrm{e}^{-V_s t^{1/\eta_s}}\right)\mathscr{H}(t-Z_s)\\ &+ \mathscr{K}_1\left(1 - \mathrm{e}^{-Q_s t^{1/\eta_s}} - Q_s t^{1/\eta_s}\mathrm{e}^{-Q_s t^{1/\eta_s}}\right)\bar{\mathscr{H}}(t-Z_s)\\ &+ \mathscr{K}_1\left(1 - \mathrm{e}^{-U} - U\mathrm{e}^{-U}\right)\mathscr{H}(t-Z_s),\end{aligned} \tag{4.8}$$

$$\begin{aligned}\Upsilon_1(t;s) =& 2\pi\lambda\, \mathfrak{b}_{\text{OUT}}^{-2}\mathfrak{a}_{\text{OUT}}\left(\mathfrak{a}_{\text{OUT}}^{-1} + \mathfrak{a}_{\text{OUT}}^{-1}\ln(\mathfrak{a}_{\text{OUT}}) - \mathrm{e}^{-T_s t^{1/\eta_s}} - T_s t^{1/\eta_s}\mathrm{e}^{-T_s t^{1/\eta_s}}\right)\mathscr{H}(t-Z_s)\\ &+ \pi\lambda\,\kappa_s^{-2}t^{2/\eta_s}\bar{\mathscr{H}}(t-Z_s) + \pi\lambda\left(\mathfrak{b}_{\text{OUT}}^{-1}\ln(\mathfrak{a}_{\text{OUT}})\right)^2\mathscr{H}(t-Z_s),\end{aligned} \tag{4.9}$$

$\mathscr{H}(\cdot)$ is the Heaviside function, $\bar{\mathscr{H}}(t) = 1 - \mathscr{H}(t)$ and

$$\begin{aligned} \mathscr{K}_1 &= 2\pi\lambda\, \mathfrak{a}_{\mathrm{LOS}}\mathfrak{b}_{\mathrm{LOS}}^{-2}, & \mathscr{K}_2 &= 2\pi\lambda\, \mathfrak{a}_{\mathrm{LOS}}\mathfrak{a}_{\mathrm{OUT}}(\mathfrak{b}_{\mathrm{LOS}} + \mathfrak{b}_{\mathrm{OUT}})^{-2}, \\ U &= \mathfrak{b}_{\mathrm{LOS}}\mathfrak{b}_{\mathrm{OUT}}^{-1}\ln(\mathfrak{a}_{\mathrm{OUT}}), & W &= (\mathfrak{b}_{\mathrm{LOS}} + \mathfrak{b}_{\mathrm{OUT}})\mathfrak{b}_{\mathrm{OUT}}^{-1}\ln(\mathfrak{a}_{\mathrm{OUT}}), \\ Q_s &= \mathfrak{b}_{\mathrm{LOS}}\kappa_s^{-1}, & T_s &= \mathfrak{b}_{\mathrm{OUT}}\kappa_s^{-1}, \\ V_s &= (\mathfrak{b}_{\mathrm{LOS}} + \mathfrak{b}_{\mathrm{OUT}})\kappa_s^{-1}, & Z_s &= (\kappa_s\mathfrak{b}_{\mathrm{OUT}}^{-1}\ln(\mathfrak{a}_{\mathrm{OUT}}))^{\eta_s}. \end{aligned}$$

Proof. A detailed development follows from the proof of [57, Lemma 1] (which also uses [64, Section II A]). In summary the proof states that as Φ_{LOS}, Φ_{NLOS} and Φ_{OUT} are independent, then: $\Lambda_L([0,t)) = \Lambda_{L_{\mathrm{LOS}}}([0,t)) + \Lambda_{L_{\mathrm{NLOS}}}([0,t)) + \Lambda_{L_{\mathrm{OUT}}}([0,t))$. However, since the path-loss of the links in OUT is $+\infty$, then $\Lambda_{L_{\mathrm{OUT}}}([0,t)) = 0$. To derive the intensity measures for $s = \{\mathrm{LOS}, \mathrm{NLOS}\}$, by following similar steps as in [64, Lemma 1] we can finally write:

$$\Lambda_s([0,t)) = 2\pi\lambda \int_0^{\infty} \mathscr{H}\left(t - (\kappa_s r)^{\eta_s}\right) p_s(r)\mathrm{d}r. \tag{4.10}$$

□

Finally, we have that users are attached to the BS providing the smallest-path loss. Thus, for the typical UE located in $\mathscr{O}$, we have that:

$$L_0 = \min\left\{ \min_{x\in\Phi_{\mathrm{LOS}}} \{L_{\mathrm{LOS}}(x,0)\}, \min_{x\in\Phi_{\mathrm{NLOS}}} \{L_{\mathrm{NLOS}}(x,0)\}, \underbrace{\min_{x\in\Phi_{\mathrm{OUT}}} \{L_{\mathrm{OUT}}(x,0)\}}_{+\infty} \right\}. \tag{4.11}$$

Hence, by using the definition of the contact distribution function of a PPP in (2.18), which represents the CDF of the distance to the nearest neighbor, we have that:

$$\mathbb{P}(L_0 \leq t) = 1 - \exp(-\Lambda([0,t))). \tag{4.12}$$

4.3 Performance indicators formulation

4.3.1 SINR analysis

As done in Chapter 3, when we refer to a typical user or a typical BS and when the context is clear, we write for simplicity $d(i) = d(0,i)$, $h(0,i) = h(i)$ and $L(0,i) = L(i)$.

Moreover, as stated in the previous section we would like to analyze the performance of generic RBs located in each part of the spectrum, i.e., RBs located in B_u and B_d.

Downlink SINR

The DL SINR at a RB $\tau_d \in B_d$, of a typical user linked to a BS $x \in \Phi^{(\text{mode})}$ can be written as:

$$\gamma_d^{(\text{mode})}(\tau_d, s) = \frac{G^{(\max)} P^{(\text{mode})} h_s L_0^{-1}}{I_d^{(\text{mode})}(\tau_d) + \sigma^2}, \tag{4.13}$$

where mode$\in \{\text{FD, HD}\}$, $s \in \{\text{LOS, NLOS}\}$, σ^2 is the noise power and

$$\begin{aligned} I_d^{(\text{mode})}(\tau_d) \;=\; & \sum_{x' \in \Phi^{(\text{FD})}} G(x')\, \rho P_d\, h(x')\, L(x')^{-1} - \mathbb{1}\left[x \in \Phi^{(\text{FD})}\right] G^{(\max)} \rho P_d\, h_s\, L_0^{-1} \\ & + \sum_{x'' \in \Phi^{(\text{HD})}} G(x'')\, P_d\, h(x'')\, L(x'')^{-1} - \mathbb{1}\left[x \in \Phi^{(\text{HD})}\right] G^{(\max)} P_d\, h_s\, L_0^{-1} \\ & + \sum_{y' \in \Psi_u^{(\text{FD})}} G(y')\, P_u h(y') L(y')^{-1}. \end{aligned} \tag{4.14}$$

The first line of (4.14) represents the interference coming from FD BSs. The indicator function subtracts the intended received power (numerator of (4.13)) in case x is a FD-enabled BS. The second line is for the interference caused by the HD BSs, where the indicator function, once again, prevents to count the intended received power twice. The third line is for the interference generated by UL users scheduled by FD BSs.

Furthermore, the DL SINR at a RB $\tau_u \in B_u$, for a UE strictly scheduled by a FD-enabled BS $x \in \Phi^{(\text{FD})}$ is:

$$\gamma_d^{(\text{FD})}(\tau_u, s) = \frac{G^{(\max)} \rho P_d\, h_s L_0^{-1}}{I_d^{(\text{FD})}(\tau_u) + \sigma^2}, \tag{4.15}$$

where

$$I_d^{(\text{FD})}(\tau_d) = \sum_{x' \in \Phi^{(\text{FD})} \setminus \{x\}} G(x')\, \rho P_d\, h(x')\, L(x')^{-1} + \sum_{y' \in \Psi_u} G(y')\, P_u h(y') L(y')^{-1}. \tag{4.16}$$

We insist on the fact that a DL transmission occurs at a RB $\tau_u \in B_u$, if and only if the BS is in FD-mode. Let us notice that when comparing (4.14) to (4.16), we have that the latter expression only suffers from the interference coming from other FD-enabled BSs, as HD BSs only transmit in B_d. Moreover, in $I_d^{(\text{mode})}(\tau_d)$ we take into account the interference from all UL users, and not only by the UEs scheduled by FD BSs, since every scheduled user transmits in B_u.

Uplink SINR

We can write the UL SINR at RB $\tau_u \in B_u$, when the typical BS x is connected to a UE y as:

$$\gamma_u^{(\text{mode})}(\tau_u, s) = \frac{G^{(\max)} P_u \, h_s \, L_0^{-1}}{I_u^{(\text{mode})}(\tau_u) + \sigma^2}, \tag{4.17}$$

where mode$\in \{\text{FD, HD}\}$, $s \in \{\text{LOS, NLOS}\}$ and

$$\begin{aligned} I_u^{(\text{mode})}(\tau_u) = & \sum_{x' \in \Phi^{(\text{FD})}} G(x') \, \rho P_d \, h(x') \, L(x')^{-1} + \mathbb{1}\left[x \in \Phi^{(\text{FD})}\right] \left(I_{\text{RSI}} - G(0) \rho P_d \, h_s \, L_0^{-1}\right) \\ & + \sum_{y' \in \Psi_u \setminus \{y\}} G(y') \, P_u h(y') L(y')^{-1}. \end{aligned} \tag{4.18}$$

In (4.18), I_{RSI} is the RSI and $G(0)$ is the net self-interference gain, i.e., $G_{\text{d}}^{(\min)} \cdot G_{\text{d}}^{(\max)}$ or $\left(G_{\text{d}}^{(\max)}\right)^2$ (see (4.4)). Regarding the first line of $I_u^{(\text{mode})}(\tau_u)$, the first term represents the interference generated by all BSs operating in FD and the second term represents the self-interference when the typical BS is as well in FD-mode. The second line is for the interference generated by all UL users.

Furthermore, the UL SINR at a RB $\tau_d \in B_d$ when the user is strictly scheduled by a BS $x \in \Phi^{(\text{FD})}$, is given by:

$$\gamma_u^{(\text{FD})}(\tau_d, s) = \frac{G^{(\max)} P_u \, h_s \, L_0^{-1}}{I_u^{(\text{FD})}(\tau_d) + \sigma^2}, \tag{4.19}$$

where

$$\begin{aligned} I_u^{(\text{FD})}(\tau_d) = & \sum_{x' \in \Phi^{(\text{FD})} \setminus \{x\}} G(x') \, \rho P_d \, h(x') \, L(x')^{-1} + I_{\text{RSI}} \\ & + \sum_{x'' \in \Phi^{(\text{HD})}} G(x'') \, P_d \, h(x'') \, L(x'')^{-1} + \sum_{y' \in \Psi_u^{(\text{FD})} \setminus \{y\}} G(y') \, P_u h(y') L(y')^{-1}. \end{aligned} \tag{4.20}$$

Let us recall that we only have UL transmissions at a RB $\tau_d \in B_d$ when the BS is operating in FD-mode. Moreover, we can observe that when comparing (4.18) to (4.20), we have that the latter expression suffers additionally from the interference coming from other HD-enabled BSs transmitting in this part of the spectrum. However, in $I_u^{(\text{FD})}(\tau_d)$ the interference from UEs is only generated by the ones scheduled by FD BSs and not all of them as in (4.18).

4.3.2 Coverage probability analysis

For each duplex-mode we have that the coverage probability can be expressed as:

$$\mathscr{P}_m^{(\text{mode})}(\tau,\Gamma) = \mathscr{P}_m^{(\text{mode})}(\tau,\Gamma,\text{LOS}) + \mathscr{P}_m^{(\text{mode})}(\tau,\Gamma,\text{NLOS}), \tag{4.21}$$

where $m \in \{d,u\}$, mode $\in \{\text{FD, HD}\}$. The terms $\mathscr{P}_m^{(\text{mode})}(\tau,\Gamma,s)$ for $s \in \{\text{LOS, NLOS}\}$ depend on the probability of occurrence of each link state and are further defined below in Proposition 4.4.1, Proposition 4.4.2 and Theorem 4.4.1.

Moreover, we can as well define a general expression for the DL and UL coverage probability. In this regard, we know that a BS operates in FD with probability p. Then it holds that:

$$\mathscr{P}_m(\tau,\Gamma) = \begin{cases} p\ \mathscr{P}_m^{(\text{FD})}(\tau,\Gamma) + (1-p)\ \mathscr{P}_m^{(\text{HD})}(\tau,\Gamma), & \text{if } \tau \in B_m, \\ \mathscr{P}_m^{(\text{FD})}(\tau,\Gamma), & \text{otherwise.} \end{cases} \tag{4.22}$$

4.3.3 Spectral efficiency analysis

We carried out the SINR analysis be differentiating both parts of the frequency-domain spectrum, i.e., B_u from B_d. Hence, by using Lemma 2.5.5, (2.74) and (2.75), we can write the average spectral efficiency for each duplex-mode as:

$$\mathscr{A}_m^{(\text{mode})} = \frac{1}{B_u + B_d} \sum_{\tau\in\Omega} \int_0^\infty \frac{\mathscr{P}_m^{(\text{mode})}(\tau,\Gamma)}{\ln(2)(1+\Gamma)} \mathrm{d}\Gamma, \tag{4.23}$$

where $m \in \{u,d\}$ and mode $\in \{\text{FD, HD}\}$. However, as we have that BSs are FD with probability p, we can proceed as in (3.33) and write the general expression for the ASE of ULs and DLs as:

$$\mathscr{A}_m = p\mathscr{A}_m^{(\text{FD})} + (1-p)\mathscr{A}_m^{(\text{HD})}. \tag{4.24}$$

The same holds for the cell ASE which is equivalent to (3.34):

$$\mathscr{A}_c = p\left(\mathscr{A}_u^{(\text{FD})} + \mathscr{A}_d^{(\text{FD})}\right) + (1-p)\left(\mathscr{A}_u^{(\text{HD})} + \mathscr{A}_d^{(\text{HD})}\right). \tag{4.25}$$

Finally, we can write the FD-to-HD ASE ratio in (2.78), as a function of (p,ρ), i.e.:

$$\vartheta_m(p,\rho) = \frac{\mathscr{A}_m(p,\rho)}{\mathscr{A}_m^{(\text{HD})}}. \tag{4.26}$$

4.4 Analytical performance evaluation

4.4.1 Preliminaries

In order to derive closed-form expressions for the coverage probability and spectral efficiency, we consider the following assumption.

Assumption 4.4.1. *The interference from an equipment (BS or UE) to another is negligible.*

It is important to highlight that this assumption does not suppress the RSI in FD uplinks, nor the presence of noise in the network and can also be found in other works, e.g. [56, 57, 65]. Its accuracy is validated in Section 4.5.

With Assumption 4.4.1, the DL SINRs in (4.13) and (4.15) become:

$$\gamma_d^{(\text{mode})}(\tau, s) = \frac{G^{(\max)} P^{(\text{mode})} h_s}{\sigma^2 L_0}, \ \forall \tau \in \Omega, \tag{4.27}$$

where $s \in \{\text{LOS}, \text{NLOS}\}$. On the other hand, for the UL the SINRs for a BS $x \in \Phi$ in (4.17) and (4.19) become:

$$\gamma_u^{(\text{mode})}(\tau, s) = \frac{G^{(\max)} P_u h_s}{(I_{\text{RSI}} \, \mathbb{1}[x \in \Phi^{(\text{FD})}] + \sigma^2) L_0}, \ \forall \tau \in \Omega. \tag{4.28}$$

Hence, we observe that for these two new expressions, the SINRs are independent of the location of the RB in the frequency-domain spectrum (bandwidth).

4.4.2 Coverage probability

Proposition 4.4.1 (Downlink coverage probability)**.** *By taking into account* (4.12) *we can write the DL coverage probability as:*

$$\mathscr{P}_d^{(\text{mode})}(\tau, \Gamma, s) = \int_0^\infty Q\left(\ln\left(\Gamma t \frac{\sigma^2}{G^{(\max)} P^{(\text{mode})}}\right) - \mu_s\right) \dot{\Lambda}_{L_s}([0,t)) \exp\left(-\Lambda_L([0,t))\right) \mathrm{d}t, \tag{4.29}$$

where mode $\in \{\text{FD}, \text{HD}\}$*,* $s \in \{\text{LOS}, \text{NLOS}\}$*,* $Q(\cdot)$ *is the Q-function and* $\dot{\Lambda}_{L_s}(\cdot)$ *is the derivative of* Λ_{L_s} *with respect to t, i.e.:*

$$\dot{\Lambda}_{L_{\text{LOS}}}([0,t)) \;=\; \dot{\Upsilon}_0(t; \text{LOS}), \tag{4.30}$$

$$\dot{\Lambda}_{L_{\mathrm{NLOS}}}([0,t)) \quad = \quad \dot{\Upsilon}_1(t;\mathrm{NLOS}) - \dot{\Upsilon}_0(t;\mathrm{NLOS}), \tag{4.31}$$

with

$$\dot{\Upsilon}_0(t;s) = \mathscr{K}_2(V_s^2/\eta_s)t^{2/\eta_s-1}\mathrm{e}^{-V_s t^{1/\eta_s}}\mathscr{H}(t-Z_s) + \mathscr{K}_1(Q_s^2/\eta_s)t^{2/\eta_s-1}\mathrm{e}^{-Q_s t^{1/\eta_s}}\bar{\mathscr{H}}(t-Z_s), \tag{4.32}$$

$$\dot{\Upsilon}_1(t;s) = 2\pi\lambda\kappa_s^{-2}\eta_s^{-1}t^{2/\eta_s-1}\bar{\mathscr{H}}(t-Z_s) + 2\pi\lambda\mathfrak{b}_{OUT}^{-2}\mathfrak{a}_{OUT}T_s^2\eta_s^{-1}t^{2/\eta_s-1}\mathrm{e}^{-T_s t^{1/\eta_s}}\mathscr{H}(t-Z_s). \tag{4.33}$$

Proof. Straightforward application of [57, Proposition 1] to our model. □

Remark 4.4.1. *Since the Q function is a monotonically non-increasing function, if* $P^{(\mathrm{mode})}$ *or* $G^{(\max)}$ *increase then the DL coverage probability increases as well.*

Proposition 4.4.2 (Uplink coverage probability for HD)**.**

$$\mathscr{P}_u^{(\mathrm{HD})}(\tau,\Gamma,s) = \int_0^\infty Q\left(\ln\left(\Gamma t\frac{\sigma^2}{G^{(\max)}P_u}\right) - \mu_s\right)\dot{\Lambda}_{L_s}([0,t))\exp\left(-\Lambda_L([0,t))\right)\mathrm{d}t, \tag{4.34}$$

where mode $\in \{\mathrm{HD}\}$ *and* $s \in \{\mathrm{LOS}, \mathrm{NLOS}\}$.

Proof. Similar to Proposition 4.4.1. □

Theorem 4.4.1 (Uplink coverage probability for FD)**.**

$$\begin{aligned}\mathscr{P}_u^{(\mathrm{FD})}(\tau,\Gamma,s) = \int_0^\infty \dot{\Lambda}_{L_s}([0,t))\Bigg[&Q\left(\ln\left(\Gamma t\frac{\tilde{\beta}\rho P_d+\sigma^2}{G^{(\max)}P_u}\right)-\mu_s\right)\left(1-\frac{(2\pi-\Theta_d)^2}{(2\pi)^2}\right)\\ &+Q\left(\ln\left(\Gamma t\frac{\alpha\rho P_d+\sigma^2}{G^{(\max)}P_u}\right)-\mu_s\right)\frac{(2\pi-\Theta_d)^2}{(2\pi)^2}\Bigg]\exp\left(-\Lambda_L([0,t))\right)\mathrm{d}t,\end{aligned} \tag{4.35}$$

where $s \in \{\mathrm{LOS},\mathrm{NLOS}\}$.

Proof. By using Proposition 4.4.2 and noticing that I_{RSI} is a random variable, we can derive $\mathscr{P}_u^{(\text{FD})}(\Gamma,\tau,s)$ by computing:

$$\begin{aligned}
&\mathbb{E}_{I_{\text{RSI}}}\left[\int_0^{\infty} Q\left(\ln\left(\Gamma t\frac{\left(I_{\text{RSI}}+\sigma^2\right)}{G^{(\max)}P_u}\right)-\mu_s\right)\dot{\Lambda}_{L_s}([0,t))\exp\left(-\Lambda_L([0,t))\right)\mathrm{d}t\right]\\
&=\int_0^{\infty}\dot{\Lambda}_{L_s}([0,t))\exp\left(-\Lambda_L([0,t))\right)Q\left(\ln\left(\Gamma t\frac{\left(\alpha\rho P_d+\sigma^2\right)}{G^{(\max)}P_u}\right)-\mu_s\right)\mathbb{P}\left(\Delta\theta>\Theta_d\right)\mathrm{d}t\\
&+\int_0^{\infty}\dot{\Lambda}_{L_s}([0,t))\exp\left(-\Lambda_L([0,t))\right)Q\left(\ln\left(\Gamma t\frac{\left(\tilde{\beta}\rho P_d+\sigma^2\right)}{G^{(\max)}P_u}\right)-\mu_s\right)\mathbb{P}\left(\Delta\theta\leq\Theta_d\right)\mathrm{d}t.
\end{aligned} \tag{4.36}$$

where $s\in\{\text{LOS},\text{NLOS}\}$. Further, we compute $\mathbb{P}(\Delta\theta>\Theta_d)$ by assuming uniform angles of UL and DL users. Further, we proceed by considering a plane described by a square of side 2π and then calculating the surface in which the difference between two points is greater than Θ_d, resulting in $\mathbb{P}(\Delta\theta>\Theta_d)=(2\pi-\Theta_d)^2/(2\pi)^2$. □

Remark 4.4.2. *Notice that when the BS beamwidth, $\Theta_d\to 0$, i.e., when we have a very thin beam steered towards the users, then $\mathbb{P}(\Delta\theta>\Theta_d)\to 1$. Hence, the UL coverage probability is maximized since the RSI is only characterized by $\alpha\rho P_d$. However, $\alpha=\beta G_d^{(\min)}G_d^{(\max)}\neq 0$, then since the Q function is a monotonically non-increasing function, if P_d increases then the UL coverage probability decreases. The previous case is indeed the classical problem studied along this thesis, i.e., for imperfect self-IC, the greater the transmission power, the greater the UL degradation.*

4.4.3 Spectral efficiency

Theorem 4.4.2 (Average spectral efficiency)**.** *As we now have that the DL and UL SINRs are given respectively by* (4.27) *and* (4.28)*. We can write the ASE as done in* (2.77)*, i.e.:*

$$\mathscr{A}_m^{(\text{mode})}=\alpha_m^{(\text{mode})}\int_0^{\infty}\frac{\mathscr{P}_m^{(\text{mode})}(\tau,\Gamma)}{\ln(2)(1+\Gamma)}\mathrm{d}\Gamma. \tag{4.37}$$

for mode $\in \{\text{FD, HD}\}$ *and* $m \in \{u,d\}$. *Therefore,* (4.24) *results is:*

$$\mathscr{A}_m = p\int_0^{\infty} \frac{\mathscr{P}_m^{(\text{FD})}(\tau,\Gamma)}{\ln(2)(1+\Gamma)}\mathrm{d}\Gamma + \frac{(1-p)}{2}\int_0^{\infty} \frac{\mathscr{P}_m^{(\text{HD})}(\tau,\Gamma)}{\ln(2)(1+\Gamma)}\mathrm{d}\Gamma. \tag{4.38}$$

4.5 Simulation and performance evaluation

We focus our analysis in the 28 GHz band, given the interest of commercial deployments for 5G in this part of the spectrum. We simulate the network according to Table 4.1 which is based on [65, 66]. Contrary to the analytical framework, simulations take into account the whole interference. As in Chapter 3, the value of λ is derived from the ISD. For comparison, we simulate a sub-6 GHz network according to the urban micro-cell model in [54], with central carrier frequency of 2.6 GHz, path-loss functions $28+22\log_{10}(r)+20\log_{10}(2.6)$ for LOS and $22.7+36.7\log_{10}(r)+26\log_{10}(2.6)$ for NLOS, shadowing standard deviations $\sigma_{\text{LOS}} = 3$ dB and $\sigma_{\text{NLOS}} = 4$ dB, $p_{\text{LOS}}(r) = \min(18/r,1)(1-\exp(-r/36))+\exp(-r/36)$, $p_{\text{OUT}} = 0$, $B = 20$ MHz and omnidirectional antennas.

Fig. 4.2 shows the coverage probability, as a function of Γ for different values of p. First of all, it is possible to notice that the curves saturate at a probability considerably less than one. This is due to the fact that a high average cell radius was considered (this behaviour is in line with the results found in [57]). But the conclusions regarding the behaviour of the curves should not vary for other smaller radius (apart from the higher saturation levels). This value of R_c was chosen, given the interest of analyzing the performance of a mmWave-based networks not over-densified, since this reduces deployment costs and radiation levels. In this regard, we want to show that even under this condition, it is still possible to increase the

Table 4.1 Simulation parameters

Parameter	Value	Parameter	Value
B	400 MHz	RB bandwidth	720 KHz
P_d	30 dBm	P_u	23 dBm
β	-100 dB	$\Theta_d = \Theta_u$	30°
$G_d^{(\max)} = G_u^{(\max)}$	20 dB	$G_d^{(\min)} = G_u^{(\min)}$	-10 dB
$(\kappa_{\text{LOS}}, \eta_{\text{LOS}})$	(30.7 dB, 2)	$(\kappa_{\text{NLOS}}, \eta_{\text{NLOS}})$	(24.66 dB, 2.92)
$(\mathfrak{a}_{\text{LOS}}, \mathfrak{b}_{\text{LOS}})$	(1, 1/67.1)	$(\mathfrak{a}_{\text{OUT}}, \mathfrak{b}_{\text{OUT}})$	($\exp(5.2)$, 1/30)
$(\mu_{\text{LOS}}, \sigma_{\text{LOS}})$	(0, 5.8 dB)	$(\mu_{\text{NLOS}}, \sigma_{\text{NLOS}})$	(0, 8.7 dB)
Noise figure	10 dB	Noise density	-174 dBm/Hz
$(\sigma_{\text{LOS}}, \sigma_{\text{NLOS}})$	(5.8, 8.7) dB	R_c	225 m

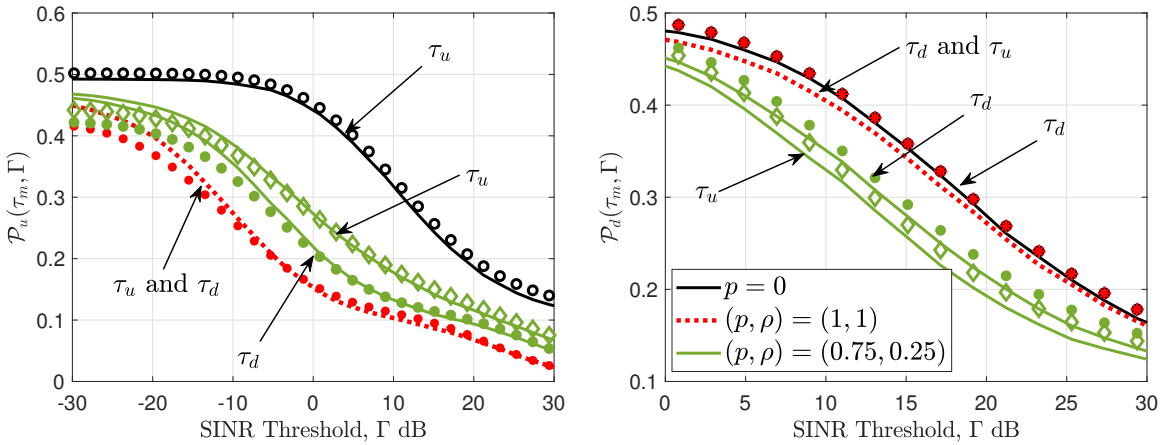

(a) UL coverage probability.

(b) DL coverage probability.

Fig. 4.2 Coverage probability, $\mathscr{P}_m^{(\text{mode})}(\tau,\Gamma)$. Markers are for analytical results.

ASE performance of the system. Further, we observe that simulated and analytical results match well, supporting Assumption 4.4.1. Results also show that DL outperforms UL, which under the validation of the previous assumption (that states that the interference between different equipment is negligible), is explained by the fact that $P_d > P_u$. Further, by focusing in the UL (Fig. 4.2 (a)), we see that τ_u outperforms τ_d when $p \neq \{0,1\}$. This was expected as τ_d is only used by BSs in FD-mode, hence the RSI is always considered, whereas τ_u is also used by HD BSs (with no RSI), consequently enhancing the performance. Regarding the DL in Fig. 4.2 (b), we see that the all-HD and FD (with $\rho = 1$) curves, almost match. Validating again Assumption 4.4.1 and more particularly equation (4.27), which shows that for $\rho = 1$ the HD and FD curves should be equivalent. Yet the curves do not match exactly, as in practice (simulation) there is a remaining interference. This interference is created since we have that: $\Theta_m \neq 0$, creating in fact some interference between equipment.

Fig. 4.3 shows the coverage probability as a function of ρ, for different values of p. For the UL in Fig. 4.3 (a), we see that for a fixed ρ and $\Gamma = -10$ dB, the performance of τ_u decreases with p, yet not due to interference coming from other links (as Assumption 4.4.1 is validated), but to the adoption of FD which generates RSI. This is clearly proven by the perfect self-IC case ($\beta = 0$), where the UL coverage probability is constant for all p's. The previous argument is further supported by the behavior of τ_d (only used by FD BSs) which does not vary with p. Concerning the impact of ρ, a similar conclusion is derived, as greater ρ's generate a higher RSI, degrading the UL performance. Thus, in terms of UL coverage probability, smaller values of p and ρ are preferable.

For the DL in Fig. 4.3 (b), the performance of both τ_u and τ_d is practically independent of p, since the inter-cell interference is negligible compared to a sub-6 GHz case (see the

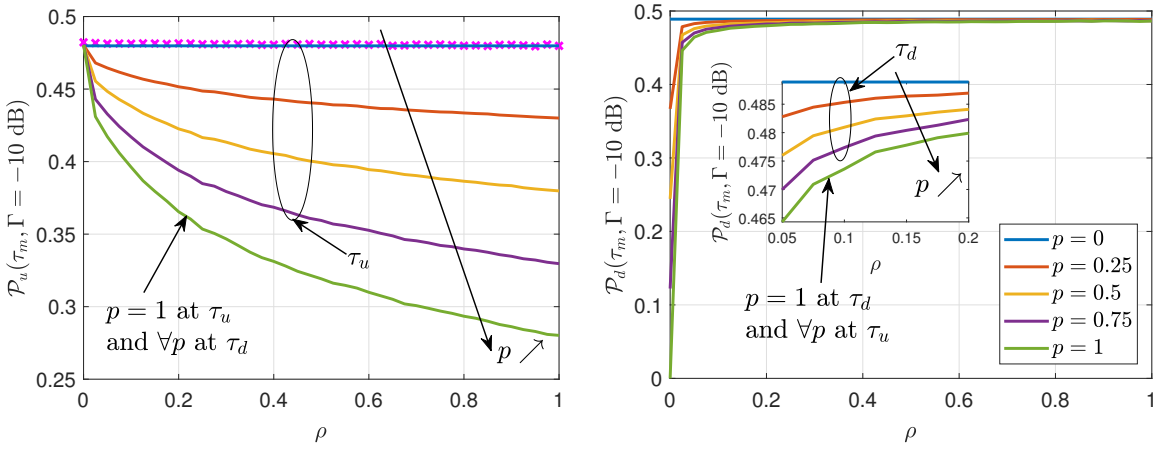

(a) UL coverage probability vs. ρ.

(b) DL coverage probability vs. ρ.

Fig. 4.3 Coverage probability for $\Gamma = -10$ dB. Markers are for $\beta = 0$.

previous Chapter). The slight dependence on p for τ_d happens at extremely small values of ρ, where the transmission power of FD DLs is heavily reduced. Further, the performance is enhanced with ρ, as transmit and receive power increase with ρ on the DL without adding interference, as in sub-6 GHz. Thus, for the DL coverage probability higher values of p and ρ are preferable.

The ASE performance of the system for different (p, ρ, β) configurations is depicted in Fig. 4.4. As it is for the coverage probability, Fig. 4.4 (a) shows that for the UL small values of ρ and p are preferable, whereas for the DL and cell, in Fig. 4.4 (c) and (d), it is the opposite. For $\beta = 0$ in Fig. 4.4 (b), the UL performance is independent of ρ (also seen in Fig. 4.3 (a)), since there is no RSI, but it grows with p, as FD always outperforms HD in terms of ASE if the noise-plus-interference is the same for both cases. Additionally, results confirm that an hybrid FD/HD deployment is not required in mmWave, since the links are maximized for $p = 1$ or $p = 0$. Yet it demonstrates the interest of performing power control at FD BSs with imperfect self-IC ($\beta \neq 0$). We can indeed observe that for $\rho = 0.1$, the UL ASE remains almost unchanged, while still enabling an enhancement of the DL performance.

Furthermore, Table 4.2 (a) shows the ASE performance of HD networks in sub-6 GHz and 28 GHz, noticing a superiority of mmWaves. Table 4.2 (b) presents the links ASEs for a sub-6 GHz network where all BSs are in FD-mode, for different β's and no power control. Results show once again that if the self-IC is not perfect, i.e., $\beta \neq 0$, the UL is heavily degraded ($\vartheta_u = 0.67$). Table 4.2 (c) also displays the links ASEs for an FD network, for different ρ's and β's. As with HD, mmWave also increases the ASE of FD networks. In fact, for $\beta = -100$ dB, if $\rho = 0.13$, there is an enhancement of 133% in the UL, 85% in the DL and 100% in the cell (when compared to its sub-6 GHz counterpart). Moreover, UL degradation

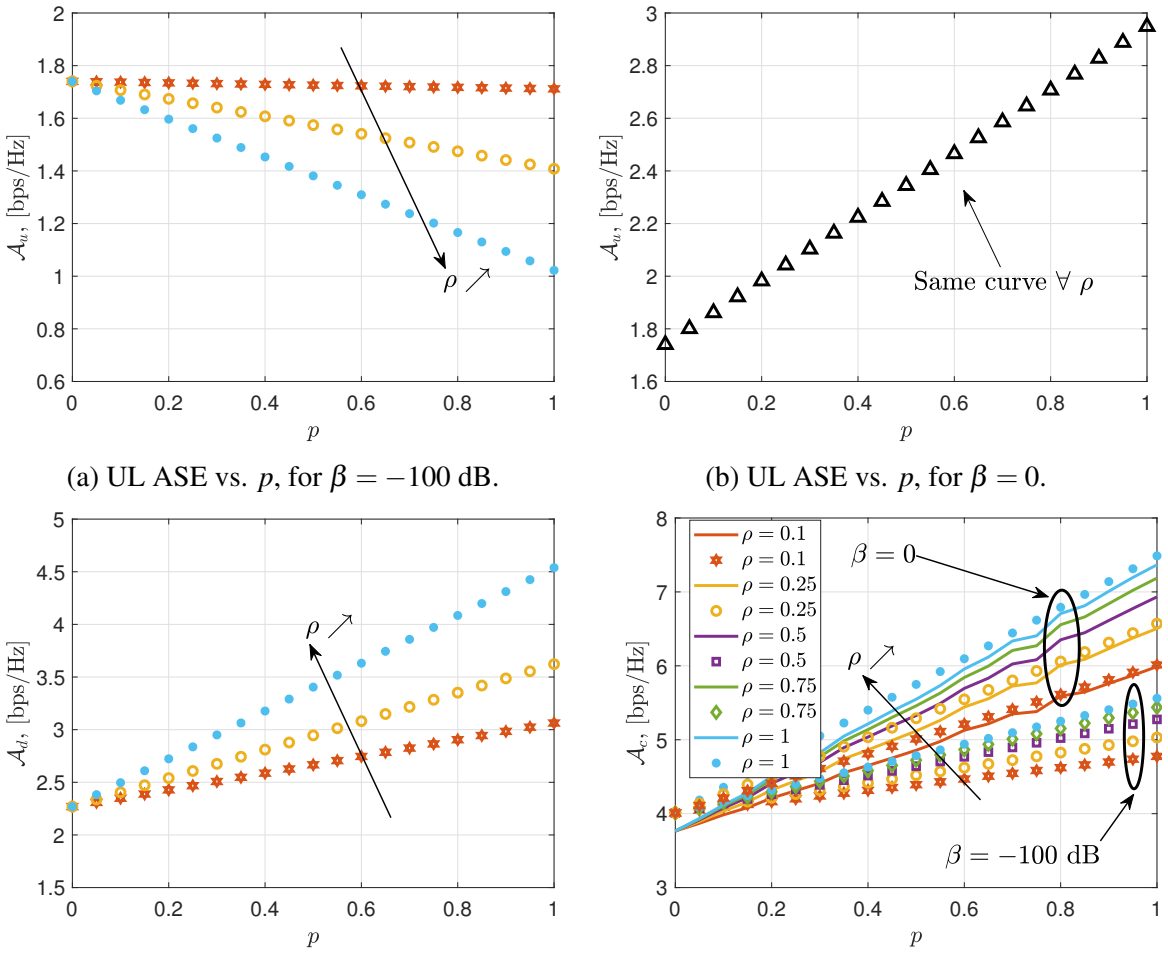

(a) UL ASE vs. p, for $\beta = -100$ dB.

(b) UL ASE vs. p, for $\beta = 0$.

(c) DL ASE vs. p.

(d) Cell ASE vs. p.

Fig. 4.4 ASE performances. Markers are for analytical results.

is avoided ($\vartheta_u = 1$), while still enhancing the DL and cell performances ($\vartheta_d = 1.36$ and $\vartheta_c = 1.21$). Additionally, for $\beta = 0$, each link almost doubles the performance of the HD system, closely approaching the ASE of an ideal FD system ($\vartheta_m = 2$).

As FD enhances the system ASE, an operator may be interested in relaxing its coverage probability floor level. In this regard, it is possible to find a $\rho = \rho^*$, such that $\rho_{\text{DL}}^{(\text{min})} \leq \rho^* \leq \rho_{\text{UL}}^{(\text{max})}$, where $\rho_{\text{DL}}^{(\text{min})}$ is the minimum acceptable ρ to achieve the expected DL coverage probability and $\rho_{\text{UL}}^{(\text{max})}$ is the highest value of ρ to obtain a given UL coverage probability threshold. As an example, let us suppose that an operator tolerates a coverage probability loss at $\Gamma = -10$ dB of 20% and 10% in the UL and DL, respectively, when compared to a HD network. By analyzing Fig. 4.3, $\rho_{\text{UL}}^{(\text{max})} = 0.15$ and $\rho_{\text{DL}}^{(\text{min})} = 0.025$. If the operator interest is to favor the UL performance, $\rho^* = \rho_{\text{DL}}^{(\text{min})}$, while for a DL maximization $\rho^* = \rho_{\text{UL}}^{(\text{max})}$. Table 4.2 (d), shows the ASEs for these cases, observing that in each configuration it is

Table 4.2 Simulated ASEs (bps/Hz) and ASE gains with respect to HD ($\vartheta_m(p,\rho)$).

HD ASE: 2.6 GHz		
$\mathscr{A}_u$	$\mathscr{A}_d$	$\mathscr{A}_c$
1.03	1.10	2.13

HD ASE: 28 GHz		
$\mathscr{A}_u$	$\mathscr{A}_d$	$\mathscr{A}_c$
1.61	2.20	3.81

(a) HD performance under a sub-6 GHz and 28 GHz environment.

FD ASE: 2.6 GHz	$\beta=-100$ dB			$\beta=0$		
	$\mathscr{A}_u$	$\mathscr{A}_d$	$\mathscr{A}_c$	$\mathscr{A}_u$	$\mathscr{A}_d$	$\mathscr{A}_c$
	0.69	1.62	2.30	1.21	1.62	2.83
$\vartheta_m(1,1)$	0.67	1.47	1.08	1.17	1.47	1.33

(b) Sub-6 GHz FD network ($p=1$) for different β values.

FD ASE: 28 GHz	$\beta=-100$ dB, $\rho=0.13$			$\beta=0$, $\rho=1$		
	$\mathscr{A}_u$	$\mathscr{A}_d$	$\mathscr{A}_c$	$\mathscr{A}_u$	$\mathscr{A}_d$	$\mathscr{A}_c$
	1.61	3.00	4.61	3.17	4.21	7.38
$\vartheta_m(1,\rho)$	1.00	1.36	1.21	1.97	1.91	1.93

(c) mmWave FD network ($p=1$) for different ρ and β values.

FD ASE: 28 GHz $\beta=-100$ dB	$\rho^*=\rho_{\text{DL}}^{(\min)}=0.025$			$\rho^*=\rho_{\text{UL}}^{(\max)}=0.15$		
	$\mathscr{A}_u$	$\mathscr{A}_d$	$\mathscr{A}_c$	$\mathscr{A}_u$	$\mathscr{A}_d$	$\mathscr{A}_c$
	2.22	2.11	4.33	1.55	3.06	4.61
$\vartheta_m(1,\rho)$	1.38	0.96	1.14	0.96	1.39	1.21

(d) mmWave FD network ($p=1$) for $\rho_{\text{DL}}^{(\min)}$ and $\rho_{\text{UL}}^{(\max)}$.

FD ASE: 28 GHz $\beta=-100$ dB	$\rho^*=\text{mean}(\rho_{\text{DL}}^{(\min)},\rho_{\text{UL}}^{(\max)})=0.0875$		
	$\mathscr{A}_u$	$\mathscr{A}_d$	$\mathscr{A}_c$
	1.73	2.71	4.44
$\vartheta_m(1,\rho)$	1.07	1.23	1.17

(e) mmWave network for $\rho=\text{mean}(\rho_{\text{DL}}^{(\min)},\rho_{\text{UL}}^{(\max)})$.

not possible to improve the performance of all links simultaneously. In this regard for a $\rho^*=(\rho_{\text{DL}}^{(\min)}+\rho_{\text{UL}}^{(\max)})/2$, we see in Table 4.2 (e) that all links outperform their HD counterpart.

4.6 Summary and final remarks

In this chapter we analyze if implementing hybrid FD/HD capabilities in base stations (as the model presented in Chapter 3) is needed when considering mmWaves and beamforming. First, we observe that mmWave-based networks outperform sub-6 GHz ones in terms of spectral efficiency. This results from increased beamforming capabilities at the BS in this

band. On this matter, and as we observe from the results, transmissions in the mmWave part of the spectrum suffer from a greater attenuation. This suggests that it is preferable to consider smaller cell radius to obtain greater coverage probabilities. However, we show that if we consider radii of the same order of magnitude as the ones in sub-6 GHz cases (to avoid an over-densification of the network), we can still considerably gain in spectral efficiency due to the steering of signals.

Second, we also show that hybrid FD/HD deployments are not required in mmWave-plus-beamforming scenarios. In fact, the limiting factor is related to the self-interference cancellation capabilities of FD-enabled base stations, rather than to the co-channel interference between different equipment. The reason is that the network is indeed close to being noise-limited. Hence, we could arguably say that systems in which effective beamforming capabilities are possible, are the most favourable ones towards FD deployments. As, not only ULs are not degraded, but also DL gains can be even higher. In this regard, we see that if FD BSs are not capable of perfectly canceling their self-interference, reducing their transmission power avoids UL degradation, while still enabling a DL spectral efficiency improvement with respect to a mmWave HD system. This is not only positive in terms of UL degradation, but also regarding the energy consumption of the network which is going to be a key issue in next generation wireless systems.

Chapter 5

A cellular full-duplex non-orthogonal multiple access rate adaptation algorithm

From the previous results, we know that hybrid FD/HD networks are a good solution for reducing the UL degradation caused by BS-to-BS co-channel interference that arises when using the same resources for UL and DL in FD. However, with this type of solution the global interference level is reduced at the expense of restraining or simply not allowing BSs to adopt the FD-mode and favour HD when the radio conditions are not ideal.

A promising approach to cope with uplink interference is non-orthogonal multiple access. NOMA is a method that allows a transceiver, e.g. a BS, to serve multiple users in the same radio resource. This is achieved by multiplexing the different messages in a different domain at the transmitter side, e.g. performing power-domain multiplexing or superposition coding. Then, successive interference cancellation (SIC) is applied at the receiver side, to decode and mitigate the interference among the superposed signals [67].

In this chapter, we propose an alternative approach which adds NOMA- and SIC-capabilities to FD BSs. The idea here is to still be able to solve the UL degradation issue, however by keeping BSs in a fixed FD-mode. This since constantly switching back and forth between HD/FD to reduce the BS-to-BS co-channel interference, may incur additional complexities in terms of data signalization, resource management, allocation of users and scheduling

5.1 Background

SIC has been studied for several years in the literature of cellular networks in order to allow multi-user transmissions on the same radio resource, see e.g. [36–40]. Only recently, this technique has been proposed in conjunction with FD. In particular, the implementation of NOMA in FD-based networks shows to be a good prospect to manage the additional interference experienced in these systems [68–74]. In [68], authors show the superiority of FD-NOMA over HD-NOMA but insist on the necessity to reduce co-channel interference. In [69, 71], authors focus on a single cell and try to reduce interference at the downlink user. Reference [70] tackle the problem of cross-tier interference, again on the downlink. In several studies, FD-NOMA is envisioned at relays or for device-to-device communications [72–74].

To the best of our knowledge, there is no solution available to directly mitigate the BS-to-BS interference and, thus, directly attack the UL degradation experienced in traditional FD-based networks. In the literature, SIC is preferably used at the UE, while BS capabilities are higher and BS-to-BS communication is arguably easier to achieve.

5.2 System model

As in the previous chapters, we consider a cellular network in which BSs locations are modeled by a homogeneous PPP, Φ, of spatial density λ on $\mathbb{R}^2$. The average cell radius is $R_c = 1/\sqrt{\pi\lambda}$. UEs are attached to their closest BS. In this regard, the network can be seen as a Voronoi tessellation of the network area, in which the coverage region of each BS is represented by its Voronoi cell. We assume that the density of UEs is large with respect to λ, to ensure that there are at least two users per cell.

BSs operate in FD-mode, while UEs are in HD-mode. Hence, only the three-node FD model is taken into account in this chapter. Ω is the set of RBs over the system bandwidth B_T, where every RB has a bandwidth of ω. The resource utilization ratio of ULs and DLs is $\alpha_u^{(\mathrm{FD})} = \alpha_d^{(\mathrm{FD})} = 1$. We consider a full buffer traffic model. Among the UL and DL users attached to a BS, one is randomly scheduled on every RB $\tau \in \Omega$. We then have the two point processes $\Psi_u^{(\tau)}$ and $\Psi_d^{(\tau)}$ of scheduled UL and DL users, respectively. By construction, $\Psi_u^{(\tau)}$ and $\Psi_d^{(\tau)}$ have the same density as Φ, as a realization can be obtained by drawing uniformly two points in every Voronoi cell of Φ. Moreover, as they are drawn from the same point process of active users, there are also inter-dependent. We make however the simplifying assumption that they are independent, as done in Chapter 3.

As all RBs are statistically equivalent, we now omit in the notation the dependence on τ, and without loss of generality we simply write $\Psi_m^{(\tau)}$ as Ψ_m, $m \in \{u, d\}$.

5.2.1 Transmission and propagation model

UEs and BSs transmit powers are denoted P_u and P_d, respectively. We assume that users have omnidirectional antennas, with an antenna gain of $G_u = 1$. As shown in Chapter 4, this is a worst case scenario from the perspective of users, as beamforming at UE side greatly improves FD performance. Further, we adopt the same model as the one in Chapter 4 for BSs, where the FD transceiver is conceived by using separated antennas for DL and UL as shown in Section 1.2 (see Fig. 1.5). Thus, we adopt a side- and main-lobe model for BS antennas with gains $G_d^{(\min)}$ and $G_d^{(\max)}$, respectively. The beamwidth of the main-lobe is described by the angle Θ_d. Hence, the side-lobe of gain $G_d^{(\min)}$ covers the angle $2\pi - \Theta_d$. Every BS steers two main lobes, in the direction of the scheduled UL UE and the scheduled DL UE, respectively (as depicted in Fig. 4.1).

Accordingly, we can relate to Fig. 2.3 and assume the following net average gains between elements in the network:

- $G \triangleq G_d^{(\max)} G_u$, between a BS and a scheduled UE,
- $G' \triangleq (1 - \Theta_d/(2\pi)) G_d^{(\max)} G_u + (\Theta_d/2\pi) G_d^{(\min)} G_u$, between a BS and a UE scheduled by another cell,
- $\breve{G} \triangleq G_d^{(\min)} G_d^{(\min)}$, between two BSs,
- $\tilde{G} \triangleq G_u^2$, between two UEs,
- G_{RSI}, for the self-interference between the transmitter of a FD BS and its own receiver.

By focusing in the FD BS transceiver, we notice that as it simultaneously receives and transmits signals, the RSI in (4.4) is the result from the interference between the lobes pointing towards the DL user and the other in the direction of the UL user. Hence, we have that in average:

$$G_{\text{RSI}} = \left(\frac{2\pi - \Theta_d}{2\pi}\right)^2 G_d^{(\max)} G_d^{(\min)} + \left(1 - \left(\frac{2\pi - \Theta_d}{2\pi}\right)^2\right) G_d^{(\max)2}, \tag{5.1}$$

For the signal propagation model, let us reconsider the model presented in (2.48) and Fig. 2.3. However, in this chapter we assume that $\kappa = \kappa'$ and $\eta = \eta'$. Further, Rayleigh fading channels are considered, hence once again the channel gain $h(i, j)$ (see (2.48)) is an exponential RV with mean 1.

For a typical user located in 0, we denote $L_0 = (\kappa R_0)^\eta$ the deterministic path-loss to its serving BS in x, where $R_0 = \min_{x' \in \Phi} d(0, x')$. When we refer to a typical user or a typical

BS and when the context is clear, we write $d(i) = d(0,i)$, $h(0,i) = h(i)$ and $L(0,i) = L(i)$ for simplicity.

5.2.2 NOMA model

In a power domain NOMA transmission [75, Chapter 6], a set $\tilde{\mathscr{U}}$ of transmitters transmit signals to a common receiver on the same radio resource. At the receiver, Successive Interference Cancellation (SIC) is performed to retrieve each transmitted information. The SIC decoder is characterized by a decoding order, i.e., a permutation function $\pi : \tilde{\mathscr{U}} \to \tilde{\mathscr{U}}$. For $i \in \tilde{\mathscr{U}}$, $\pi(i)$ represents the i-th decoded transmitter, and conversely the order at which transmitter q is decoded is given by $\pi^{-1}(q)$. Consequently, the i-th decoded signal is only subject to interference coming from transmitters $\pi(j)$, such that $j > i$.

5.2.3 SINR formulations

Downlink SINR

For this chapter, we define the DL SINR of a user located in y and served by a BS in x as, $\gamma_d(x,y)$, which can be written as:

$$\gamma_d(x,y) = \frac{GP_d hL(x,y)^{-1}}{I_{\mathrm{BS}}^{(d)}(x,y) + I_{\mathrm{UE}}^{(d)}(y) + \sigma^2}, \tag{5.2}$$

where

$$I_{\mathrm{BS}}^{(d)}(x,y) = \sum_{x' \in \Phi \setminus \{x\}} G' P_d h(x',y) L(x',y)^{-1}, \tag{5.3}$$

is the interference coming from other BSs,

$$I_{\mathrm{UE}}^{(d)}(y) = \sum_{y' \in \Psi_u \setminus \{y\}} \tilde{G} P_u h(y,y') L(y,y')^{-1}, \tag{5.4}$$

is the interference from UL users, and σ^2 is the thermal noise power. When y is the typical DL user, we write $\gamma_d^{(0)} \triangleq \gamma_d(x,0)$, $I_{\mathrm{BS}}^{(d)} \triangleq I_{\mathrm{BS}}^{(d)}(x,0)$, $I_{\mathrm{UE}}^{(d)} \triangleq I_{\mathrm{UE}}^{(d)}(0)$, where x is the closest BS to y.

Uplink SINR

Let us consider a BS in x serving in UL a user in y and assume that the BS is able to successively suppress the interference from a set $\mathscr{U}$ of neighboring BSs. The set $\tilde{\mathscr{U}} =$

$\mathscr{U} \cup \{y\}$ defined in Section 5.2.2 is now formed by the UL user and the neighboring BSs. In this setting, the UL user is the last one to be decoded, i.e., $\pi(y) > \pi(i)$ for all $i \in \mathscr{U}$. This choice does not necessarily achieves the capacity region border; it is however the optimal choice for the UL user. For this user, we define the UL SINR at the BS, $\gamma_u(y,x)$, as:

$$\gamma_u(y,x) = \frac{GP_u h(y,x)L(y,x)^{-1}}{I_{\text{BS}}^{(u)}(y,x;\mathscr{U}) + I_{\text{UE}}^{(u)}(y,x) + I_{\text{RSI}} + \sigma^2}, \tag{5.5}$$

where

$$I_{\text{BS}}^{(u)}(y,x;\mathscr{U}) = \sum_{x' \in \Phi \setminus \{\{x\} \cup \mathscr{U}\}} \breve{G}\, P_d h(x',x)L(x',x)^{-1} \tag{5.6}$$

is the interference coming from other BSs at BS y,

$$I_{\text{UE}}^{(u)}(y,x) = \sum_{y' \in \Psi_u \setminus \{y\}} G' P_u h(y',x)L(y',x)^{-1} \tag{5.7}$$

is the interference from all other scheduled UL users and I_{RSI} is the RSI power of a BS given by:

$$I_{\text{RSI}} = \beta G_{\text{RSI}} P_d, \tag{5.8}$$

where $\beta \in [0,1]$ is the same constant we have used in the previous chapters and that is related to the performance of the self-IC used at the BS receiver, i.e., β characterizes the effective remaining RSI with respect to the transmitted power. When x is the typical BS, we write $\gamma_u^{(0)} \triangleq \gamma_u(y,0)$, $I_{\text{BS}}^{(u)}(\mathscr{U}) \triangleq I_{\text{BS}}^{(u)}(y,0;\mathscr{U})$, $I_{\text{UE}}^{(u)} \triangleq I_{\text{UE}}^{(u)}(y,0)$, where y is the scheduled UE.

BS-to-BS SINR

For our proposed scheme, we need to define the BS-to-BS SINR for a transmission occurring from a BS x' to a BS x. The BS-to-BS SINR is given by:

$$\gamma_b(x',x) = \frac{\breve{G} P_d h(x',x)L(x',x)^{-1}}{I_{\text{BS}}(x',x) + I_{\text{UE}}(x) + I_{\text{RSI}} + \sigma^2}, \tag{5.9}$$

where

$$I_{\text{BS}}(x',x) = \sum_{x'' \in \Phi \setminus \{x,x'\}} \breve{G}\, P_d h(x'',x)L(x'',x)^{-1} \tag{5.10}$$

is the interference from all other BSs,

$$I_{\text{UE}}(x) = \sum_{y \in \Psi_u} G' P_u h(y,x)L(y,x)^{-1} \tag{5.11}$$

is the interference coming from all UL users. When x is the typical BS, we write $\gamma_b^{(0)}(x') \triangleq \gamma_b(x',0)$. When x is the typical BS and x' is its n-th closest BS, $n \in \mathbb{N}$, we write $\gamma_b^{(n)} \triangleq \gamma(x',0)$, $I_{\text{BS}}^{(n)} \triangleq I_{\text{BS}}(x',0)$, and $I_{\text{UE}}^{(b)} \triangleq I_{\text{UE}}(0)$.

Remark 5.2.1. *From* (5.6)*, we know that a BS in x is able to decode the interference from a set of BSs, $\mathscr{U}(x)$. Hence, to calculate I_{BS} in* (5.10)*, we could eventually decode some of the interfering BSs. However, for the following development, we do not analyze a particular decoding order for the interfering BSs. Therefore,* (5.10) *represents a worst case scenario for the later computation of capacities between BSs.*

5.2.4 Coverage probability, capacity and rate

Let us recall Section 2.5.2 where we defined the instantaneous capacity and coverage probability for ULs and DLs[1]. In this chapter though, we are also interested in the links between BSs. Hence, we consider the coverage probability, $\mathbb{P}(\gamma_m > \Gamma)$, and capacity, $\mathscr{C}_m = \omega \log_2(1+\gamma_m)$, for all links $m \in \{u,d,b\}$. In particular, on the UL, the capacity depends on the set $\mathscr{U}$ of BSs whose interference can be suppressed and we explicitly write $\mathscr{C}_u(\mathscr{U})$. Moreover, the ergodic capacity shown in (2.72), i.e., the Shannon capacity averaged over the distribution of γ_m, provides upper bounds for the achievable data rates on a given link. We denote $\mathscr{R}_m$ the actual data rate chosen on link m and we have[2] that $\mathscr{R}_m \leq \mathscr{C}_m$. Notice that in this sense, the rate may be considered as equal or a fraction of the throughput in (2.74). In the following, we may omit the location of the scheduled user and write $\mathscr{R}_m(x) = \mathscr{R}_m(x,y)$, $m \in \{u,d\}$, when it is clear from the context.

5.3 Rate adaptation approach

5.3.1 Algorithm

Our goal is to minimize as much as possible the impact of $I_{\text{BS}}^{(u)}$ on the UL performance. Algorithm 1 shows the proposed approach. A BS $x \in \Phi$ proceeds as follows:

[1] In this chapter though, we do not refer to any duplex 'mode' as all BSs are in FD.

[2] In theory, any arbitrary data rate can be chosen strictly less than the capacity. In practice, a finite set of data rates are achievable. For simplicity, we assume a continuous set of available data rates less or equal to the link capacity.

Algorithm 1 FD-NOMA Rate Adaptation (run at BS x)

1: **Input**: Φ, M, $\nu^\star$
2: **Output**: $\mathscr{R}_d(x)$, $\mathscr{R}_u(x)$
3: **Init**: $J(x;M) \leftarrow \emptyset$
4: $I_M(x) \leftarrow$ BSs with the M smallest path-losses $L(x,x')$, $x' \in \Phi$
5: $I_M(x) \leftarrow \textsc{Sort}(I_M(x))$
6: Send message to $I_M(x)$
7: **for** Every message received from x'' **do**
8: $\quad J(x;M) \leftarrow J(x;M) \cup \{x''\}$
9: $\quad$ Estimate $h(x,x'')$
10: $\quad$ Compute $\mathscr{C}_b(x,x'')$ ▷ using the estimation of $h(x,x'')$ and (5.9)
11: **end for**
12: $\mathscr{C}_{\min}(x;M) \leftarrow \min\{C_b(x,x''), x'' \in J(x;M)\}$
13: Compute $\mathscr{C}_d(x)$ ▷ using DL SINR expression (5.2)
14: $\nu(x) \leftarrow$ (5.14)
15: $\mathscr{R}_d \leftarrow$ (5.13)
16: $\mathscr{U}(x) \leftarrow$ (5.15) ▷ using $\mathscr{R}_d(x')$, $x' \in I_M(x)$
17: $\mathscr{R}_u(x) \leftarrow$ (5.16)
18: **return** $\mathscr{R}_d$, $\mathscr{R}_u$

1. Let $I_M(x)$ be the set of the M strongest interfering BSs averaging out fast fading (step 4). With our channel model, $I_M(x)$ is also the set of M closest BSs. Let $J(x;M)$ be the set of BSs for which x is a strong interferer, i.e., $J(x;M) = \{x'' \in \Phi \,|\, x \in I_M(x'')\}$ (step 8). We estimate for every x'' the Shannon capacity between x and x'' (step 10). We define (step 12):

$$\mathscr{C}_{\min}(x;M) \triangleq \min_{x'' \in J(x;M)} \mathscr{C}_b(x,x''), \tag{5.12}$$

2. BS x chooses a DL rate as follows (step 15):

$$\mathscr{R}_d(x) = \nu(x)\,\mathscr{C}_d(x), \tag{5.13}$$

where (step 14)

$$\nu(x) \triangleq \max\left(\min\left(\frac{\mathscr{C}_{\min}(x;M)}{\mathscr{C}_d(x)}, 1\right), \nu^\star\right) \tag{5.14}$$

and $\nu^\star \in [0,1]$ is a system parameter that characterizes the maximum DL rate and $1-\nu^\star$ is the maximum loss factor tolerated by BS x on the DL. Let $\mathscr{U}$ be the set of BSs that can be decoded, i.e. (step 16),

$$\mathscr{U}(x) = \{x' \in I_M(x) \,|\, \mathscr{R}_d(x') \leq \mathscr{C}_b(x',x)\}. \tag{5.15}$$

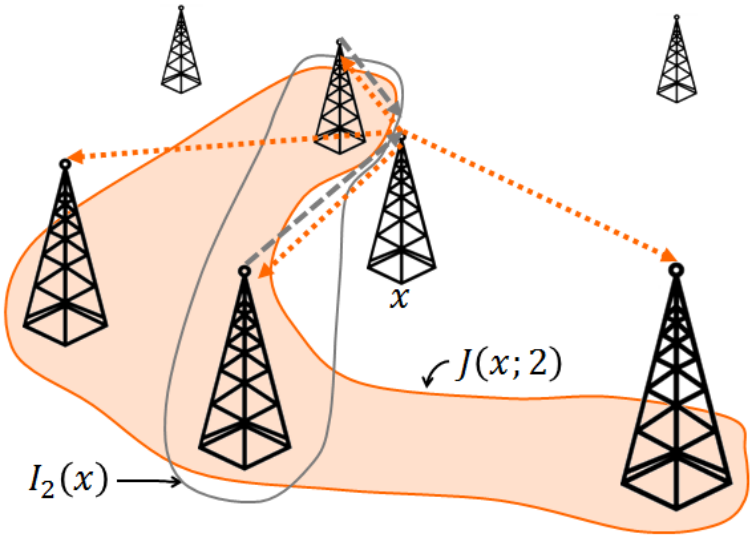

Fig. 5.1 Representation of the interference sets $I_M(x)$ and $J(x)$ for $M = 2$.

3. BS x chooses an UL rate as follows (step 17):

$$\mathscr{R}_u(x) = \mathscr{C}_u(x; \mathscr{U}(x)). \tag{5.16}$$

Before continuing, it is important to mention that in sequel when the context is clear we write $J(x) = J(x;M)$. Further, when x is the typical BS we write $\mathscr{R}_d^{(0)} \triangleq \mathscr{R}_d(0)$, $\mathscr{C}_d^{(0)} \triangleq \mathscr{C}_d(0)$ and $\mathscr{C}_{\min}^{(0)}(M) \triangleq \mathscr{C}_{\min}(0;M)$. Moreover, when the n-th neighbor of the typical BS located in x' is at a distance r, i.e., $d(0,x') = r$, then we write $\mathscr{C}_b^{(n)}(r) \triangleq \mathscr{C}_b^{(n)}(0,x')$, $\mathscr{C}_d(r) \triangleq \mathscr{C}_d(x')$ and $\mathscr{R}_d(r) \triangleq \mathscr{R}_d(x')$.

A graphical representation of the interference sets $I_M(x)$ and $J(x)$ for a BS $x \in \Phi$ is depicted in Fig. 5.1. In the figure, BSs that fall inside the region covered by the gray-bold line are the two closest and stronger interferers of the BS in x, i.e., they represent $I_2(x)$. The gray-dashed arrows represent their signals towards x and are the ones that might actually be cancelled due to our solution. In this regard, these signals can in fact be cancelled if their respective DL rates are lower than the capacity between them and the BS in x. Further, the BSs that fall inside the region covered by the orange surface are the BSs that are strongly interfered by the BS in x for the given value of M, i.e., $J(x)$. The orange-dotted arrows are the signals used for BSs in $J(x)$ to decide that x is a strong interferer.

Remark 5.3.1. *If $\mathscr{C}_{\min}(x) \geq \mathscr{C}_d(x)$, then BS x can be decoded by all BSs in $J(x)$, i.e., for which it is a strong interferer. In this case, there is no need to degrade the DL rate of BS x to allow SIC at the BSs it interferes, so that $\nu(x) = 1$ and $\mathscr{R}_d(x) = \mathscr{C}_d(x)$ in* (5.13) *and* (5.14)*.*

Remark 5.3.2. *If $\mathscr{C}_{\min}(x) < \mathscr{C}_d(x)$, BS x can choose to degrade its DL rate in order to be decoded by the BSs it interferes. The higher the degradation, the higher the number of BSs that will be able to suppress its interference. In this regard, $1-\nu^\star$ sets a maximum tolerable DL rate degradation. If additionally $\mathscr{C}_{\min}(x)/\mathscr{C}_d(x) \geq \nu^\star$, the BS can set its DL rate to $\mathscr{C}_{\min}(x)$ and still be decoded by all BSs in $J(x)$.*

Remark 5.3.3. *On the UL, the capacity depends on the ability of BS x to suppress the interference from BSs in $I_M(x)$ and, thus, depends in* (5.16) *on the set $\mathscr{U}(x)$.*

Remark 5.3.4. *When $\nu^\star = 0$, BSs accept any degradation on the DL and we have thus always $\mathscr{R}_d(x') \leq \mathscr{C}_b(x',x)$. As a consequence, $|\mathscr{U}(x)| = M$ and the M strongest interferers can be suppressed.*

5.3.2 Network topology

There are two possible architectures for the implementation of the proposed approach: a distributed architecture or a centralized radio access network (CRAN). In both cases, the estimation of channels $h(x,x')$ between two BSs (step 9) is based on pilot signals broadcast by every BS for its normal operation.

Distributed Architecture

In a distributed architecture, BSs are directly connected between them through a reliable and low latency transport network. In this scenario, the algorithm and the data processing are run at every BS, as suggested by Algorithm 1. The distributed approach allows a simplified

architecture because it does not involve any new equipment. It is scalable in the sense that the amount of calculations and message exchanges depends locally only on M. NOMA-SIC decoding is performed locally and so with no additional delay. However, it requires additional computation capability at every BS and computation power cannot be mutualized. At last, when new BSs are added or existing BSs are suppressed, this should be discovered by every neighboring BS. This process may take more time than in a centralized approach.

CRAN

Under a CRAN topology, a central entity manages the different BSs in a given area and run the proposed algorithm on behalf of them. This architecture reduces the amount of signalling as BSs communicate only with the CRAN. Processing powers can be mutualized. Any update in the number of BSs is easily taken into account by the algorithm. Among the drawbacks, an additional equipment is required and the communication between two neighboring CRANs should be managed. At last, the processing at the CRAN implies a delay that could be incompatible with low latency services.

5.4 Analytical performance analysis

5.4.1 Preliminary results

As Φ is a homogeneous PPP, we have that $f_R(r,n)$ in (2.19) represents the PDF of the distance between a typical BS and its n-th nearest neighbor. Moreover, since we consider that UL and DL users are independent PPs drawn inside the Voronoi cell of each BS, then we have that the distance distribution between a scheduled UE and its serving BS is given by $f_{R_0}(r)$ in (2.41) (following the result proposed in [47, Section II-G]).

5.4.2 Coverage probability

In this subsection, we derive the coverage probabilities for DL, BS-BS link and UL.

Dowlink coverage probability

Theorem 5.4.1 (Downlink coverage probability)**.** *The DL coverage probability of a typical user,* $\mathscr{P}_d(\Gamma) \triangleq \mathbb{P}(\gamma_d^{(0)} > \Gamma)$*, is given by:*

$$\mathscr{P}_d(\Gamma) = \int_0^\infty f_{R_0}(r)\mathscr{L}\{I_{\mathrm{BS}}^{(d)}\}(r,\Gamma)\mathscr{L}\{I_{\mathrm{UE}}^{(d)}\}(r,\Gamma)N_d(r,\Gamma)\mathrm{d}r, \tag{5.17}$$

where $N_d(r,\Gamma) = \exp\left(-\Gamma(\kappa r)^{\eta}\sigma^2(GP_d)^{-1}\right)$, f_{R_0} *is given by* (2.41), $\mu = P_u/P_d$ *and*

$$\mathscr{L}\left\{I_{BS}^{(d)}\right\}(r,\Gamma) = \exp\left(-2\pi\lambda\int_r^{\infty}\left(1-\exp\left(-\Gamma\frac{G'}{G}(r/z)^{\eta}\right)\right)z\mathrm{d}z\right), \tag{5.18}$$

$$\mathscr{L}\left\{I_{UE}^{(d)}\right\}(r,\Gamma) = \exp\left(-2\pi\int_0^{\infty}\lambda_u(z)\left(1-\exp\left(-\Gamma\mu\frac{\tilde{G}}{G}\frac{(\kappa r)^{\eta}}{(\tilde{\kappa}z)^{\tilde{\eta}}}\right)\right)z\mathrm{d}z\right), \tag{5.19}$$

$$\lambda_u(z) = \lambda\left(1-\exp\left(-(9/4)\sqrt{\lambda}z\right)+0.5\lambda z^2\exp\left(-(5/4)\lambda z^2\right)\right), \tag{5.20}$$

$$\mathscr{F}_d(r,\Gamma) \triangleq \mathscr{L}\{I_{\mathrm{BS}}^{(d)}\}(r,\Gamma)\mathscr{L}\{I_{\mathrm{UE}}^{(d)}\}(r,\Gamma)N_d(r,\Gamma). \tag{5.21}$$

Proof. The proof follows from Lemma 2.5.3. However, as done in [76, Section 2] and [77], in this chapter we neglect the effect of fast fading on the interference and replace it by its mean value. Thus, when computing $\mathscr{L}\{I_{\mathrm{BS}}^{(d)}\}(r,\Gamma)$ and $\mathscr{L}\{I_{\mathrm{UE}}^{(d)}\}(r,\Gamma)$ we do not take the expectation with respect to h. So, for instance, we skip (2.55d) in order to obtain (5.18) and, correspondingly, we do the same for (5.19). □

Remark 5.4.1. *In* (5.20) *we consider* (2.46) *to model the density of interfering UL users towards a typical UE.*

Remark 5.4.2. *Note that the DL coverage probability under our model is the same as the one achieved in a traditional FD network, where all BSs work under FD. In contrast, and as we will see further in Theorem 5.4.4, the DL rate does depend on M and* $\nu^{\star}$.

Remark 5.4.3. *Note that if* $I_{\mathrm{UE}}^{(d)} = 0$ *and* $\mathscr{L}\{I_{\mathrm{UE}}^{(d)}\} = 1$, *then* (5.17) *is exactly the DL coverage probability of a HD network, see e.g. results in Section 2.5.1 and Section 3.3.3. If UEs are able to beamform their signal with a very thin beam towards their serving BS,* $\tilde{G} \to 0$ *with a high probability and, according to* (5.19), $\mathscr{L}\{I_{\mathrm{UE}}^{(d)}\} \to 1$, *this shows that omnidirectional UE antennas represent a worst case for FD. In the same way, when* $\tilde{\eta} \to +\infty$, *i.e., when the environment between UEs in different cells is highly obstructed,* $\mathscr{L}\{I_{\mathrm{UE}}^{(d)}\} \to 1$.

Corollary 5.4.1. *The probability density function (PDF) of* $\gamma_d^{(0)}$ *is given by* $f_{\gamma_d^{(0)}}(\Gamma) \triangleq (\partial/\partial\Gamma)\,\mathbb{P}(\gamma_d^{(0)} \leq \Gamma) = (\partial/\partial\Gamma)\,1 - \mathscr{P}_d(\Gamma)$, *i.e.:*

$$\begin{aligned} f_{\gamma_d^{(0)}}(\Gamma) = \int_0^\infty f_{R_0}(r)\mathscr{F}_d(r,\Gamma)(\kappa r)^\eta \cdot \left[\frac{\sigma^2}{GP_d} + 2\pi\lambda\frac{G'}{G}\int_r^\infty \exp\left(-\Gamma\frac{G'}{G}(r/z)^\eta\right)\frac{z}{(\kappa z)^\eta}\mathrm{d}z \right. \\ \left. +2\pi\lambda\mu\frac{\tilde{G}}{G}\int_0^\infty \exp\left(-\Gamma\mu\frac{\tilde{G}}{G}\frac{(\kappa r)^\eta}{(\tilde{\kappa}z)^{\tilde{\eta}}}\right)\frac{z}{(\tilde{\kappa}z)^{\tilde{\eta}}}\mathrm{d}z\right]\mathrm{d}r, \end{aligned} \tag{5.22}$$

where $\mathscr{F}_d(r,\Gamma)$ *is found in* (5.21).

BS-to-BS coverage probability

Theorem 5.4.2 (BS-to-BS CCDF)**.** *The complementary CDF (CCDF) of the SINR between a typical BS and its n-th closest interfering BS, i.e.,* $\mathscr{P}_b^{(n)}(\Gamma) \triangleq \mathbb{P}(\gamma_b^{(n)} > \Gamma)$, *can be approximated by:*

$$\mathscr{P}_b^{(n)}(\Gamma) = \int_0^\infty f_R(r,n)\mathscr{F}_b^{(n)}(r,\Gamma)\mathrm{d}r, \tag{5.23}$$

where

$$\mathscr{F}_b^{(n)}(r,\Gamma) = \underbrace{\mathscr{L}\{I_{\mathrm{BS}}^{(n,1)}\}(r,\Gamma)\mathscr{L}\{I_{\mathrm{BS}}^{(n,2)}\}(r,\Gamma)}_{\mathscr{L}\{I_{\mathrm{BS}}^{(n)}\}(r,\Gamma)}\mathscr{L}\{I_{\mathrm{UE}}^{(b)}\}(r,\Gamma)N_b(r,\Gamma), \tag{5.24}$$

$N_b(r,\Gamma) \triangleq \exp\left(-\Gamma(\breve{\kappa}r)^{\breve{\eta}}(\breve{G}P_d)^{-1}(I_{\mathrm{RSI}} + \sigma^2)\right)$, f_R *is given by* (2.19) *and*

$$\mathscr{L}\left\{I_{\mathrm{BS}}^{(n,1)}\right\}(r,\Gamma) = \left[\int_0^r \exp\left(-\Gamma(r/z)^{\breve{\eta}}\right)\frac{2z}{r^2}\mathrm{d}z\right]^{(n-1)}, \tag{5.25}$$

$$\mathscr{L}\left\{I_{\mathrm{BS}}^{(n,2)}\right\}(r,\Gamma) = \exp\left(-2\pi\lambda\int_r^\infty\left(1-\exp\left(-\Gamma(r/z)^{\breve{\eta}}\right)\right)z\mathrm{d}z\right), \tag{5.26}$$

$$\begin{aligned} \mathscr{L}\left\{I_{\mathrm{UE}}^{(b)}\right\}(r,\Gamma) = &\mathbb{E}_{f_{R_0}}\left[\exp\left(-2\pi\lambda\int_0^{R_0}\left(1-\exp\left(-\Gamma\mu\frac{G}{\breve{G}}\frac{(\breve{\kappa}r)^{\breve{\eta}}}{(\kappa z)^\eta}\right)\right)z\mathrm{d}z\right)\right. \\ &\left.\exp\left(-2\pi\lambda\int_{R_0}^\infty\left(1-\exp\left(-\Gamma\mu\frac{G'}{\breve{G}}\frac{(\breve{\kappa}r)^{\breve{\eta}}}{(\kappa z)^\eta}\right)\right)z\mathrm{d}z\right)\right]. \end{aligned} \tag{5.27}$$

Proof. See Appendix A.1. □

Remark 5.4.4. *Note that when $G = G'$, then there is no need to compute two separate integrals in* (5.27)*. Hence, it is not necessary to calculate the expected value and it holds that:*

$$\mathscr{L}\left\{I_{\mathrm{UE}}^{(b)}\right\}(r,\Gamma) = \exp\left(-2\pi\lambda\int_0^{\infty}\left(1-\exp\left(-\Gamma\mu\frac{G'}{\breve{G}}\frac{(\breve{\kappa}r)^{\breve{\eta}}}{(\kappa z)^{\eta}}\right)\right)z\mathrm{d}z\right). \tag{5.28}$$

Corollary 5.4.2. *The probability density function (PDF) of $\gamma_b^{(n)}$ is given by $f_{\gamma_b^{(n)}}(\Gamma) \triangleq (\partial/\partial\Gamma)\,\mathbb{P}(\gamma_b^{(n)} \leq \Gamma) = (\partial/\partial\Gamma)\,1 - \mathscr{P}_b^{(n)}(\Gamma)$, which results in:*

$$\begin{aligned} f_{\gamma_b^{(n)}}(\Gamma) = \int_0^{\infty} f_R(r,n)\Bigg[\left(-\frac{\partial}{\partial\Gamma}\mathscr{L}\left\{I_{\mathrm{BS}}^{(n,1)}\right\}(r,\Gamma)\right)\mathscr{L}\left\{I_{\mathrm{BS}}^{(n,2)}\right\}(r,\Gamma)\mathscr{L}\left\{I_{\mathrm{UE}}^{(b)}\right\}(r,\Gamma)N_b(r,\Gamma) \\ \mathscr{F}_b^{(n)}(r,\Gamma)\left(2\pi\lambda\int_r^{\infty}\exp\left(-\Gamma\frac{r^{\breve{\eta}}}{z^{\breve{\eta}}}\right)\frac{r^{\breve{\eta}}}{z^{\breve{\eta}-1}}\mathrm{d}z + \frac{(\kappa r)^{\eta}}{\breve{G}P_d}\left(I_{\mathrm{RSI}}+\sigma^2\right)\right) \\ \left(-\frac{\partial}{\partial\Gamma}\mathscr{L}\left\{I_{\mathrm{UE}}^{(b)}\right\}(r,\Gamma)\right)\mathscr{L}\left\{I_{\mathrm{BS}}^{(n,1)}\right\}(r,\Gamma)\mathscr{L}\left\{I_{\mathrm{BS}}^{(n,2)}\right\}(r,\Gamma)N_b(r,\Gamma)\Bigg]\mathrm{d}r \end{aligned} \tag{5.29}$$

where

$$\frac{\partial}{\partial\Gamma}\mathscr{L}\left\{I_{\mathrm{BS}}^{(n,1)}\right\}(r,\Gamma) = -\frac{(n-1)}{\mathscr{L}\left\{I_{\mathrm{BS}}^{(n,1)}\right\}(r,\Gamma)}\int_0^{r}\exp\left(-\Gamma\frac{r^{\breve{\eta}}}{z^{\breve{\eta}}}\right)\frac{2r^{\breve{\eta}-2}}{z^{\breve{\eta}-1}}\mathrm{d}z, \tag{5.30}$$

$$\begin{aligned} \frac{\partial}{\partial\Gamma}\mathscr{L}\left\{I_{\mathrm{UE}}^{(b)}\right\}(r,\Gamma) = &-\mathbb{E}_{f_{R_0}}\left[\mathscr{E}_1(R_0,\Gamma)\mathscr{E}_2(R_0,\Gamma)2\pi\lambda\int_0^{R_0}\exp\left(-\Gamma\mu\frac{G}{\breve{G}}\frac{(\breve{\kappa}r)^{\breve{\eta}}}{(\kappa z)^{\eta}}\right)z\mu\frac{G}{\breve{G}}\frac{(\breve{\kappa}r)^{\breve{\eta}}}{(\kappa z)^{\eta}}\mathrm{d}z\right] \\ &-\mathbb{E}_{f_{R_0}}\left[\mathscr{E}_1(R_0,\Gamma)\mathscr{E}_2(R_0,\Gamma)2\pi\lambda\int_{R_0}^{\infty}\exp\left(-\Gamma\mu\frac{G'}{\breve{G}}\frac{(\breve{\kappa}r)^{\breve{\eta}}}{(\kappa z)^{\eta}}\right)z\mu\frac{G'}{\breve{G}}\frac{(\breve{\kappa}r)^{\breve{\eta}}}{(\kappa z)^{\eta}}\mathrm{d}z\right], \end{aligned} \tag{5.31}$$

$$\mathscr{E}_1(R_0,\Gamma) \triangleq \exp\left(-2\pi\lambda\int_0^{R_0}\left(1-\exp\left(-\Gamma\mu\frac{G}{\breve{G}}\frac{(\breve{\kappa}r)^{\breve{\eta}}}{(\kappa z)^{\eta}}\right)\right)z\mathrm{d}z\right), \tag{5.32}$$

$$\mathscr{E}_2(R_0,\Gamma) \triangleq \exp\left(-2\pi\lambda\int_{R_0}^{\infty}\left(1-\exp\left(-\Gamma\mu\frac{G'}{\breve{G}}\frac{(\breve{\kappa}r)^{\breve{\eta}}}{(\kappa z)^{\eta}}\right)\right)z\mathrm{d}z\right). \tag{5.33}$$

Uplink coverage probability

We could proceed and try to compute the UL coverage probability from the SINR expression in (5.5) by following similar steps as for the other cases, i.e., calculate the expected values and perform the PGFL of the PPPs. However, when doing so, we observe that $\mathscr{L}\{I_{\mathrm{BS}}^{(u)}(\mathscr{U})\}$ in (5.6) is equivalent to:

$$I_{\mathrm{BS}}^{(u)} = \sum_{x' \in \Phi} \breve{G} P_d L(x')^{-1} \mathbb{1}\left\{x' \neq \mathscr{U}(x)\right\}. \tag{5.34}$$

Hence, when developing the Laplace transform (expected value) we come across with the following expression:

$$\begin{aligned} \mathbb{E}_{I_{\mathrm{BS}}^{(u)}}\left[\exp\left(-\frac{\Gamma L(r)}{GP_u} I_{\mathrm{BS}}^{(u)}\right)\right] =& \mathbb{E}\left[\exp\left(-\Gamma \frac{L(r)\breve{G}}{G\mu} \sum_{x' \in \Phi} L(x')^{-1} \mathbb{1}\left\{x' \neq \mathscr{U}(x)\right\}\right)\right], \\ =& \mathbb{E}\left[\prod_{x' \in \Phi} \exp\left(-\Gamma \frac{L(r)\breve{G}}{G\mu} L(x')^{-1} \mathbb{1}\left\{x' \neq \mathscr{U}(x)\right\}\right)\right]. \end{aligned} \tag{5.35}$$

Given the difficulties to introduce the indicator function in (5.35) into the PGFL expression[3], we proceed by assuming that the process of interfering BSs is a thinned PPP with intensity $\lambda p(r)$, where $p(r)$ is the probability that a typical BS is not able to decode and suppress the interference coming from another BS located at a distance r. We further validate this assumption by simulations in Section 5.5.

In order to characterize $p(r)$, we observe that a BS at distance r from the typical BS, is not decoded either if it is farther than the M-th closest BS (as a BS can only decode BSs in its set I_M) or if its DL rate ($\mathscr{R}_d(r)$) is greater than the capacity between this BS and the typical BS. This translates as:

$$p(r) = \mathbb{P}(r > R_M) + \mathbb{P}(r \leq R_M \wedge \mathscr{R}_d(r) > \mathscr{C}_b(r)), \tag{5.36}$$

where R_M is the RV representing the distance from a typical BS to its M-th neighboring BS, which follows the distribution $f_R(r,M)$ in (2.19).

Remark 5.4.5. *By considering Remark 5.3.4, we know that when $\nu^\star = 0$, it holds that $\mathscr{R}_d(r) \leq \mathscr{C}_b(r)$ and the typical BS can cancel the interference from all BSs in its set $I_M(\cdot)$.*

[3] In the other cases the indicator function argument only depends on the distance, yet here it depends as well on $\mathscr{U}$. See for instance the proof of Theorem 5.4.1.

Then, we have in (5.36) *that:* $\mathbb{P}(r \leq R_M \wedge \mathscr{R}_d(r) > \mathscr{C}_b(r)) = 0$. *Hence we can directly write* $p(r)$ *as:*

$$p(r) = \mathbb{P}(r > R_M) = 1 - \mathbb{P}(r \leq R_M) = 1 - \int_r^{\infty} f_R(z, M)\mathrm{d}z = 1 - \frac{\Gamma(M, \lambda\pi r^2)}{(M-1)!} \tag{5.37}$$

where $f_R(z, M)$ *is known from* (2.19).

When considering any value of $\nu^\star$, $p(r)$ can be further developed as:

$$\begin{aligned}
p(r) &= \mathbb{P}(r > R_M) + \mathbb{P}(r \leq R_M \wedge \mathscr{R}_d(r) > \mathscr{C}_b(r)), && \text{(5.38a)}\\
&= \mathbb{P}(r > R_M) + \mathbb{P}(r \leq R_M)\mathbb{P}(\mathscr{R}_d(r) > \mathscr{C}_b(r)), && \text{(5.38b)}\\
&= \mathbb{P}(r > R_M) + \mathbb{P}(r \leq R_M) \sum_{n=1}^{\infty} \mathbb{P}(\mathscr{R}_d(r) > \mathscr{C}_b^{(n)}(r)|n)\mathbb{P}(n-1) && \text{(5.38c)}\\
&= \mathbb{P}(r > R_M) + \mathbb{P}(r \leq R_M) \sum_{n=1}^{M} \mathbb{P}(\mathscr{R}_d(r) > \mathscr{C}_b^{(n)}(r)|n \leq M)\mathbb{P}(n-1), && \text{(5.38d)}
\end{aligned}$$

where (5.38b) is given by assuming that r and the DL rate at the BS in r, i.e., $\mathscr{R}_d(r)$, are independent, (5.38c) is by using the total probability Theorem, where $\mathbb{P}(n-1)$ is the probability of having exactly $(n-1)$ BSs in the disk of radius r (which is a Poisson RV, see (2.15)). Moreover, (5.38d) is due to the fact that by construction, there is only M BSs in the disk described by R_M.

Now, we know that for a BSs $x \in \Phi$, $\nu(x)$ in (5.14) can take three different values, which are described by the three following events:

$$\begin{aligned}
&E_1 : \nu(x) = \nu^\star, \text{ occurs when } \mathscr{C}_{\min}(x;M) < \mathscr{C}_d(x) \text{ and } \frac{\mathscr{C}_{\min}(x;M)}{\mathscr{C}_d(x)} \leq \nu^\star,\\
&E_2 : \nu(x) = \frac{\mathscr{C}_{\min}(x;M)}{\mathscr{C}_d(x)}, \text{ occurs when } \mathscr{C}_{\min}(x;M) < \mathscr{C}_d(x) \text{ and } \frac{\mathscr{C}_{\min}(x;M)}{\mathscr{C}_d(x)} > \nu^\star,\\
&E_3 : \nu(x) = 1, \text{ occurs when } \mathscr{C}_{\min}(x;M) \geq \mathscr{C}_d(x).
\end{aligned} \tag{5.39}$$

By analyzing a typical BS, we find general expressions for the probability of occurrence of each of these events, i.e.:

$$\mathbb{P}(E_1) \triangleq P_1(M) = \mathbb{P}\left(\mathscr{C}_{\min}^{(0)}(M) \leq \nu^\star \mathscr{C}_d^{(0)}\right), \tag{5.40}$$

$$\mathbb{P}(E_2) \triangleq P_2(M) = \mathbb{P}\left(\nu^\star \mathscr{C}_d^{(0)} < \mathscr{C}_{\min}^{(0)}(M) < \mathscr{C}_d^{(0)}\right), \tag{5.41}$$

$$\mathbb{P}(E_3) \triangleq P_3(M) = \mathbb{P}\left(\mathscr{C}_{\min}^{(0)}(M) \geq \mathscr{C}_d^{(0)}\right). \tag{5.42}$$

Hence, if we use the law of total probabilities, we can expand $p(r)$ in (5.38d) as:

$$\begin{aligned} p(r) = \mathbb{P}(r \leq R_M) \sum_{n=1}^{M} \Bigg[& \underbrace{\mathbb{P}\left(\nu^\star \mathscr{C}_d(r) > \mathscr{C}_b^{(n)}(r) \middle| n \leq M, \mathscr{C}_{\min}^{(0)}(M) \leq \nu^\star \mathscr{C}_d(r)\right)}_{\text{Term } E_1} P_1(M) \\ & + \underbrace{\mathbb{P}\left(\mathscr{C}_{\min}^{(0)}(M) > \mathscr{C}_b^{(n)}(r) \middle| n \leq M, \nu^\star \mathscr{C}_d(r) \leq \mathscr{C}_{\min}^{(0)}(M) \leq \mathscr{C}_d(r)\right)}_{\text{Term } E_2} P_2(M) \\ & + \underbrace{\mathbb{P}\left(\mathscr{C}_d(r) > \mathscr{C}_b^{(n)}(r) \middle| n \leq M, \mathscr{C}_{\min}^{(0)}(M) \geq \mathscr{C}_d(r)\right)}_{\text{Term } E_3} P_3(M) \Bigg] \frac{(\lambda \pi r^2)^{(n-1)}}{(n-1)!} \mathrm{e}^{-\lambda \pi r^2} + \mathbb{P}(r > R_M). \end{aligned} \tag{5.43}$$

However, we observe that there are possible simplifications in 'Term E_2' and 'Term E_3'. In the first place, for 'Term E_2', by knowing that $n \leq M$, then $\mathscr{C}_{\min}^{(0)}(M) \leq \mathscr{C}_b^{(n)}$, $\forall n$. Hence, the probability that $\mathscr{C}_{\min}^{(0)}(M) > \mathscr{C}_b^{(n)}(r)$ is zero. On the other hand, for 'Term E_3', we have that the second condition states that $\mathscr{C}_{\min}^{(0)}(M) \geq \mathscr{C}_d(r)$. Thus, $\mathbb{P}(\mathscr{C}_d(r) > \mathscr{C}_b^{(n)}) = 0$. Therefore, $p(r)$ results in:

$$p(r) = \mathbb{P}(r > R_M) + \mathbb{P}(r \leq R_M) \sum_{n=1}^{M} \mathbb{P}\left(\nu^\star \mathscr{C}_d(r) > \mathscr{C}_b^{(n)}(r)\right) P_1(M) \frac{(\lambda \pi r^2)^{(n-1)}}{(n-1)!} \mathrm{e}^{-\lambda \pi r^2}. \tag{5.44}$$

Remark 5.4.6. *Notice that by setting $\nu^\star = 0$ in* (5.44)*, we also obtain* (5.37)*.*

Remark 5.4.7. *For a fixed value of M, $P_1(M)$ and $\mathbb{P}(\nu^\star \mathscr{C}_d(r) > \mathscr{C}_b^{(n)}(r))$ increase with $\nu^\star$. Hence, $p(r)$ increases as well, i.e., it is less probable that a BS can decode its interferers when $\nu^\star$ is high. Therefore, low values of $\nu^\star$ are preferable to enhance the UL performance.*

Remark 5.4.8. *Let us notice that $p(r) \geq 1 - \mathbb{P}(r \leq R_M)$. This is obvious since we cannot decode more than M BSs. Moreover, since $\mathbb{P}(r \leq R_M)$ is a monotonically increasing function of r, then for $\nu^\star = 0$, $p(r)$ is monotonically decreasing.*

Finally, since we assume that PPPs of scheduled users and BSs are independent, we can consider that the DL capacity of the BS in r, i.e., $\mathscr{C}_d(r)$, distributes as $\mathscr{C}_d^{(0)}$. Therefore, we write:

$$\mathbb{P}\left(\nu^\star \mathscr{C}_d(r) > \mathscr{C}_b^{(n)}(r)\right) = \mathbb{P}\left(\nu^\star \mathscr{C}_d^{(0)} > \mathscr{C}_b^{(n)}(r)\right) \tag{5.45a}$$

$$= \mathbb{P}\left(\nu^\star \log_2\left(1+\gamma_d^{(0)}\right) > \log_2\left(1+\gamma_b^{(n)}(r)\right)\right), \tag{5.45b}$$

$$= 1 - \mathbb{P}\left(\gamma_b^{(n)}(r) > \left(1+\gamma_d^{(0)}\right)^{\nu^\star} - 1\right), \tag{5.45c}$$

$$= 1 - \mathbb{E}_{\gamma_d^{(0)}}\left[\mathscr{F}_b^{(n)}\left(r, \left(1+\gamma_d^{(0)}\right)^{\nu^\star} - 1\right)\right], \tag{5.45d}$$

where $\mathscr{F}_b^{(n)}(\cdot,\cdot)$ is defined in (5.24) and we can substitute (5.45d) in (5.44). With this, we can proceed with the following theorem.

Theorem 5.4.3 (UL Coverage Probability)**.** *The UL coverage probability of a typical BS, $\mathscr{P}_u(\Gamma) \triangleq \mathbb{P}(\gamma_u^{(0)} > \Gamma)$, can be approximated by:*

$$\mathscr{P}_u(\Gamma) = \int_0^\infty f_{R_0}(r)\mathscr{L}\left\{I_{BS}^{(u)}(\mathscr{U})\right\}(r,\Gamma)\mathscr{L}\left\{I_{UE}^{(u)}\right\}(r,\Gamma)N_u(r,\Gamma)\mathrm{d}r, \tag{5.46}$$

where $N_u(r,\Gamma) = \exp\left(-\Gamma(\kappa r)^\eta (GP_u)^{-1}(I_{RSI}+\sigma^2)\right)$, f_{R_0} is given by (2.41) *and*

$$\mathscr{L}\left\{I_{UE}^{(u)}\right\}(r,\Gamma) = \exp\left(-2\pi\int_0^\infty \lambda_u^{(BS)}(z)\left(1-\exp\left(-\Gamma\frac{G'}{G}(r/z)^\eta\right)\right)z\mathrm{d}z\right), \tag{5.47}$$

$$\mathscr{L}\left\{I_{BS}^{(u)}(\mathscr{U})\right\}(r,\Gamma) = \exp\left(-2\pi\lambda\int_0^\infty p(z)\left(1-\exp\left(-\Gamma\frac{\breve{G}}{G\mu}\frac{(\kappa r)^\eta}{(\breve{\kappa}z)^{\breve{\eta}}}\right)\right)z\mathrm{d}z\right), \tag{5.48}$$

$$\lambda_u^{(\mathrm{BS})}(z) = \lambda\left(1-\exp\left(-(13/2)\lambda z^2\right) + (2/7)\lambda z^2\exp\left(-(13/9)\lambda z^2\right)\right). \tag{5.49}$$

Proof. See Appendix A.2. □

Remark 5.4.9. *In* (5.49) *we consider* (2.47) *to model the density of interfering UL users towards a typical BS.*

Remark 5.4.10. *For $\nu^\star = 0$, when $M \to \infty$, then $\mathbb{P}(r \leq R_M) \to 1$. Hence, $p(r) \to 0$, i.e., there is no BS-to-BS co-channel interference since for this scenario $\mathscr{L}\{I_{BS}^{(u)}(\mathscr{U})\}(r,\Gamma) = 1$ and we obtain the maximum performance for ULs.*

The UL coverage probability of Theorem 5.4.3 can be computed as soon as the distribution of $\mathscr{C}_{\min}(M)$ in $P_1(M)$ is available (see (5.40)). Given the technical difficulties to derive this distribution, we rely in the next section on an approximation.

5.4.3 Approximation of the distribution of $\mathscr{C}_{\min}$

For our approximation, we assume that for a given value of M, the following holds:

$$\mathscr{C}_{\min}^{(0)}(M) \approx \mathscr{C}_b^{(M')}, \tag{5.50}$$

where M' is an integer. This approximation is sustained by numerical observations and we will provide the mapping between M and M' in Section 5.5 for our simulation parameters.

Under the previous assumption, we have that $P_1(M)$, $P_2(M)$ and $P_3(M)$ in (5.40), (5.41) and (5.42), respectively, result in:

$$P_1(M) \approx 1 - \mathbb{E}_{\gamma_d^{(0)}}\left[\mathscr{P}_b^{(M')}\left(\left(1+\gamma_d^{(0)}\right)^{\nu^\star} - 1\right)\right], \tag{5.51}$$

$$P_2(M) \approx \mathbb{E}_{\gamma_d^{(0)}}\left[\mathscr{P}_b^{(M')}\left(\left(1+\gamma_d^{(0)}\right)^{\nu^\star} - 1\right)\right] - \mathbb{E}_{\gamma_d^{(0)}}\left[\mathscr{P}_b^{(M')}\left(\gamma_d^{(0)}\right)\right], \tag{5.52}$$

$$P_3(M) \approx \mathbb{E}_{\gamma_d^{(0)}}\left[\mathscr{P}_b^{(M')}\left(\gamma_d^{(0)}\right)\right]. \tag{5.53}$$

5.4.4 Average data rates

Theorem 5.4.4 (Average DL rate)**.** *The average DL data rate is given by:*

$$\mathbb{E}[\mathscr{R}_d] = \overline{\mathscr{C}}_{\min}^{(0)}(M)P_2(M) + \overline{\mathscr{C}}_d^{(0)}\left(\nu^\star P_1(M) + P_3(M)\right) \tag{5.54}$$

where

$$\overline{\mathscr{C}}_d^{(0)} = \omega \mathbb{E}\left[\log_2\left(1+\gamma_d^{(0)}\right)\right] = \omega \int_0^{\infty} \frac{\mathscr{P}_d(\Gamma)}{\log(2)(1+\Gamma)} \mathrm{d}\Gamma, \tag{5.55}$$

$$\overline{\mathscr{C}}_{\min}^{(0)}(M) = \mathbb{E}\left[\mathscr{C}_{\min}^{(0)}(M)\right] \approx \omega \mathbb{E}\left[\log_2\left(1+\gamma_b^{(M')}\right)\right] = \omega \int_0^{\infty} \frac{\mathscr{P}_b^{(M')}(\Gamma)}{\log(2)(1+\Gamma)} \mathrm{d}\Gamma. \tag{5.56}$$

Proof. See Appendix A.3. □

Remark 5.4.11. *For $M \to \infty$, we have that $\overline{\mathscr{C}}_{\min} \to 0$. Thus, $P_3(M) \to 0$, $P_1(M) \to 1$, and* (5.54) *results in:*

$$\mathbb{E}[\mathscr{R}_d] = \overline{\mathscr{C}}_d^{(0)} \nu^{\star}. \tag{5.57}$$

Hence, we obtain that the mean DL rate is directly proportional to $\nu^{\star}$. In the general case, for a fixed M, the mean DL rate is an increasing function of $\nu^{\star}$ since P_1 is non-decreasing and P_2 is non-increasing with $\nu^{\star}$.

Remark 5.4.12. *For $\nu^{\star} = 1$, $P_2(M) = 0$ and $P_3(M) = 1 - P_1(M)$. Thus,* (5.54) *becomes:*

$$\mathbb{E}[\mathscr{R}_d] = \overline{\mathscr{C}}_d^{(0)}, \tag{5.58}$$

which is independent of M and equivalent to the mean channel capacity of a FD network (i.e. maximum achievable DL rate under our setting). This reaffirms the zero degradation loss tolerance imposed by a value of $\nu^{\star} = 1$.

Theorem 5.4.5 (Average UL rate)**.** *Since for all BS $x \in \Phi$, $\mathscr{R}_u(x) = \mathscr{C}_u(x; \mathscr{U}(x))$, the average UL rate and capacity are the same. In this regard, we have that:*

$$\mathbb{E}[\mathscr{R}_u] = \overline{\mathscr{C}}_u^{(0)} = \omega \int_0^{\infty} \frac{\mathscr{P}_u(\Gamma)}{\ln(2)(1+\Gamma)} d\Gamma. \tag{5.59}$$

Proof. Similar to (5.55). See Appendix A.3 for further details. □

5.5 Simulation and performance evaluation

In this Section we study the performance of the proposed model under realistic network parameters and we validate the assumptions made to derive the mathematical model, i.e.:

- The scheduled UL and DL UEs locations are modeled by homogeneous PPPs of intensity λ. In simulations, DL and UL UEs are drawn uniformly in the Voronoi cell of every BS.
- The point process of interfering BSs of a typical BS is given by thinning Φ according to the probability $p(r)$ of retaining a point at a distance r. In the simulations, the sets I_M and J are built according to Algorithm 1.
- $\mathscr{C}_{\min}(M)$ is approximated by $\mathscr{C}_b^{(M')}$ for some mapping between M and M'. In the simulation, we compute exactly $\mathscr{C}_{\min}(M)$.
- Antenna gains between equipment are calculated by computing average gains.

5.5.1 Simulation settings

As we have seen in Chapters 2, 3 and 4, cases in which BSs are not capable of steering their beams towards their intended users (omnidirectional antennas), represent a 'worst case scenario' for FD deployments, since the co-channel interference is high in this type of networks. This is specially harmful, as the BS-to-BS interference critically impacts the UL performance and even when the DL performance is enhanced with respect to HD, the gains could still be higher and profit from lower interference and/or higher received signal powers. We take as a base the latter case to validate our mathematical development and analyze the effectiveness of our algorithm. In this sense, we study the impact of the two parameters that characterize our solution, i.e., $\nu^\star$ and M, on the performance of ULs and DLs.

We later examine the effectiveness of our algorithm for different RSI levels. Finally, we continue with analyzing the performance of our model under the scenario in which BSs are able to perform beamforming towards their scheduled users. For this case, we use as benchmark the antenna parameters of BSs in Chapter 4 (see Table 4.1), i.e., $G^{(\max)} = 20$ dBi, $G^{(\min)} = -10$ dBi and $\Theta_d = 30^\circ$.

We simulate a network according to the values found in Table 5.1, which are based on [78, 79]. According to these references, we consider the urban micro (UMi) case model with NLOS channels. These types of channels are considered due to the low probability of being in LOS in UMi (since it is given by $p_{\text{LOS}}(r) = \min(18/r, 1)(1 - \exp(-r/36)) + \exp(-r/36)$, as in Section 4.5). Moreover, the values of $(\kappa, \tilde{\kappa}, \check{\kappa})$ and $(\eta, \tilde{\eta}, \check{\eta})$ are calculated

Table 5.1 General simulation parameters

Parameter	Value	Parameter	Value
f_c	3.5 GHz	W	100 MHz
ω	360 kHz	R_c	100 m
Noise density	-174 dBm/Hz	Noise figure	8 dB
UE height	1.5 m	BS height	10 m
P_u	23 dBm	G_u	0 dBi
P_d	30 dBm	β	-110 dB
$G_d^{(\max)}$	20 dBi	$G_d^{(\min)}$	-10 dBi
Θ_d	30°	(κ, η)	(9.18, 3.53)
$(\check{\kappa}, \check{\eta})$	(7.77, 3.53)	$(\tilde{\kappa}, \tilde{\eta})$	(κ, η)

by using the UMi-NLOS path-loss expression in [79, Section 7.4], i.e., $35.3\log_{10}(r)+22.4+21.3\log_{10}(f_c)-0.3(h_{Rx}-1.5)$, where h_{Rx} is the receiver height. It is important to highlight that the UMi-NLOS path-loss model is also considered for BS-to-BS links. This sis due to the fact that SC BSs are usually deployed below roof tops, which also decreases the likelihood of having LOS links.

5.5.2 Model validation

The performance of the BS-to-BS CCDF introduced in (5.23) is shown Fig. 5.2. We can firstly notice that there is a gap between theory and simulation for $n = 1$. Let us recall that when analyzing the BS-to-BS CCDF, the interference is computed by considering all UL users and by dividing the interference of BSs in two subsets: one for the BSs in between the typical BS and its n-th neighbor[4], and other for the rest of the interfering BSs. Hence, we can observe that with our mathematical approach, when $n = 1$, it holds for set of interfering BSs inside the disk of radius R_M that $\mathscr{L}\{I_{\text{BS}}^{(n,1)}\} = 1$ (see (5.25)). This means that the previous term does not impacts the BS-to-BS performance. However, to compute the interference component regarding the all other BSs, i.e., $\mathscr{L}\{I_{\text{BS}}^{(n,2)}\}$, we have an integral evaluated from r to $+\infty$. Thus, the n-th closest neighboring BS, which is in fact at a distance r from the typical BS ends up interfering as well. Consequently, we consider for this case significantly more interference than the one that is actually received by the typical BS, reason why we obtain a lower performance through the theoretical curve. For values of $n > 1$, results match well, validating the assumptions regarding the position of active UEs and the independence between the interference generated by UL users and BSs. Moreover, we observe that the

[4] BSs inside the disk of radius R_M.

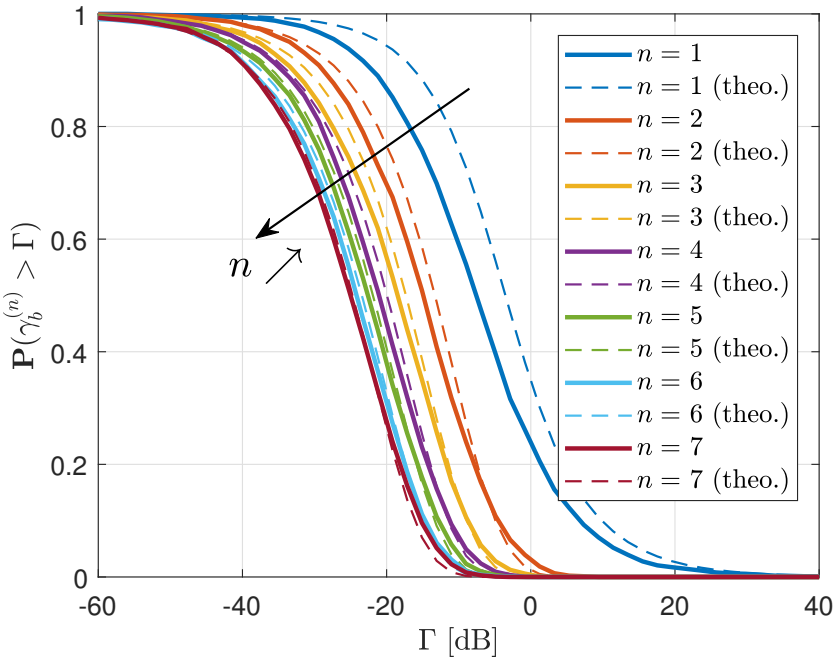

Fig. 5.2 BS-to-BS coverage probability for different values of n, where the bold lines are for simulations and dashed lines for analytical results.

performance decreases with n. This is evident since both base stations are farther apart between each other.

Fig. 5.3 shows the distribution of $\mathscr{C}_{\min}(M)$, obtained by simulations and the theoretical value of $\mathscr{C}_b^{(M')}$, which is obtained by computing $\mathbb{P}(\log(1+\gamma_b^{(M')}))$ (see (5.23)). Firstly, we observe that theory and simulations match well for each pair M and M'. Particularly, we notice that when $M \leq 3$, it holds that $M' = M$. However, for greater values of M, e.g. for $M = \{4,5\}$, we have that $M' > M$, implying that as M increases, $\mathscr{C}_{\min}(M)$ decreases with a higher rate than $\mathscr{C}_b^{(M)}$. This is due to the fact that for each BS in x, $\mathscr{C}_{\min}(x;M)$ depends on the size of the set $J(x;M)$ as seen in (5.12), i.e., the set of BSs for which the BS in x is a strong interferer. Indeed, the size of this set is not necessarily equal to M, as it is in fact the case for the set $I_M(\cdot)$. For instance, we know that when we compute $\mathscr{C}_b^{(M)}$, the capacity corresponds to the one between a BS and its M-th closest neighbor. But, on the other hand, for the same value of M, when we calculate $\mathscr{C}_{\min}(M)$, we do not necessarily compute the capacity to M-th closest neighbor. In fact, it can correspond to a BS placed at a greater distance than R_M. Unfortunately, even when we can find a good mapping for the values of M and their corresponding M', we cannot assure that the relationship observed in Fig. 5.3 will be the same for another set of network parameters. Hence, for a different configuration we would have to proceed to map the values of M and M' again.

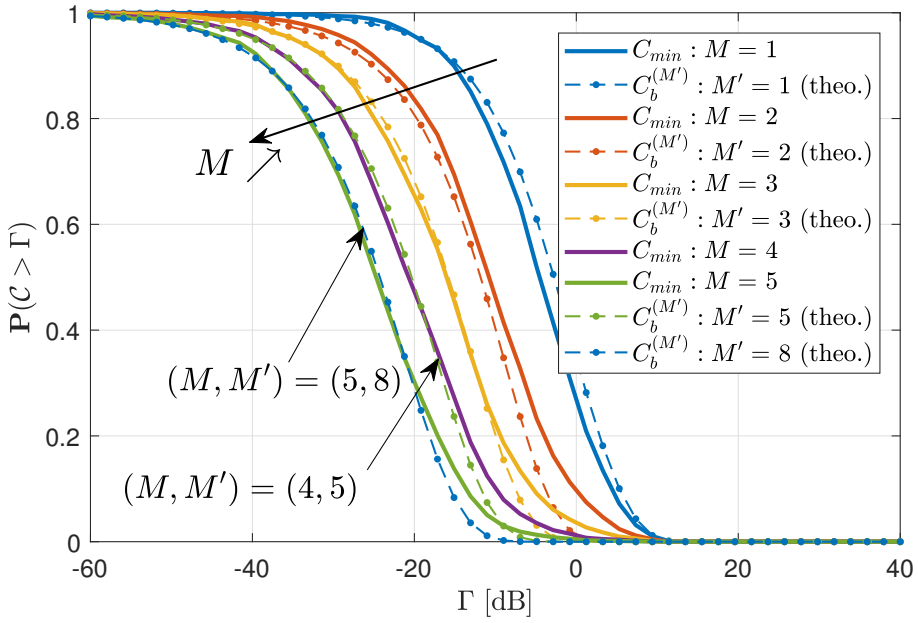

Fig. 5.3 Mapping between $\mathscr{C}_{\min}(M)$ and $\mathscr{C}_b^{(M')}$, where the bold lines are for simulations of $\mathscr{C}_{\min}$ and the marked-dashed lines for analytical results.

We plot in Fig. 5.4 $p(r)$ as a function of r for $v^\star = 0$ and $v^\star = 0.1$. Simulated-based results are obtained by actually computing the probability that a typical BS is not able to decode another BS located at a distance $\|r + \Delta r\|$, where $\Delta r > 0$. For the analytical results we use (5.44) and the mapping between M and M' in Fig. 5.3 to approximate $P_1(M)$ in (5.51). For both values of $v^\star$, $v^\star = 0$ in Fig. 5.4 (a) and $v^\star = 0.1$ in Fig. 5.4 (b), we can see that the probability of not being decodable increases with r. This is logical, given that the probability of being outside the disk described by the radius R_M is high when the value of r is high. Particularly, for the behavior of $p(r)$ when $v^\star = 0$, we see that the probability of being able to decode a BS increases with M. This, since for $v^\star = 0$, the only condition needed for an interfering BS to be decoded is to be inside the disk described by R_M. Hence, the greater the value of M, the greater the probability to be inside the disk, i.e., the lower the value of $p(r)$.

On the other hand, for $v^\star = 0.1$ in Fig. 5.4 (b), we observe that results have the same behavior for $M = \{1, 2, 3, 4\}$, even when the gap between curves slightly increases for the last value. For $M = 5$ the analytical curve behaves differently between $150 \leq r \leq 200$ m. However, the overall behavior is similar, which validates our approach (i.e., thinning of the process of interfering BSs according to $p(r)$). Further, we can see that by omitting the setting in which $M = 1$ and by particularly focusing in small distances, e.g. $0 \leq r \leq 100$, the probability of being able to decode a BS does not increase with M. This is different to

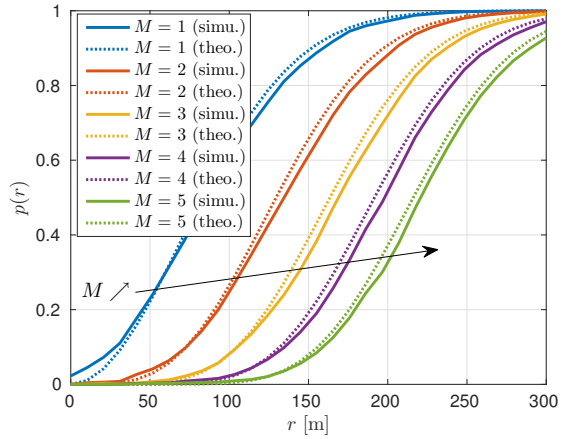

(a) $\nu^\star = 0$.

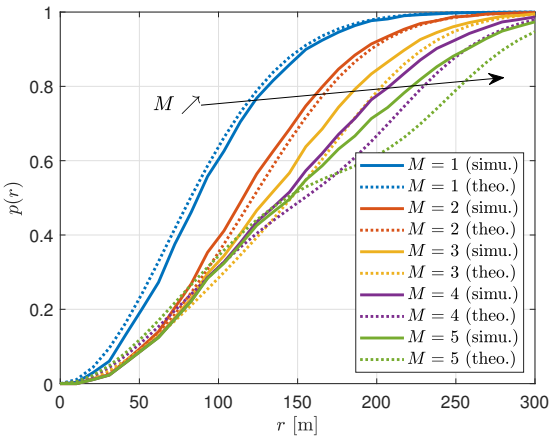

(b) $\nu^\star = 0.1$.

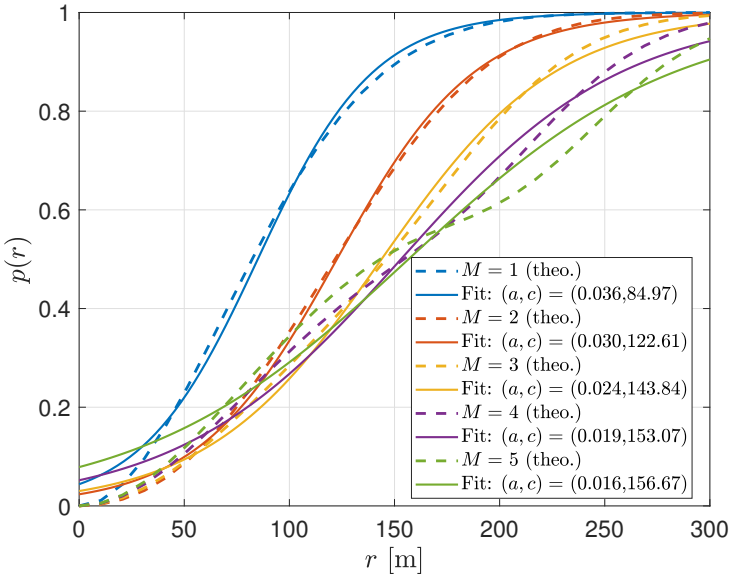

(c) Sigmoid function fitting for $\nu^\star = 0.1$.

Fig. 5.4 Behavior of $p(r)$, i.e., probability of not being able to decode a BS at a distance r. (a) is for $\nu^\star = 0$, (b) is for $\nu^\star = 0.1$ and (c) is the result after fitting the theoretical result for $\nu^\star = 0.1$ with a simple sigmoid function.

what it is observed for $\nu^\star = 0$. This can be explained since for this regime a BS is with high probability inside the disk of radius R_M, thus the value of $p(r)$ in (5.44) is mostly dictated by $\mathbb{P}(\nu^\star \mathscr{C}_d(r) > \mathscr{C}_b^{(n)}(r))$, which decreases with M. However, when r is large, e.g. $r \geq 200$, $p(r)$ mostly depends on the probability of being inside the disk of radius R_M. Then, the probability of decoding a BS increases with M, since for a fixed value of r, $p(r)$ decreases with M.

When $\nu^\star = 0$, $p(r)$ does not have a complex expression (see Remark 5.4.5). Thus, we can directly proceed to evaluate the UL coverage probability. However, for all values of $\nu^\star \neq 0$, the analytical expression of $p(r)$ is complex. Therefore, obtaining its numerical value is a time consuming task, which makes it difficult for us to study the UL coverage probability in (5.46). By analyzing Fig. 5.4 (b) however, we can note that the behavior of $p(r)$ can eventually be approximated by a simpler function. In this regard, we fit $p(r)$ with a sigmoid

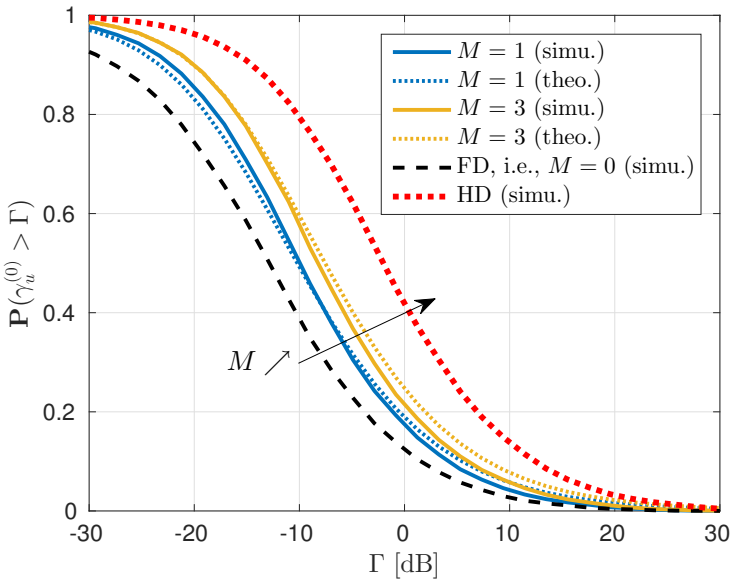

(a) $\nu^\star = 0$.

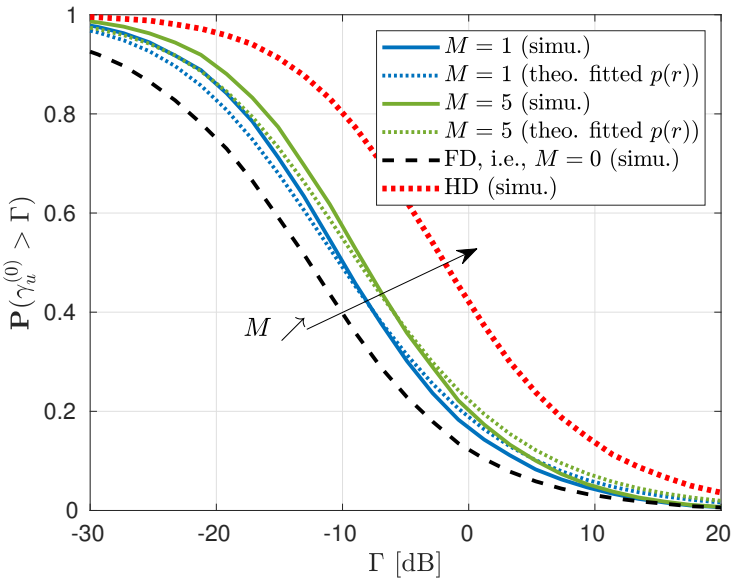

(b) $\nu^\star = 0.1$ and $p(r)$ fitted with sigmoid function.

Fig. 5.5 UL coverage probability for $\nu^\star = 0$ and $\nu^\star = 0.1$, and different values of M.

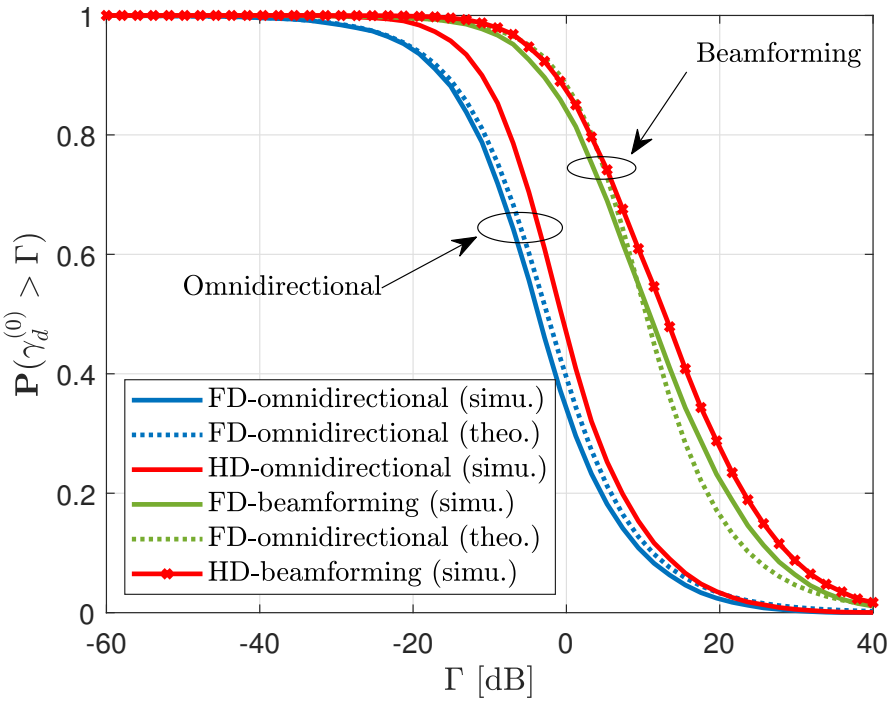

Fig. 5.6 DL coverage probability for BSs with omnidirectional and beamforming-capable antennas.

function $1/(1+\exp(-a(r-c)))$, where a and c are constants. We plot in Fig. 5.4 (c) the resulting curves for the different values M. We will now validate this simplification by studying the UL coverage probability.

The UL coverage probability for $v^\star = 0$ and $v^\star = 0.1$ are shown in Fig. 5.5. For $v^\star = 0$ in Fig. 5.5 (a) we compute $p(r)$ by using (5.37). For $v^\star = 0.1$ in Fig. 5.5 (b), we proceed by using the simplified version of $p(r)$ obtained by fitting it with the sigmoid function (see Fig. 5.4 (c)). Firstly, we observe that for both cases, results match well. For $v^\star = 0.1$, analytical curves experience a slightly lower coverage probability than simulations for low SINR values, e.g. -30 dB $\leq \Gamma \leq -10$ dB. This can be explained since the fitted functions for $M = 1$ and $M = 5$ are moderately higher than $p(r)$ for small values of r, to some degree increasing the interfering of BSs. Moreover, we can appreciate from both figures that the coverage probability is improved as M increases. However, when analyzing Fig. 5.5 (b), we notice that when $v^\star = 0.1$, even though we obtain performance gains when varying the value of M from $M = 1$ to $M = 5$, there is actually not a significant difference between the two scenarios. This shows that since BS antennas are omnidirectional, in order to further improve the UL coverage probability by using our algorithm, it is necessary to consider very high values of M. Yet, as we will discuss below, reasonable and realistic values of M actually

allow to considerably enhance the average UL data rate with respect to the traditional FD case.

Interestingly though, we note that even with a value of $M = 1$, a gain of 3 dB is already obtained with respect to the traditional FD network (for both cases). In fact, $\nu^\star = 0$ and $\nu^\star = 0.1$ have close UL coverage probability performances for $M = 1$. Yet, we see that if we set $\nu^\star = 0$ and $M = 3$, the UL coverage probability is slightly higher than the one achieved when fixing $\nu^\star = 0.1$ and $M = 5$. This effect will be later discussed when analyzing the mean UL rate.

Finally, we plot in Fig. 5.6 the DL coverage probability, where we notice that analytical and simulation results match well for both omnidirectional and beamforming cases. This is not actually a new result for us (with respect to the previous chapters), since we can recall that the DL coverage is independent of M and $\nu^\star$.

5.5.3 Impact of $\nu^\star$ and M

The mean UL rate as a function of M, for different values of $\nu^\star$, is depicted in Fig. 5.7 (a). Firstly, we see that FD (i.e., $M = 0$) has a performance 38% lower than that of HD. Moreover, and as expected from the previous analysis (see for example Remark 5.4.7) we notice that the UL data rate is enhanced as $\nu^\star$ decreases, since this reduces the DL rate, allowing to decode more BS-to-BS unwanted signals. In fact, we observe that for very low values of $\nu^\star$, e.g. $\nu^\star \leq 0.06$ it is even possible to outperform the HD performance. Hence, the HD data rate does not acts as an upper bound when implementing our solution. In this regard, we see that the mean UL rate is extremely sensible to the value of $\nu^\star$ under this regime, e.g. notice how much the performance varies in the interval $\nu^\star \in [0, 0.1]$. However, as we will further see, low values of $\nu^\star$ are detrimental to the DL rate. Furthermore, we can notice that even for a $\nu^\star = 1$, which is the value that obtains the lower gains, the FD UL rate is also outperformed. In this regard, if we set $M = 4$ and $\nu^\star = 1$ we achieve a 25% gain with respect to FD and reduce the loss to a 23% when compared to HD, which shows the potential of our solution under these scenarios. The UL performance though, is less sensible as $\nu^\star$ increase. Indeed, the gains are arguably marginals when $\nu^\star$ goes from 1 to 0.7 (this explains why we do not show the curves in-between).

On the other hand, from the figure we observe that the UL performance improves when M increases. It could be said that this is intuitive, since $I_M(\cdot)$ gets larger with M, thus we can eventually cancel more BSs. Yet, we could not derive this directly from the expression of $p(r)$ in (5.44). We can notice though that even for $M = 1$, our solution outperforms the traditional FD case. Indeed, if we consider $M = 1$ and $\nu^\star = 0.6$ we obtain a 24% gain with respect to FD and the loss compared to HD is reduced to 23%. Moreover, we notice that for a

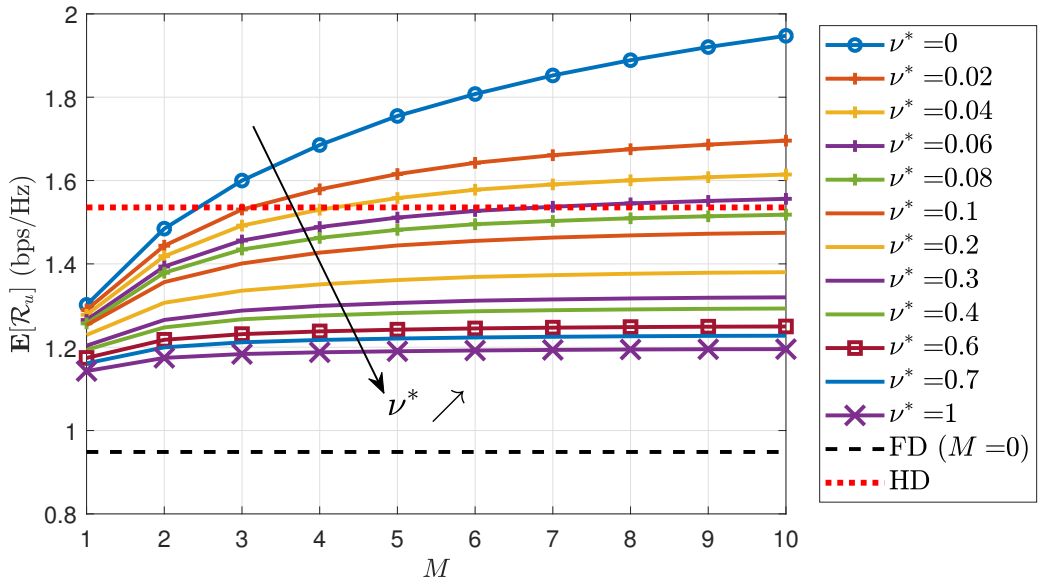

(a) Mean UL rate.

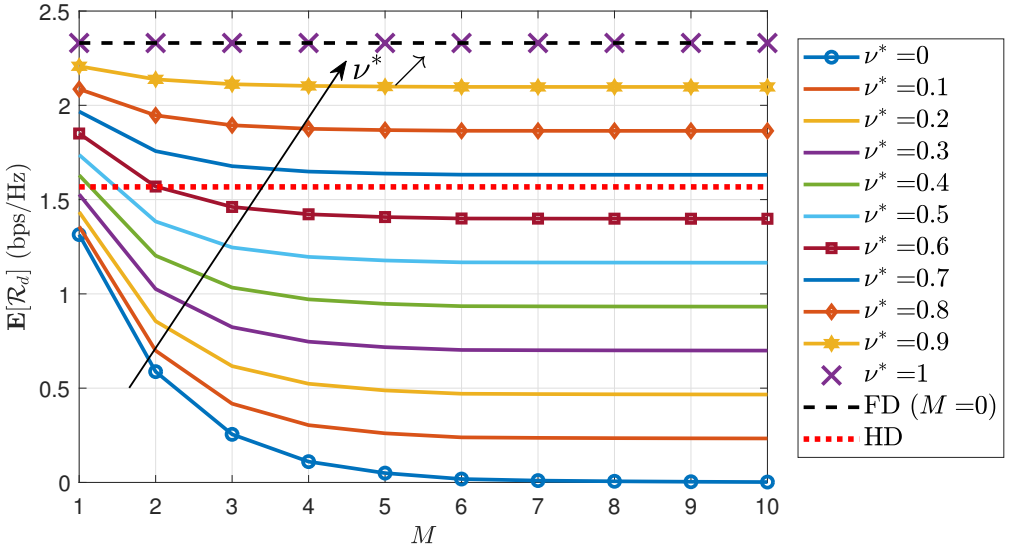

(b) Mean DL rate.

Fig. 5.7 Mean UL and DL rates as a function of M, for different values of $\nu^\star$, when considering omnidirectional antennas.

fixed value of $\nu^\star$, the UL gains become marginal as M increases. This, allows us to pick low values of M without considerably achieving lower performance gains. Indeed, due to SIC error propagation constraints, M cannot be chosen arbitrarily large [80]. As a consequence, we could in fact operate with values of $M = 2$ and $\nu^\star = 0.6$, with which we increase the FD performance by approximately 30%.

Further, the mean DL rate is seen in Fig. 5.7 (b). We clearly see that the DL behavior is totally opposite to the one of the UL. In the first place, we see that FD achieves a performance that is 49% higher than the one of HD. Regarding the impact of $\nu^\star$, we notice that low values of this parameter critically impair the DL rate. In fact, $\nu^\star = 0$ represents the worst possible value for DLs, which is in contrast the best one for ULs. For the DL, the value of $\nu^\star$ can arbitrarily degrade the rate and set it to be equal to $\mathscr{C}_{\text{min}}$. However, it is possible surpass the HD performance for some values of $\nu^\star$, e.g. all $\nu^\star \geq 0.7$ independently of M. Moreover, and differently from what is seen with ULs, the FD DL rate (i.e., when $M = 0$) acts as an upper bound, so independently of the value of $\nu^\star$ we can not surpass the FD performance. Only with $\nu^\star = 1$ we can achieve the FD data rate.

Regarding M, we observe (as well) an opposite behavior when compared to the UL. For the DLs, the rate decreases with M. However, we observe that our solution can outperform the HD case even for $M = 1$. As a matter of fact, when $M = 1$ and $\nu^\star = 0.6$, our solution obtains a 18% gain with respect to HD.

At this point, since the UL and DL performances behave in the opposite way according to variation of $\nu^\star$ and M, we could arguably say that our solution also enables to trade-off UL for DL gain, as it is the case with the solution presented in Chapter 3. However, fixing $\nu^\star = 1$ and $M = 4$ allows us to maintain the performance of FD DL (i.e., 49% gain with respect to HD), while enhancing the FD UL in a 25% and satisfying the constraints of SIC.

5.5.4 Impact of residual self-interference

From the numerical application results of Section 2.5.1, we know that the value of β plays a critical role for ULs. Hence, in this part, we are interested in studying how our solution performs when considering different β values. Since we know that the DL performance is independent of the RSI, in this section we only analyze the effect on ULs.

Firstly, the UL coverage probability for different values of β is depicted in Fig. 5.8. We plot two cases, one in which the self-IC is perfect, i.e., $\beta = 0$, and other in which $\beta = -100$ dB (hence, a greater value if compared to the one previously used in Sections 5.5.2 and 5.5.3). For both scenarios we analyze the behavior when setting $M = 1$ and $M = 10$, and we also show the FD performance (i.e., $M = 0$). From the figure, we observe that not only the UL coverage probability of FD is improved when the RSI is lower (i.e., when β is smaller), but also that the performance of our solution is enhanced. This is due to the fact that when the RSI is low compared to noise and co-channel interference, then by implementing our algorithm we can more effectively increase the SINR value, since the RSI component might become negligible. In this regard, we notice that when $\beta = -100$ dB, by setting $M = 1$ we improve the UL coverage probability by 2 dB, and when $M = 10$ by 4.1 dB. However, when

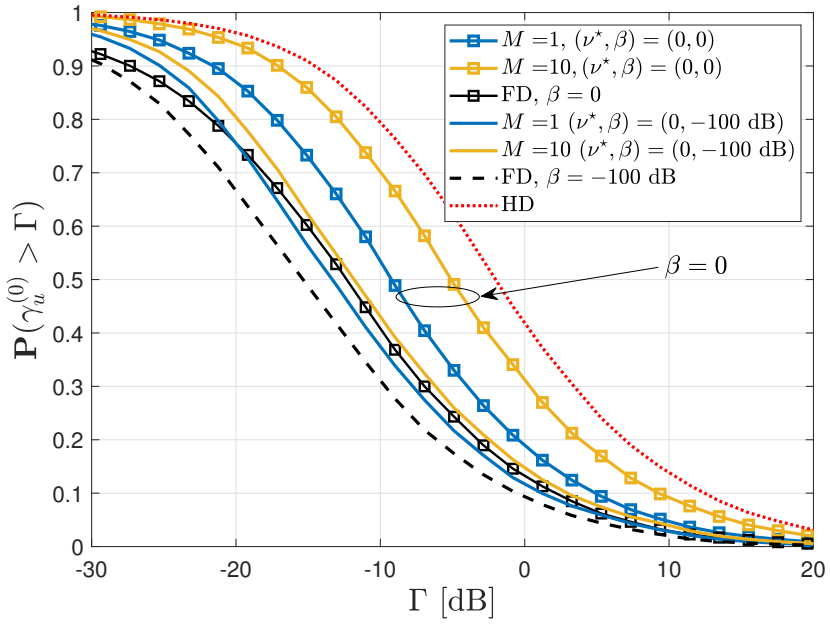

Fig. 5.8 UL coverage probability for different values of β.

$\beta = 0$, a value of $M = 1$ increases the coverage probability by 4.1 dB and for $M = 10$ by 8.2 dB. In fact, this last setting is considerably close to the UL coverage probability of a HD-based system.

The mean UL rate for $\beta = 0$ and $\beta = -100$ dB are shown in Fig. 5.9. We can firstly notice from the case in which $\beta = 0$ in Fig. 5.9 (a), that the rate of FD now is indeed only slightly higher than the one achieved for $\beta = -110$ dB in Fig. 5.7 (a). This indicates that the realistic value of β chosen to model our system (i.e., $\beta = -110$ dB) is favourable and that the interference mostly comes from other equipment (specially from BSs). However, this small performance enhancement for FD when we consider perfect self-IC, translates into higher rates when implementing our solution. In fact, and as opposed to the case in which $\beta = -110$ dB in Fig. 5.7 (a), now we can outperform HD with values of $\nu^\star = 0$ and $\nu^\star = 0.1$. Moreover, if we set $\nu^\star = 1$ (in order not to degrade the DL performance of FD) and $M = 4$, we outperform FD by a 31% (instead of 25% as before with $\beta = -110$ dB).

On the other hand, as we just saw with the UL coverage probability, when the value of β increases, the mean data rate performance is also worsen. Indeed, from Fig. 5.9 (b), we observe that when $\beta = -100$ dB, the gap between HD and FD is considerably increased (see the double-arrow indicating the difference between curves). The FD now has a 56% loss with respect to HD. In this regard, since now the RSI component is higher, suppressing the interference from other BSs is not as effective as before, since the UL SINR is still impaired

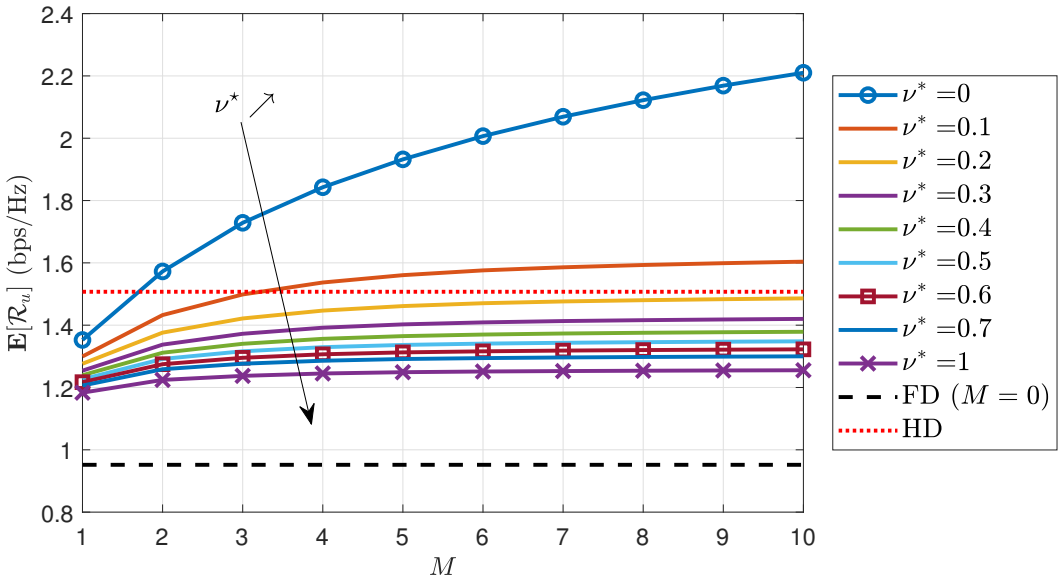

(a) Mean UL rate for perfect self-IC ($\beta = 0$).

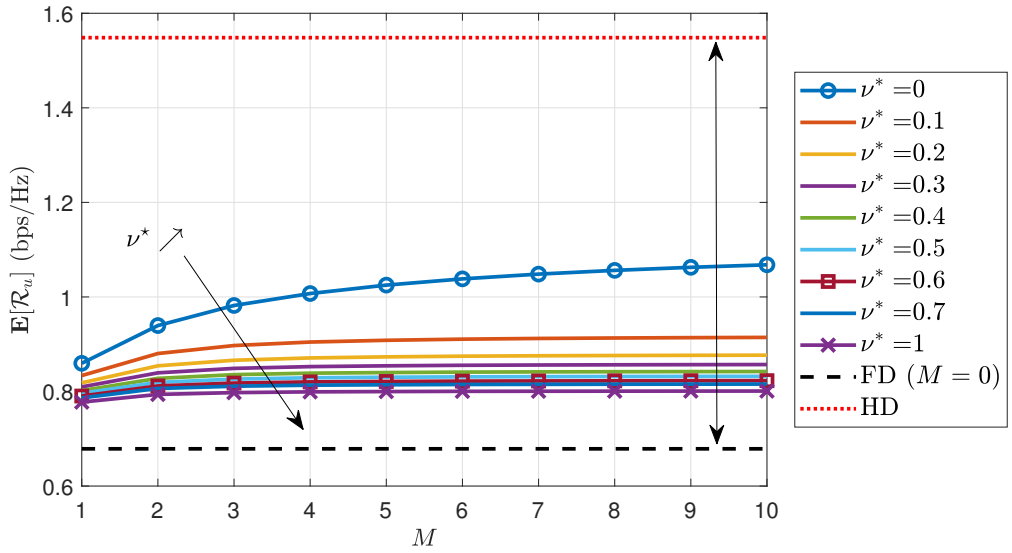

(b) Mean UL rate for $\beta = -100$ dB.

Fig. 5.9 Mean UL rates for different RSI values (i.e., β), when considering omnidirectional antennas.

by the self-interference. So, even when our solution enables to enhance the performance of FD, the gains are considerably lower. Actually, by setting $\nu^\star = 1$ and $M = 4$, we improve the FD performance by a 18%, but we are still far from HD.

We summarize in Table 5.2 the recommended configurations of our solution under different values of β. Let us recall that ϑ_m represents the ratio between FD and HD ASEs,

Table 5.2 Recommended settings of our solution for different values of β.

	Solution: $(\nu^\star, M)$	UL						DL	
		$\beta = 0$		$\beta = -110$ dB		$\beta = -100$ dB			
		$\vartheta_u - 1$	$\digamma_u$	$\vartheta_u - 1$	$\digamma_u$	$\vartheta_u - 1$	$\digamma_u$	$\vartheta_d - 1$	$\digamma_d$
(a)	$(1,0)$	-37%	-	-38%	-	-56%	-	$+49\%$	-
(b)	$(1,4)$	-17%	$+31\%$	-23%	$+25\%$	-48%	$+18\%$	$+49\%$	0%
(c)	$(0.6,1)$	-19%	$+28\%$	-23%	$+24\%$	-49%	$+16\%$	$+18\%$	-20%

for links $m \in \{u,d\}$. However, since we here study normalized mean rates, the expression $\vartheta_m - 1$ in the table depicts the rate gains (losses) with respect to HD. Furthermore, we define $\digamma_m$, for $m \in \{u,d\}$, as the rate gains with respect to a FD network. Particularly, case (a) in the table (i.e., when $(\nu^\star, M) = (1,0)$) represents a FD network. Case (b) represents the scenario in which the FD DL gain is maintained, while enhancing the FD UL and satisfying practical constraints of SIC. This could in fact be seen as the best configuration. Case (c) is an intermediate setting that has a similar behavior to (b). Nevertheless, SIC is only performed along one interfering BS. Thus, the previous case is especially useful when high SIC computing capabilities are not available.

5.5.5 Impact of antenna directivity

The mean UL and DL rates when using the antenna model of Chapter 4 can be found in Fig. 5.10. For the UL, in Fig. 5.10 (a) we observe that our system performs similarly as for the omnidirectional case, i.e., the UL rate is enhanced when $\nu^\star$ decreases and M decreases. However, and as before, the gains become marginal for greater values of M. Moreover, we notice that now the performance of FD is only 4% lower than the one of HD. Hence, with beamforming, FD does not experiences a critical UL degradation. On this matter, our solution enables to improve the performance of FD[5], yet the gains are not substantial. So our solution is arguably not useful in scenarios where the interference between BSs is not high, since the complexity of the system increases when considering our model, while obtaining marginal gains.

For the DL, we notice again in Fig. 5.10 (b) that the mean rate follows a similar behavior as in the omnidirectional antenna scenario, i.e., the higher $\nu^\star$ or the lower M, the better the DL performance. Yet, we see now that the mean DL rate of FD outperforms the one of HD by a 78%. Hence, the enhancement of FD with respect to HD is higher when considering beamforming-capable BSs, rather than when these use omnidirectional antennas (as already

[5]It can even outperform the one of HD, yet for values of $\nu^\star$ that completely impair the DL (as for the omnidirectional case).

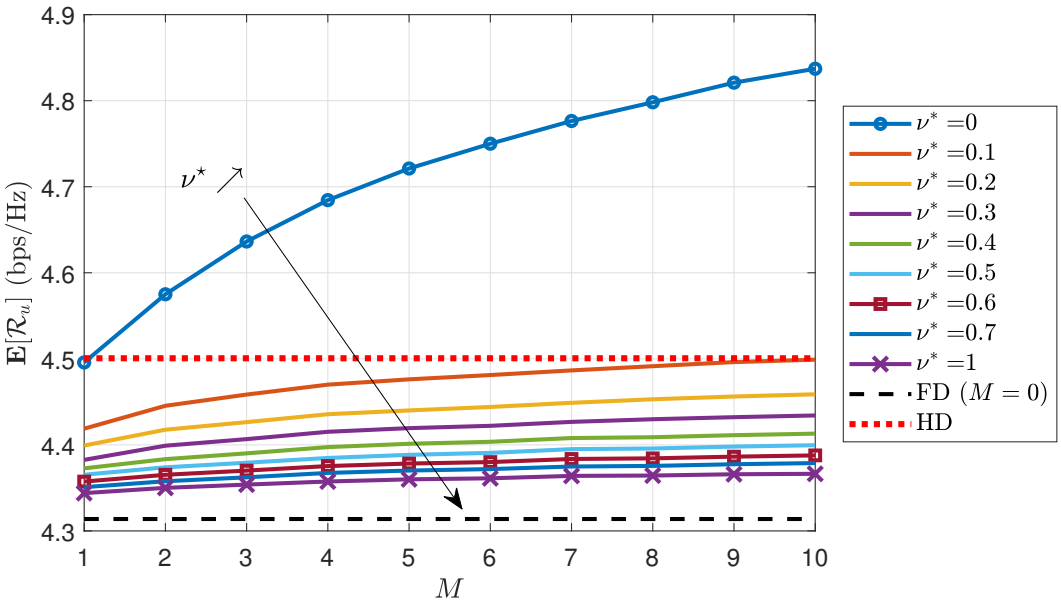

(a) Mean UL rate.

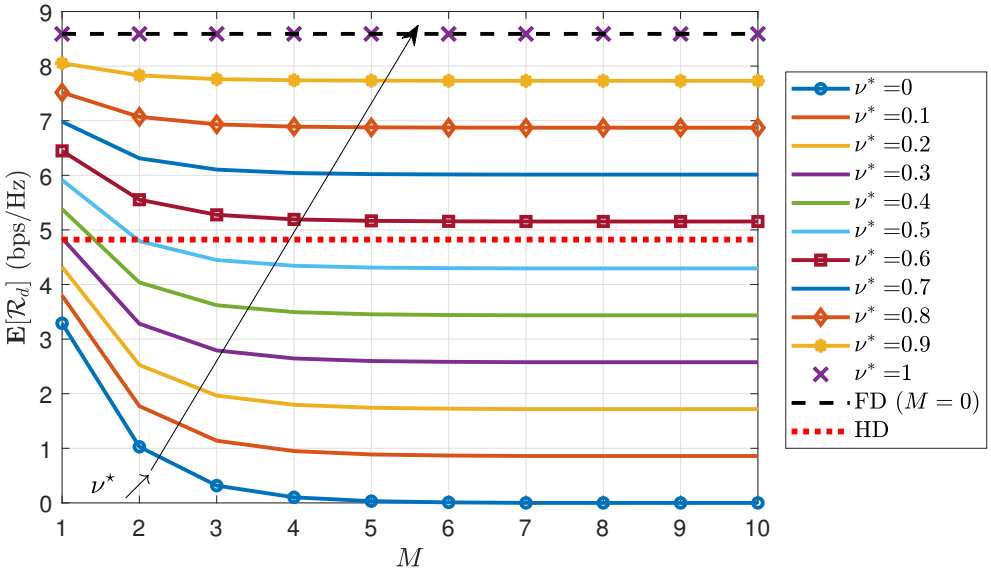

(b) Mean DL rate.

Fig. 5.10 Mean UL and DL rates as a function of M, for different values of $\nu^\star$, when considering directional antennas in the BSs.

seen in Chapter 4). Now, since the performance of FD is higher, then lower values of $\nu^\star$ enable to equal the mean DL rate achieved by a HD system. In this context, we can set for example $M = 1$ and $\nu^\star = 0.3$. But, given that FD does not experiences a high UL degradation

and the DL performance almost doubles the one of HD, once again we can argue that our solution is not needed for these scenarios.

The DL coverage probability for both omnidirectional and beamforming-capable antennas in BSs can be seen in Fig. 5.6. For the latter case, we observe that analytical and simulation results also match well. Particularly, the curves for the beamforming case have a slightly different behavior, because we consider the average antenna gains[6]. This is not entirely accurate in reality, but still we show that our approach is a good approximation. We further notice that the performance is considerably improved when having higher directivity of antennas. In this sense, although the FD coverage probability in the omnidirectional case is not heavily degraded, the gap between HD and FD is even smaller for the beamforming case. This is due to the fact that not only the BS-to-BS interference is reduced, but also the DL SINR increased.

5.6 Summary and final remarks

In this chapter we study an algorithm that, by using NOMA and successive interference cancellation, enables FD BSs to cancel the BS-to-BS interference that impair their UL performance. The solution depends on the coordination between interfering stations and the correct exchange of this information relies on the DL data rate management of each cell. In this regard, the solution is characterized by two parameters, M and $\nu^\star$. The first represents the maximum number of BSs that each cell can eventually cancel and the second, the tolerated DL rate reduction in each cell.

The model shows to be promising in scenarios in which FD ULs are critically degraded. This is particularly the case when equipment in the network have omnidirectional antennas. For this case, by setting $\nu^\star = 1$, our solution enables to maintain the favourable DL rate gains obtained by FD (when compared to a HD network), while considerably reducing the UL degradation experienced by FD ULs. In this regard, higher UL gains are obtained when decreasing the value of $\nu^\star$. However, this impairs the DL performance, which is an advantage presented by FD. On this matter, extremely low values of the latter parameter (e.g. $\nu^\star = 0$) arbitrarily degrades the DL, turning the problem around, i.e., we gain in ULs, but lose in the DL. On this matter though, there is no need to alternated between duplex-modes, as done in Chapter 3. When using the algorithm presented in this chapter, BSs can always operate in a FD-fashion, which not only simplifies the management of resources, but as well, the complexity of transceivers.

[6]Gains are computed by using the probabilities of being in the direction of a side-lobe or a main lobe assuming random uniform directions.

On the other hand, we observe that when BSs are capable of steering their signals towards their scheduled users, BS-to-BS and BS-to-UE interference are significantly reduced. Hence, FD by itself performs well since ULs do not experience a critical degradation and DL gains can be further improved. This suggests that no additional solution is actually needed and the feasibility of FD rests in the capability of transceivers to effectively cancel the self-interference, the management of signalization, user plane data and the communications protocols, among others.

Finally, as seen in Section 1.3.3, there are other systems or situations that can relate with the BS-to-BS interference present in full-duplex. In this regard, we clearly see that the algorithm proposed in this chapter can be adapted and implemented in some of these previous scenarios. In fact, since the algorithm was initially thought to be used by BSs, it could be (arguably) simple to directly adapt it to be used by generic HD-enabled BSs. Indeed, our solution could be installed in 4G and 5G BSs that operate in near frequency bands and that interfere between each other.

Chapter 6

Conclusions and future works

Full-duplex is a principle that was long held as impractical due to the high self-interference that arises when transmitting and receiving in the same frequency channel. Indeed, without self-IC, FD is not possible in practice. Yet, advances in hardware and signal processing allow to obtain levels of residual self-interference that could make us consider FD as a feasible/practical technique. This technique seems very promising because next generation mobile networks will offer not only higher data rates but also more efficient ways of using resources, especially energy and spectrum resources. In this regard and under ideal conditions, FD promises to double the spectral efficiency and/or the throughput of wireless communication systems. However, due to imperfect self-IC none of these upper bounds is reached. Moreover, under a cellular context, the simultaneous use of resources by multiple cells generates additional co-channel interference, which takes FD systems even farther away from the expected performance levels.

In this thesis we analyze networks in which FD-capabilities are only achievable by base stations, while users equipment continue to operate in half-duplex. Having a BS in FD, while it serves simultaneously one uplink and downlink user is known as the three-node FD architecture. This relies on the fact that complex and costly self-interference cancellation systems are more easily implemented in BSs, which do not count with the same space, energy and cost constraints as UEs. Interestingly, we observe that even when the interference floor is higher in FD, DLs in three-node FD cellular networks improve their performance with respect to HD. This can be explained by the fact that BSs have higher transmission powers for the useful signal while new interferers have low power. This is also due to the absence of self-interference at the UEs. On the contrary, ULs are heavily degraded. The latter issue is not only due to the residual self-interference component, yet also to the strong BS-to-BS interference which is generated when propagation characteristics allow signals to travel in the direction of other BSs. In this sense, UEs transmission powers are not comparable with the

ones of BSs, thus the received UL signals are generally not high enough to achieve acceptable signal-to-interference-plus-noise ratio levels. This effect is observable even when self-IC is perfect.

We focus our work in the study of alternatives that can help reduce the impaired ULs in FD-based networks, while still profiting of the gains achieved in DLs. As previously mentioned, omnidirectional antennas at the BSs represent a worst case scenario for FD. In this case indeed, BS-to-BS and BS-to-UE interference is increased compared to a beamforming scenario. As a consequence, ULs are strongly impaired and, on the other hand, DLs cannot fully exploit the additional resources provided by FD. We start by proposing a duplex-switching policy in which BSs can choose whether to operate in HD- or FD-mode depending on the position of their scheduled users. The criterion of FD adoption in each cell depends, in this sense, on two parameters. One, which goes hand in hand with the position of the UL user. Another, which focuses on the position of the DL user. The first parameter forces BSs to adopt FD only when the propagation conditions are adequate towards the scheduled UL user. This mechanism reduces the UL degradation. On the other hand, the second parameter restricts FD adoption to when a minimum distance is met between the scheduled DL and UL users in the same cell. The previous mechanism allows to further improve the FD DL performance, as the UL user in the same cell is usually the strongest interfering UE. Since FD adoption in BSs depends simultaneously on both parameters, we observe that the DS policy offers a way of favouring the gains of one link against the other. However, by optimizing the parameters, the mean cell performance of the network can be maximized, outperforming both HD and FD cellular networks. Nevertheless, as it is the case with related works, our DS policy remains as a means to cope with the UL degradation by limiting the amount of FD BSs in the network, which could be considered counterproductive or disappointing.

Furthermore, and intrigued by whether a similar policy might be useful when systems are as close to being only noise-limited, we analyze hybrid FD/HD small-cell deployments while exploiting the mmWave spectrum. We see in fact that this is a favorable scenario for FD, as smaller wavelengths that allow equipment to beamform their signals towards the intended receivers, significantly reduce the co-channel interference. There is no need of having then an hybrid FD/HD deployment if the RSI values are considerably low. In this regard, we propose a novel way of modeling the self-interference according to the antenna gains and (receiving/transmitting) patterns. The model shows that as there exists a probability of having the receiver and transmitter main-lobes directly pointing in the same direction, the self-interference can be considerably increased in average. By taking into account this consideration, we propose to perform power control in the DL. Even though this may result in lower DL gains, since signals are effectively steered, we can still benefit from enhanced DLs

(with respect to HD). However, and more importantly, we have another way of minimizing the UL degradation. In fact, for a specific value of reduction of the power of BSs, we obtain zero degradation for the ULs and a 36% gain for the DLs (if compared to HD). In addition, performing power control reduces the net energy consumption of the network, which might be interesting for next generation mobile systems.

In the last part of the thesis, we propose a new solution to the UL degradation that does not limit the number of FD BSs in the network. Hence, we consider a network where all BSs simply operate in FD. For this case, we propose an algorithm to coordinate BSs, in order to allow them to cancel the BS-to-BS interference that impairs the ULs. The coordination is based on NOMA and the possibility to limit the DL rate when required, in order to allow stations to decode the signals received from a bounded set of interfering BSs. The intended UL data is recovered after performing successive interference cancellation. This operation considerably increases the UL SINR. The algorithm shows to be useful in deployments in which the BS-to-BS interference is high, e.g. when BSs have omnidirectional antennas. For this case, we can keep FD gains in the DLs while considerably reducing the UL degradation. In this particular setting, it is not necessary to balance the gains of the DLs in order to increase the one of the ULs (as it is indeed the case of our DS-policy). However, its usefulness is unclear when the system is only noise-limited, e.g. when BSs are capable of beam-steering their signals towards UEs. In fact, for this scenarios FD already achieves high SE and throughput. Hence, the solution is arguably not necessary and the limiting factor of the FD deployment is related to the self-IC capabilities and the additional complexity related to this new principle. Interestingly though, we note that the proposed algorithm can be adapted to other ecosystems that suffer from co-channel or channel-adjacent interference. This could be the case of 5G networks coexisting with current 4G networks, or in deployments based on dynamic TDD where we can have the same type of interference between BSs. So we do not limit its applicability only to FD.

6.1 Future perspectives

Along this thesis we have examined the three-node FD architecture. But eventually we could also implement FD-capabilities in UEs (this is known as the two-node FD architecture). In this regard, we might think that because users transmission powers are lower, then the residual self-interference will also be lower. Hence, the impact towards the DL performance would not be that critical. But, on the other hand, given the constraints of space, battery and costs, it is not possible to ensure that the effectiveness of the self-IC systems will be comparable to that of base stations. Therefore, it is necessary to analyze the DL performance

for different β values, to observe the actual effect of incorporating FD in users. On this matter, since the interference in DLs is higher in a two-node FD case, it may be necessary to consider other alternatives to reduce the BS-to-UE or UE-to-UE. We could take into account indeed coordinated multi-point (CoMP) systems as solutions. CoMP considers transmission and/or reception at multiple separated sites with a dynamic coordination among them to pro-actively manage the interference for the users [81, Chapter 6]. In fact, CoMP could also be useful in a three-node FD architecture to help reduce the interference and further improve the FD DL gains. Its implementation then remains attractive and could be combined, for instance, with our DS policy to simultaneously improve the DL performance and minimize the UL degradation in FD. In particular, we could arguably say that the algorithm presented in Chapter 5 is a CoMP-based solution.

Moreover and as mentioned above, next-generation networks will be heavily regulated around their power consumption. So it would be interesting as well to analyze the energy efficiency of FD and of the different models presented in this thesis. On this matter, from Chapter 1 we know that self-IC systems are conceived by implementing additional hardware and signals processing techniques. So, FD can consume a considerably higher amount of energy compared to current HD transceivers. We could in fact think on the results presented in Chapter 4, where we demonstrate that even when reducing the DL transmission power control, we can still obtain high gains if beam steering is possible. Accordingly, promising results are shown in [82]. Authors here find an optimal power control strategy, by using game theory tools that can be adopted by FD BSs in an ultra-dense network setting. Results reveal that it is not only possible to improve the energy efficiency but also ensure suitable coverage probability levels. Some other works also address this problem, yet most of them are focused in FD relaying, e.g. [83, 84].

To study the feasibility of FD in macro-cellular deployments, we have performed additional analyzes not shown in the thesis. We have observed that the algorithm proposed in Chapter 5 works well, yet only when self-IC is perfect. However, since it is not realistic to assume perfect self-IC, for current achievable values of β, the largest interference component lies in the RSI. Hence, future efforts could therefore be directed towards alternative models of self-IC to allow FD implementation macro-cell deployments, e.g. new antennas specially designed for this purpose or exploit massive MIMO capabilities. Particularly, and as far as the algorithm presented in Chapter 5 is concerned, we do not take full advantage of the qualities of NOMA. Indeed, capacity values between BSs are computed in advance and the algorithm later allows (sometimes) the cancellation of a given number of interfering BSs. Therefore, these capacities represent a worst case scenario. In this regard, we can only ensure that the system operates within the capacity region boundaries (see for instance [75,

Chapter 6]). Greater gains could though be achieved by analyzing the decoding order of the interfering BSs. Thus, additional studies can be done in this direction.

In terms of methodology analysis, we only examine in this thesis the full-buffer traffic model. However, in reality the dynamism of traffic can particularly vary between different cellular network services. In this regard, some notable efforts have been recently done to characterize the entanglement between queuing theory and stochastic geometry, see for instance [85, 86]. It would therefore be attractive to study more in depth the performance of FD-based cellular networks by considering dynamical systems on point processes. Moreover, in Chapter 5 we were not able to analytically characterize $\mathscr{C}_{\text{min}}$ in closed-form. In this regard, we approximated its behavior by numerical observations. However, works such as [87–89] suggest some notions that could be useful to achieve this goal. Moreover, we could extend the study of Chapter 5 to general cases where the strongest interferers are not necessarily the closest ones. This would allow the implementation of our solution in scenarios where the propagation of the signals are strongly related to the environment, such as indoor deployments or mmWave transmissions.

References

[1] ITU. IMT Vision – Framework and Overall Objectives of the Future Development of IMT for 2020 and Beyond. Technical report, ITU, September 2015.

[2] Theodore Rappaport. *Wireless Communications: Principles and Practice*. Prentice Hall, 2 edition, August 2002.

[3] Sanjay Goyal, Pei Liu, and Shivendra S. Panwar. User Selection and Power Allocation in Full-Duplex Multicell Networks. *IEEE Transactions on Vehicular Technology*, 66(3):2408–2422, March 2017.

[4] Boya Di, Siavash Bayat, Lingyang Song, Yonghui Li, and Zhu Han. Joint User Pairing, Subchannel, and Power Allocation in Full-Duplex Multi-User OFDMA Networks. *IEEE Transactions on Wireless Communications*, 15(12):8260 – 8272, December 2016.

[5] Sanjay Goyal, Pei Liu, Shivendra S. Panwar, Robert A. Difazio, Rui Yang, and Erdem Bala. Full duplex cellular systems: Will doubling interference prevent doubling capacity? *IEEE Communications Magazine*, 53(5):121–127, May 2015.

[6] Zhongshan Zhang, Keping Long, Athanasios V. Vasilakos, and Lajos Hanzo. Full-Duplex Wireless Communications: Challenges, Solutions, and Future Research Directions. *Proceedings of the IEEE*, 104(7):1369–1409, July 2016.

[7] Dongkyu Kim, Hyungsik Ju, Sungsoo Park, and Daesik Hong. Effects of Channel Estimation Error on Full-Duplex Two-Way Networks. *IEEE Transactions on Vehicular Technology*, 62(9):4666–4672, November 2013.

[8] Ahmed Masmoudi and Tho Le-Ngoc. Channel Estimation and Self-Interference Cancellation in Full-Duplex Communication Systems. *IEEE Transactions on Vehicular Technology*, 66(1):321–334, January 2017.

[9] Zhongshan Zhang, Xiaomeng Chai, Keping Long, Athanasios V. Vasilakos, and Lajos Hanzo. Full Duplex Techniques for 5G Networks: Self-Interference Cancellation, Protocol Design, and Relay Selection. *IEEE Communications Magazine*, 53(5):128–137, May 2015.

[10] Melissa Duarte, Ashutosh Sabharwal, Vaneet Aggarwal, Rittwik Jana, K. K. Ramakrishnan, Christopher W. Rice, and N. K. Shankaranarayanan. Design and Characterization of a Full-Duplex Multiantenna System for WiFi Networks. *IEEE Transactions on Vehicular Technology*, 63(3):1160–1177, March 2014.

[11] Aimin Tang and Xudong Wang. A-Duplex: Medium Access Control for Efficient Coexistence Between Full-Duplex and Half-Duplex Communications. *IEEE Transactions on Wireless Communications*, 14(10):5871 – 5885, October 2015.

[12] Ertugrul Basar, Miaowen Wen, Raed Mesleh, Marco Di Renzo, Yue Xiao, and Harald Haas. Index Modulation Techniques for Next-Generation Wireless Networks. *IEEE Access*, 5:16693 – 16746, August 2017.

[13] Weijun Tang, Suili Feng, Yuan Liu, and Yuehua Ding. Hybrid Duplex Switching in Heterogeneous Networks. *IEEE Transactions on Wireless Communications*, 15(11):7419 – 7431, November 2016.

[14] Jemin Lee and Tony Q. S. Quek. Hybrid Full-/Half-Duplex System Analysis in Heterogeneous Wireless Networks. *IEEE Transactions on Wireless Communications*, 14(5):2883 – 2895, May 2015.

[15] Sanjay Goyal, Pei Liu, Sha Hua, and Shivendra Panwar. Analyzing a Full-Duplex Cellular System. In *47th Annual Conference on Information Sciences and Systems (CISS)*, March 2013.

[16] Hirley Alves, Carlos H. M. de Lima, Pedro H. J. Nardelli, Richard Demo Souza, and Matti Latva-aho. On the Average Spectral Efficiency of Interference-Limited Full-Duplex Networks. In *9th International Conference on Cognitive Radio Oriented Wireless Networks and Communications (CROWNCOM)*, pages 550 – 554, June 2014.

[17] Ahmad AlAmmouri, Hesham ElSawy, Osama Amin, and Mohamed-Slim Alouini. In-Band α-Duplex Scheme for Cellular Networks: A Stochastic Geometry Approach. *IEEE Transactions on Wireless Communications*, 15(10):6797–6812, October 2016.

[18] Hesham ElSawy, Ahmad AlAmmouri, Osama Amin, and Mohamed-Slim Alouini. Can Uplink Transmissions Survive in Full-duplex Cellular Environments? In *22th European Wireless Conference*, May 2016.

[19] Rongpeng Li, Yan Chen, Geoffrey Ye Li, and Guangyi Liu. Full-Duplex Cellular Networks. *IEEE Communications Magazine*, 55(4):184–191, April 2017.

[20] Ashutosh Sabharwal, Philip Schniter, Dongning Guo, Daniel W. Bliss, Sampath Rangarajan, and Risto Wichman. In-Band Full-Duplex Wireless: Challenges and Opportunities. *IEEE Journal on Selected Areas in Communications*, 32(9):1637–1652, September 2014.

[21] Melissa Duarte, Chris Dick, and Ashutosh Sabharwal. Experiment-Driven Characterization of Full-Duplex Wireless Systems. *IEEE Transactions on Wireless Communications*, 11(12):4296–4307, December 2012.

[22] Ira Brodsky, Joel Brand, and Mayank Jain. Freedom of Frequency: How the Quest for In-Band Full-Duplex Led to a Breakthrough in Filter Design. *IEEE Microwave Magazine*, 20(2):36 – 43, February 2019.

[23] Evan Everett, Achaleshwar Sahai, and Ashutosh Sabharwal. Passive Self-Interference Suppression for Full-Duplex Infrastructure Nodes. *IEEE Transactions on Wireless Communications*, 13(2):680–694, January 2014.

[24] Achaleshwar Sahai, Gaurav Patel, Chris Dick, and Ashutosh Sabharwal. On the Impact of Phase Noise on Active Cancelation in Wireless Full-Duplex. *IEEE Transactions on Vehicular Technology*, 62(9):4494–4510, November 2013.

[25] Ville Syrjälä, Mikko Valkama, Lauri Anttila, Taneli Riihonen, and Dani Korpi. Analysis of Oscillator Phase-Noise Effects on Self-Interference Cancellation in Full-Duplex OFDM Radio Transceivers. *IEEE Transactions on Wireless Communications*, 13(6):2977 – 2990, June 2014.

[26] George C. Alexandropoulos and Melissa Duarte. Joint Design of Multi-Tap Analog Cancellation and Digital Beamforming for Reduced Complexity Full Duplex MIMO Systems. In *IEEE International Conference on Communications (ICC)*, May 2017.

[27] Pablo Pascual Campo, Dani Korpi, Lauri Anttila, and Mikko Valkama. Nonlinear Digital Cancellation in Full-Duplex Devices Using Spline-Based Hammerstein Model. In *IEEE Globecom Workshops (GC Wkshps)*, December 2018.

[28] Dani Korpi, Matias Turunen, Lauri Anttila, and Mikko Valkama. Modeling and Cancellation of Self-Interference in Full-Duplex Radio Transceivers: Volterra Series-Based Approach. In *IEEE International Conference on Communications Workshops (ICC Workshops)*, May 2018.

[29] Dani Korpi, Mona Aghababaeetafreshi, Mauno Piilila, Lauri Anttila, and Mikko Valkama. Advanced Architectures for Self-Interference Cancellation in Full-Duplex Radios: Algorithms and Measurements. In *50th Asilomar Conference on Signals, Systems and Computers*, pages 1553–1557, November 2016.

[30] Visa Tapio, Markku Juntti, Aarno Pärssinen, and Kari Rikkinen. Real Time Adaptive RF and Digital Self-Interference Cancellation for Full-Duplex Transceivers. In *50th Asilomar Conference on Signals, Systems and Computers*, pages 1558 – 1562, November 2016.

[31] Tong Zhang, Ali Najafi, Chenxin Su, and Jacques C. Rudell. A 1.7-to-2.2GHz Full-Duplex Transceiver System with $>$ 50dB Self-Interference Cancellation Over 42MHz Bandwidth. In *IEEE International Solid-State Circuits Conference*, February 2017.

[32] José Mairton B. da Silva, Gábor Fodor, and Carlo Fischione. On the Spectral Efficiency and Fairness in Full-Duplex Cellular Networks. In *IEEE International Conference on Communications (ICC)*, May 2017.

[33] Technical Specification Group Services and System Aspects; Summary of Rel-15 Work Items (TR 21.915 V0.6.0 Release 15). Technical report, 3rd Generation Partnership Project (3GPP), February 2019.

[34] Shaozhen Guo, Xiaolin Hou, and Hanning Wang. Dynamic TDD and Interference Management Towards 5G. In *IEEE Wireless Communications and Networking Conference (WCNC)*, April 2018.

[35] Jalal Rachad, Ridha Nasri, and Laurent Decreusefond. Interference Analysis in Dynamic TDD System Combined or not With Cell Clustering Scheme. In *IEEE Vehicular Technology Conference (VTC Spring)*, June 2018.

[36] Matthias Wildemeersch, Tony Q. S. Quek, Marios Kountouris, Alberto Rabbachin, and Cornelis H. Slump. Successive Interference Cancellation in Heterogeneous Networks. *IEEE Transactions on Communications*, 62(12):4440–4453, December 2014.

[37] Matthias Wildemeersch, Tony Q. S. Quek, Marios Kountouris, and Cornelis H. Slump. Successive Interference Cancellation in Uplink Cellular Networks. In *IEEE 14th Workshop on Signal Processing Advances in Wireless Communications (SPAWC)*, June 2013.

[38] Xinchen Zhang and Martin Haenggi. The Performance of Successive Interference Cancellation in Random Wireless Networks. *IEEE Transactions on Information Theory*, 60(10), October 2014.

[39] Daniel Jaramillo-Ramirez, Marios Kountouris, and Eric Hardouin. Successive Interference Cancellation in Downlink Cooperative Cellular Networks. In *IEEE International Conference on Communications (ICC)*, June 2014.

[40] Lei Zhou and Wei Yu. Uplink Multicell Processing with Limited Backhaul via Per-Base-Station Successive Interference Cancellation. *IEEE Journal on Selected Areas in Communications*, 31(10):1981–1993, October 2013.

[41] Wei Lu. *New Results on Stochastic Geometry Modeling of Cellular Networks : Modeling, Analysis and Experimental Validation*. Phd. thesis, École doctorale Sciences et technologies de l'information et de la communication, Université Paris-Saclay, 2015.

[42] Martin Haenggi. *Stochastic Geometry for Wireless Networks*. Cambridge University Press, 1 edition, November 2012.

[43] Sung Nok Chiu, Dietrich Stoyan, Wilfrid S. Kendall, and Joseph Mecke. *Stochastic Geometry and Its Applications*. Wiley, 3 edition, August 2013.

[44] François Baccelli and Bartłomiej Błaszczyszyn. *Stochastic Geometry and Wireless Networks, Volume I - Theory*. Now Publishers, 2009.

[45] Marco Di Renzo. Introduction to Stochastic Geometry and Point Processes. In *Course on Random Graphs and Wireless Communications Networks, Oriel College, Oxford University*, September 2016.

[46] D. Moltchanov. Distance Distributions in Random Networks. *Ad Hoc Networks*, 10(6):1146–1166, 2012.

[47] Martin Haenggi. User Point Processes in Cellular Networks. *IEEE Wireless Communications Letters*, 6(2):258 – 261, April 2017.

[48] Jeffrey G. Andrews, Francois Baccelli, and Radha Krishna Ganti. A Tractable Approach to Coverage and Rate in Cellular Networks. *IEEE Transactions on Communications*, 59(11):3122 – 3134, November 2011.

[49] Ahmad AlAmmouri, Jeffrey G. Andrews, and François Baccelli. A Unified Asymptotic Analysis of Area Spectral Efficiency in Ultradense Cellular Networks. *IEEE Transactions on Information Theory*, 65(2):1236–1248, February 2019.

[50] Thomas D. Novlan, Harpreet S. Dhillon, and Jeffrey G. Andrews. Analytical Modeling of Uplink Cellular Networks. *IEEE Transactions on Wireless Communications*, 12(6):2669 – 2679, May 2013.

[51] Jinyi Huang, Kaiqiang Qi, Zhikun Xu, and Chenyang Yang. Hybrid Full and Half Duplex Networking. In *IEEE/CIC International Conference on Communications in China (ICCC)*, July 2016.

[52] Itsikiantsoa Randrianantenaina, Hayssam Dahrouj, Hesham Elsawy, and Mohamed-Slim Alouini. Interference Management in Full-Duplex Cellular Networks With Partial Spectrum Overlap. *IEEE Access*, 5:7567–7583, March 2017.

[53] Arman Shojaeifard, Kai-Kit Wong, Marco Di Renzo, Gan Zheng, Khairi Ashour Hamdi, and Jie Tang. Massive MIMO-Enabled Full-Duplex Cellular Networks. *IEEE Transactions on Communications*, 65(11):4734 – 4750, November 2017.

[54] Evolved Universal Terrestrial Radio Access (E-UTRA); Further Advancements for E-UTRA Physical Layer Aspects (TR 36.814 Release 9). Technical report, 3rd Generation Partnership Project (3GPP), March 2017.

[55] Tianyang Bai and Robert W. Heath. Coverage and Rate Analysis for Millimeter Wave Cellular Networks. *IEEE Transactions on Wireless Communications*, 14(2):1100 – 1114, February 2015.

[56] Sarabjot Singh, Mandar N. Kulkarni, Amitava Ghosh, and Jeffrey G. Andrews. Tractable Model for Rate in Self-Backhauled Millimeter Wave Cellular Networks. *IEEE Journal on Selected Areas in Communications*, 33(10):2196 – 2211, October 2015.

[57] Marco Di Renzo. Stochastic Geometry Modeling and Analysis of Multi-Tier Millimeter Wave Cellular Networks. *IEEE Transactions on Wireless Communications*, 14(9):5038 – 5057, September 2015.

[58] Jeffrey G. Andrews, Tianyang Bai, Mandar N. Kulkarni, Ahmed Alkhateeb, Abhishek K. Gupta, and Robert W. Heath. Modeling and Analyzing Millimeter Wave Cellular Systems. *IEEE Transactions on Communications*, 65(1):403 – 430, January 2017.

[59] Zhenyu Xiao, Pengfei Xia, and Xiang-Gen Xia. Full-Duplex Millimeter-Wave Communication. *IEEE Wireless Communications*, 24(6):136 – 143, December 2017.

[60] Weiguang Ding, Yong Niu, Hao Wu, Yong Li, and Zhangdui Zhong. QoS-aware Full-duplex Concurrent Scheduling for Millimeter Wave Wireless Backhaul Networks. *IEEE Access*, 6:25313 – 25322, April 2018.

[61] Zhongxiang Wei, Xu Zhu, Sumei Sun, Yi Huang, Ahmed Al-Tahmeesschi, and Yufei Jiang. Energy-Efficiency of Millimeter-Wave Full-Duplex Relaying Systems: Challenges and Solutions. *IEEE Access*, 4:4848 – 4860, July 2016.

[62] Tolga Dinc and Harish Krishnaswamy. Millimeter-Wave Full-Duplex Wireless: Applications, Antenna Interfaces and Systems. In *IEEE Custom Integrated Circuits Conference (CICC)*, April 2017.

[63] Xiao Liu, Lin Bai Zhenyu Xiao and, Jinho Choi, Pengfei Xia, and Xiang-Gen Xia. Beamforming Based Full-Duplex for Millimeter-Wave Communication. *Sensors*, 16(7):1130, July 2016.

[64] Bartłomiej Błaszczyszyn, Mohamed Kadhem Karray, and Holger Paul Keeler. Using Poisson processes to model lattice cellular networks. In *Proceedings IEEE International Conference on Computer Communications (INFOCOM)*, pages 773–781, April 2013.

[65] Mustafa Riza Akdeniz, Yuanpeng Liu, Mathew K. Samimi, Shu Sun, Sundeep Rangan, Theodore S. Rappaport, and Elza Erkip. Millimeter Wave Channel Modeling and Cellular Capacity Evaluation. *IEEE Journal on Selected Areas in Communications*, 32(6):1164 – 1179, June 2014.

[66] New frequency range for NR: 24.25-29.5 GHz (TR 38.815 V0.3.0). Technical report, 3rd Generation Partnership Project (3GPP), April 2018.

[67] S. M. Riazul Islam, Nurilla Avazov, Octavia A. Dobre, and Kyung sup Kwak. Power-Domain Non-Orthogonal Multiple Access (NOMA) in 5G Systems: Potentials and Challenges. *IEEE Communications Surveys & Tutorials*, 19(2):721–742, 2017.

[68] Zhiguo Ding, Pingzhi Fan, and H. Vincent Poor. On the Coexistence Between Full-Duplex and NOMA. *IEEE Wireless Communications Letters*, 7(5):692–695, October 2018.

[69] Ming Liu, Yuming Mao, Supeng Leng, and Kun Yang. Successive Interference Cancellation in Full Duplex Cellular Networks. In *2017 IEEE International Conference on Communications (ICC)*, May 2017.

[70] Lei Huang, Shengqian Han, Chenyang Yang, and Gang Wang. Full-Duplex Based Successive Interference Cancellation in Heterogeneous Networks. In *2016 IEEE 27th Annual International Symposium on Personal, Indoor, and Mobile Radio Communications (PIMRC)*, September 2016.

[71] Shahram Shahsavari, David Ramirez, and Elza Erkip. Joint User Scheduling and Power Optimization in Full-Duplex Cells with Successive Interference Cancellation. In *To appear in IEEE Asilomar Conference on Signals, Systems and Computers proceedings*, 2017.

[72] Xinwei Yue, Yuanwei Liu, Shaoli Kang, Arumugam Nallanathan, and Zhiguo Ding. Exploiting Full/Half-Duplex User Relaying in NOMA Systems. *IEEE Transactions on Communications*, 66(2):560–575, February 2018.

[73] Md. Fazlul Kader, Soo Young Shin, and Victor C. M. Leung. Full-Duplex Non-Orthogonal Multiple Access in Cooperative Relay Sharing for 5G Systems. *IEEE Transactions on Vehicular Technology*, 67(7):5831–5840, 2018.

[74] Zhengquan, Zheng Ma, Ming Xiao, Zhiguo Ding, and Pingzhi Fan. Full-Duplex Device-to-Device-Aided Cooperative Nonorthogonal Multiple Access. *IEEE Transactions on Vehicular Technology*, 66(5):4467–4471, May 2017.

[75] David Tse and Pramod Viswanath. *Fundamentals of Wireless Communication*. Cambridge University Press, 2010.

[76] Geordie George. *Device-to-Device Communication and Wearable Networks: Harnessing Spatial Proximity*. Phd. thesis, Universitat Pompeu Fabra, 2017.

[77] Jean-Marc Kelif, Marceau Coupechoux, and Philippe Godlewski. On the Dimensioning of Cellular OFDMA Networks. *Elsevier Physical Communication*, 5(1):10–21, March 2012.

[78] Guidelines for Evaluation of Radio Interface Technologies for IMT-2020 (Report ITU-R M.2412-0). Technical report, International Telecommunication Union (ITU), October 2017.

[79] Technical Specification Group Radio Access Network; Study on channel model for frequencies from 0.5 to 100 GHz (TR 38.901 Release 16). Technical report, 3rd Generation Partnership Project (3GPP), October 2019.

[80] Lou Salaün, Chung Shue Chen, and Marceau Coupechoux. Optimal Joint Subcarrier and Power Allocation in NOMA Is Strongly NP-Hard. In *IEEE International Conference on Communications (ICC)*, May 2018.

[81] Afif Osseiran, Jose F. Monserrat, and Werner Mohr. *Mobile and Wireless Communications for IMT-Advanced and Beyond*. Wiley Telecom, 1 edition, August 2011.

[82] Xiaohu Ge, Haoming Jia, Yi Zhong, Yong Xiao, Yonghui Li, and Branka Vucetic. Energy Efficient Optimization of Wireless-Powered 5G Full Duplex Cellular Networks: A Mean Field Game Approach. *IEEE Transactions on Green Communications and Networking*, 3(2):455 – 467, March 2019.

[83] Hong Shen, Zhenyao He, Wei Xu, Shulei Gong, and Chunming Zhao. Is Full-Duplex Relaying More Energy Efficient Than Half-Duplex Relaying? *IEEE Wireless Communications Letters*, 8(3):841 – 844, June 2019.

[84] Zhenyao He, Hong Shen, Wei Xu, and Chunming Zhao. Energy Efficient Joint Power Optimization for Full-Duplex Relaying. *IEEE Access*, 7:137040 – 137047, September 2019.

[85] Abishek Sankararaman and François Baccelli. Spatial Birth–Death Wireless Networks. *IEEE Transactions on Information Theory*, 63(6):3964 – 3982, June 2017.

[86] Abishek Sankararaman, François Baccelli, and Sergey Foss. Interference Queueing Networks on Grids. *The Annals of Applied Probability*, 29(5):2929 – 2987, October 2019.

[87] Michael F. Dacey. Proportion of Reflexive nth Order Neighbors in Spatial Distribution. *Geographical Analysis*, 1(4):385 – 388, October 1969.

[88] Trevor F. Cox. Reflexive Nearest Neighbours. *Biometrics*, 37(2):367 – 369, June 1981.

[89] M. F. Schilling. Mutual and Shared Neighbor Probabilities: Finite- and Infinite-Dimensional Results. *Advances in Applied Probability*, 18(2):388 – 405, June 1986.

Appendix A

Proofs Chapter 5

A.1 Proof of Theorem 5.4.2

We have that the SINR between a typical BS and its n-th closest BS is given by:

$$\gamma_b^{(n)}(r) = \frac{\breve{G}P_d h(r) L(r)^{-1}}{\underbrace{I_{\mathrm{BS}}^{(n,1)} + I_{\mathrm{BS}}^{(n,2)}}_{I_{\mathrm{BS}}^{(n)}} + I_{\mathrm{UE}}^{(b)} + I_{\mathrm{RSI}} + \sigma^2}, \tag{A.1}$$

where r is the distance between these two elements, $L(r) = (\breve{\kappa} r)^{\breve{\eta}}$, $I_{\mathrm{BS}}^{(n,1)}$ represent the interference from the exact $(n-1)$ BSs inside the disk of radius r between the typical BS and its n-th closest BS, $I_{\mathrm{BS}}^{(n,2)}$ is the interference from all BSs outside the latter disk and $I_{\mathrm{UE}}^{(b)}$ is the interference generated by all scheduled UL users.

Similarly to the development shown in Section 2.5.1 we obtain that:

$$\begin{aligned}\mathbb{P}\left(\gamma_b^{(n)}(r) > \Gamma \,\middle|\, R = r\right) &= \underbrace{\mathbb{E}_{I_{\mathrm{BS}}^{(n)}}\left[\exp\left(-\frac{\Gamma L(r)}{\breve{G}P_d} I_{\mathrm{BS}}^{(n)}\right)\right]}_{(*)} \mathbb{E}_{I_{\mathrm{UE}}^{(b)}}\left[\exp\left(-\frac{\Gamma L(r)}{\breve{G}P_d} I_{\mathrm{UE}}^{(b)}\right)\right] N_b(r,\Gamma), \\ &\triangleq \mathscr{F}_b^{(n)}(r,\Gamma).\end{aligned} \tag{A.2}$$

Recalling that $I_{\mathrm{BS}}^{(n)} = I_{\mathrm{BS}}^{(n,1)} + I_{\mathrm{BS}}^{(n,2)}$, then $(*)$ in (A.2) results in:

$$\mathbb{E}_{I_{\mathrm{BS}}^{(n,1)}}\left[\exp\left(-\frac{\Gamma L(r)}{\breve{G}P_d} I_{\mathrm{BS}}^{(n,1)}\right)\right] \mathbb{E}_{I_{\mathrm{BS}}^{(n,2)}}\left[\exp\left(-\frac{\Gamma L(r)}{\breve{G}P_d} I_{\mathrm{BS}}^{(n,2)}\right)\right]. \tag{A.3}$$

Further, we have that $I_{\text{BS}}^{(n,1)}$ can be written as:

$$I_{\text{BS}}^{(n,1)} = \sum_{x\in\Phi} \breve{G}P_d L(x)^{-1} \mathbb{1}\{\|x\| < r\}, \tag{A.4}$$

where $\|x\|$ is the distance between an interfering BS and the typical BS under study. As mentioned before, only $(n-1)$ BSs respect $\mathbb{1}\{\|x\| < L(r)\}$ in the previous equation, i.e., the $(n-1)$ BSs inside the disk of radius r whose distances to the typical BS are $\{z_1,\ldots,z_{n-1}\}$. Thus, we have that the left-hand side term of (A.3) results in:

$$\mathbb{E}_{Z_1,\ldots,Z_{n-1}}\left[\exp\left(-\Gamma\frac{L(r)}{\breve{G}P_d}\left(\frac{\breve{G}P_d}{L(z_1)}+\ldots+\frac{\breve{G}P_d}{L(z_{n-1})}\right)\right)\right] = \mathbb{E}_Z\left[\prod_{i=1}^{n-1}\exp\left(-\Gamma\frac{L(r)}{L(z_i)}\right)\right] \tag{A.5a}$$

$$= \prod_{i=1}^{n-1}\mathbb{E}_{Z_i}\left[\exp\left(-\Gamma\frac{L(r)}{L(z_i)}\right)\right] \tag{A.5b}$$

$$= \left[\int_0^r \exp\left(-\Gamma\frac{(\breve{\kappa}r)^{\breve{\eta}}}{(\breve{\kappa}d)^{\breve{\eta}}}\right)\frac{2d}{r^2}\,\mathrm{d}d\right]^{n-1} \tag{A.5c}$$

$$= \left[\frac{2}{\breve{\eta}}\Gamma^{2/\breve{\eta}}\Gamma\left(-\frac{2}{\breve{\eta}},\Gamma\right)\right]^{n-1}, \tag{A.5d}$$

where (A.5c) is derived as all distances $\{z_1,\ldots z_{n-1}\}$ are i.i.d and distribute with PDF $P_Z(z) = 2z/r^2$ (uniform distribution of points inside a disk of radius r), from which we obtain (5.25). Furthermore, we have that $I_{\text{BS}}^{(n,2)}$ can be written as:

$$I_{\text{BS}}^{(n,2)} = \sum_{x\in\Phi} \breve{G}P_d L(x)^{-1} \mathbb{1}\{\|x\| > r\}. \tag{A.6}$$

Hence, the right-hand side term of (A.3) can be expanded similar to (2.55) and by performing the PGFL we obtain (5.26).

Regarding the interference created by ULs, we can proceed similar to Lemma 2.5.2 and get:

$$\mathscr{L}\left\{I_{\text{UE}}^{(b)}\right\}(r,\Gamma) = \mathbb{E}_\Phi\left[\prod_{y\in\Psi_u}\exp\left(-\Gamma\mu\frac{G(y)}{\breve{G}}\frac{(\breve{\kappa}r)^{\breve{\eta}}}{(\kappa z)^{\eta}}\right)\right], \tag{A.7}$$

where $G(y)$ represents the net antenna gain between the UL user in y and the typical BS. Then, we can apply the PGFL of the PPP of scheduled UL users. However, the closest UE which is at distance R_0 is the one served by the typical BS, thus the net antenna gain between both elements is the maximum possible, i.e., G. For the rest, they are all farther than R_0 and their gains are G'. Consequently, by dividing the integral inside in the expression resulting

from the PGFL and taking the expected value with respect to R_0, we obtain (5.27). Finally, by integrating (A.2) over the distribution of $f_R(r,n)$, we obtain (5.23).

A.2 Proof of Theorem 5.4.3

We approximate the process of interfering BSs by applying a $p(r)$-thinning rule to the original process of BSs Φ, where $p(r)$ is the probability that a typical BS is not able to suppress the interference coming from another BS located at a distance r. From this, we obtain (5.46) by following similar steps to the ones of Theorem 5.4.1 and Theorem 5.4.2.

A.3 Proof of Theorem 5.4.4

By using the total expectation theorem we have that:

$$\mathbb{E}[\mathscr{R}_d] = \sum_{i}^{3} \mathbb{E}\left[\mathscr{R}_d \,\middle|\, E_i\right] \mathbb{P}\left[E_i\right], \tag{A.8a}$$

$$= \nu^{\star}\omega\mathbb{E}\left[\log_2\left(1+\gamma_d^{(0)}\right)\right] P_1(M) + \mathbb{E}\left[\mathscr{C}_{\min}^{(0)}\right] P_2(M) + \omega\mathbb{E}\left[\log_2\left(1+\gamma_d^{(0)}\right)\right] P_3(M), \tag{A.8b}$$

where this last results is obtained by using the three possible values that ν can take and the respective probability of each of these events.

When assuming that $\mathscr{C}_{\min}^{(0)}(M) \sim \log_2(1+\gamma_b^{(M')})$, for a given $M' \geq M$, we have that (A.8b) results in:

$$\omega\mathbb{E}\left[\log_2\left(1+\gamma_d^{(0)}\right)\right] \left(\nu^{\star}P_1(M) + P_3(M)\right) + \omega\mathbb{E}\left[\log_2\left(1+\gamma_b^{(M')}\right)\right] P_2(M). \tag{A.9}$$

Hence, from positivity of the SINRs in (5.2) and (5.9), $\mathbb{E}_{\gamma_m}\left[\log_2\left(1+\gamma_m\right)\right]$, for $m \in \{d,b\}$, we can write:

$$\mathbb{E}\left[\log_2\left(1+\gamma_m\right)\right] = \int_0^{\infty} \mathbb{P}\left(\log_2\left(1+\gamma_m\right) > \Gamma\right) \mathrm{d}\Gamma = \int_0^{\infty} \frac{\mathbb{P}\left(\gamma_m > \Gamma\right)}{\ln(2)(1+\Gamma)} \mathrm{d}\Gamma, \tag{A.10}$$

which concludes the proof.